

## COUNTERCURRENT DISTRIBUTION OF HIGH-BOILING NEUTRAL OILS FROM A LOW-TEMPERATURE COAL TAR

Patricia A. Estep, Clarence Karr, Jr., William C. Warner,  
and Edward E. Childers

U. S. Department of the Interior, Bureau of Mines  
Morgantown Coal Research Center, Morgantown, W. Va.

### INTRODUCTION

In a comprehensive investigation of the composition of low-temperature bituminous coal tar it was necessary to analyze the high-boiling neutral oil fractions in the range 275° to 344° C. The method selected for this was fractionation by distillation, further separation by countercurrent distribution (CCD), and final analysis by infrared and ultraviolet spectrophotometry. A recent review on countercurrent distribution (10) shows that relatively little work has been done on the CCD of high-boiling neutral polynuclear compounds and nothing on separation of natural mixtures by this method. Golumbic (8) has reported an investigation of the partition coefficient of 18 polynuclear compounds in the solvent system cyclohexane/80 percent ethanol and proposed this solvent system for the analysis of the heavy-oil fractions of coal-hydrogenation products. Chang (5) reported on the partition coefficient of 24 aromatic compounds in  $\beta, \beta'$ -oxydipropionitrile/isooctane and proposed this solvent system for CCD separations of petroleum fractions and oils derived from coal tars. Mold (11) has recently conducted work on the CCD of polycyclic aromatic compounds with a solvent system containing tetramethyluric acid but did not analyze natural mixtures. The present work fully demonstrates the capabilities of CCD, supplemented by infrared and ultraviolet spectroscopy for the separation and analysis of complex high-boiling neutral aromatic coal tar, shale oil, or petroleum components. It was found that class separations were sufficient to allow reliable spectrophotometric analyses to be applied. Many specific isomers occurring in sufficiently large enough amounts were individually determined.

### EXPERIMENTAL

Preliminary Fractionation by Distillation. - The neutral oil used in this work was obtained from a low-temperature West Virginia bituminous coal tar. Previous reports (3, 4) have presented the analysis of this material for fractions up to the present boiling range, using gas-liquid chromatography. In two separate distillations, the 29 neutral oil fractions analyzed in the present work were obtained, these representing 33.46 wt pct of the total neutral oil (the total neutral oil distilling up to about 360° C represents 16.92 wt pct of the tar). Complete data for the first of these distillations, including analysis of fractions 1 to 8, is included in a previous paper (3). The second distillation was made on a 47.2 g charge, giving 38.7 g distillate, 7.7 g residue, and 0.9 g loss and hold up. This material was distilled at 3.0 mm Hg with a reflux ratio of 20 to 1 in a spinning band still. Equivalent atmospheric boiling points were estimated from a standard nomograph. Infrared and ultraviolet spectra were obtained on all distillate fractions. These were combined on the basis of qualitative similarity to give 14 samples which were each fractionated by countercurrent distribution.

Countercurrent Distribution. - The instrument used was a Craig 60-tube all-glass model with an automatic fraction collector. The tube capacity for each phase was 40 ml. The instrument was operated to give 120 transfers and 60 tubes were collected in the fraction collector. Each distribution was made with a charge of 500 milligrams, obtained by using the proper volume of a solution of known concentration of the distillate fraction in the upper phase. The upper phase solvent was spectral grade isooctane, and the lower phase was a 90 wt pct ethanol in water mixture. This solvent system was chosen on the basis of its ability to separate various aromatic hydrocarbons from each other. A thorough investigation was conducted on anthracene, a typical component of these neutral oil fractions. Its partition coefficient in a variety of solvent pairs was determined, and the final choice was made for that in which the value was nearest 1. This placed the bulk of the material where enough tubes could be efficiently utilized in the separations. The solvent system choice was also limited to those mixtures sufficiently immiscible to give complete separation of layers during the preset instrument cycling time. The distributions were carried out at 26° C, and the solvents were pre-equilibrated at the same temperature. This pre-equilibration produced a volume change for equal volumes to 1.83 parts 90 wt pct ethanol per 1.00 parts isooctane after equilibration. The equilibrated solvents were used in making all necessary dilutions for ultraviolet analysis.

Spectrophotometric Analysis. - Ultraviolet spectra were obtained on the contents of all CCD tubes, taken directly from the instrument, on a Perkin-Elmer Model 350 spectrophotometer. Infrared spectra were obtained on a Perkin-Elmer Model 21 spectrophotometer equipped with a Perkin-Elmer 6x ultramicro sampling unit mounted in the sample beam. The sample holder, designed to mount the ultramicrocavity cells in this unit, has been described (6). Sample preparation preceding infrared analysis was as follows:

The contents of a single tube after ultraviolet analysis were placed in a 150-ml distillation flask and dry nitrogen passed slowly into the flask through a glass tube extending nearly to the bottom of the flask where the tube was drawn into a fine tip. The nitrogen flowed out through the side arm. When the solvent was completely removed, the material was transferred from this flask by means of a 6-in. hypodermic needle and syringe and several washings of carbon disulfide into a small tared tapered tube. The CS<sub>2</sub> was evaporated from this small tube with nitrogen through a syringe needle. It was seen from infrared spectra that the last traces of CS<sub>2</sub> could be removed by this method. The small amount of liquid material in the tip of this tube was first weighed and then transferred with the aid of a 50 μl microsyringe to an ultramicrocavity NaCl cell (purchased from the Barnes Engineering Company). Samples were run undiluted in these cells whenever possible. When there was not enough sample recovered to fill the cell cavity, the material was diluted with CS<sub>2</sub> and the infrared spectrum obtained in solution.

Determination of Distribution Curves. - The amount of material recovered in each tube was plotted to obtain a weight distribution for each run. The amount of material in a single tube typically ranged from 0.5 to 21 milligrams. Ultraviolet absorbance distribution curves also were prepared at various key wavelengths for each run. These were used for the determination of peak tubes of major components and in the quantitative analysis. When there was no peak tube discernible on the distribution plot for minor or trace components determined to

be present from spectra, it was possible to resolve the "envelope" of ultraviolet absorbance into its component parts. Since the countercurrent distributions are essentially Gaussian and symmetrical, it is possible to construct individual absorbance distribution curves by following the appearance and disappearance of individual bands in consecutive fractions and noting the peak tubes from spectra. This procedure was also helpful in determining which bands belonged to the same compound.

## RESULTS AND DISCUSSION

The results of the distillations are given in Table 1. On the basis of the qualitative information from ultraviolet and infrared spectra, the constituents from each CCD fractionation were distinguished and assigned numbers. It was essential to number these constituents since they frequently appeared in more than one run. A total of 51 separate identifications were made in this 69° C boiling range, and these are shown in Table 2.

The quantitative analyses for aromatics were conducted in the ultraviolet using absorptivities at characteristic bands where interferences from other constituents were at a minimum. Absorbance values were obtained from the curves already described. Where the ultraviolet absorption bands for components overlapped too greatly, their relative amounts could generally be estimated from their infrared bands. In those instances where very similar isomers overlapped extensively, they were analyzed as a class rather than as individual compounds. The qualitative and quantitative analyses of each class are described under separate headings.

From the quantitative data obtained for each constituent, plots of milligrams vs. tube number were prepared. Figures 1, 2, and 3 show these distribution curves for only 3 of the 14 neutral oil fractions. These are for CCD numbers 4, 9, and 14. Tubes are numbered from 0 to 59 in the direction of transfer in the instrument and from 0 up in the order of use in the fraction collector. The numbers on the distribution curves in Figures 1, 2, and 3 refer to some of the constituents listed in Table 2. The weight-percent of each constituent in the neutral oil was obtained from the distribution curves and the weights of the original distillate fractions. These quantitative results are summarized in Table 3.

o-Dimethylphthalate. - Identification of this compound was made by infrared spectroscopy. Its location in the lower tube numbers of the lower phase is in line with its polarity.

Carbazoles. - The weak but significant polar character of the unsubstituted nitrogen atom of carbazoles places this class in the lower numbered tubes of the lower phase, beginning with the parent structure in tube 27 of CCD No. 9. Subsequent runs show the peak tube to shift to tubes 29 and 31, indicating methylation, and both infrared and ultraviolet spectra confirmed the presence of monomethyl carbazoles. The quantitative determination of carbazole and its methyl derivatives was straightforward, using the absorption band at 230 to 240  $\mu$ . For the determination of the mixed monomethyl isomers, the absorptivity data used was obtained from available samples of 1- and 2-methylcarbazole. Infrared literature spectra were available for the 3- and 4-methylcarbazoles (12), and ultraviolet was available for 3-methylcarbazole (9).

Long-chain Aliphatic Hydrocarbons. - These were effectively separated from aromatic hydrocarbons in the first 15 tubes of the fraction collector in each CCD run. Infrared analysis (7) showed this aliphatic material to consist of five classes:  $\alpha$ -olefins, branched  $\alpha$ -olefins, trans-internal olefins, n-alkanes, and 2-methylalkanes. Since the CCD solvent system was selected for optimum separation of aromatics, there was only a small separation by class for the aliphatic compounds. In Table 2 each class was assigned a single number throughout the entire boiling range although boiling points indicate a change in molecular weight from  $C_{15}$  through  $C_{20}$ .

Alkyl naphthenes. - According to Bellamy (2), the infrared bands observed at 10.72, 10.50, 10.27, and 9.73  $\mu$  in aliphatic fractions can be assigned to the ring deformation vibrations of six-membered ring naphthenes. An estimate of their concentration was made using data from literature spectra (1).

Aliphatic Carbonyl. - The carbonyl bands at 5.72 to 5.93  $\mu$  along with the  $CH_2$  rocking vibration at 13.88  $\mu$  were assigned to aliphatic carbonyl, either ketones or esters. The fairly long chain, as indicated by the intensity of the 13.88  $\mu$  band, balances the polar effect of the carbonyl group to place them in tubes 56 to 58 of the fraction collector. Estimates of concentration for this class were made by using absorptivity data for the carbonyl band from pure samples of aliphatic esters.

Naphthalenes. - Alkyl naphthalenes were identified in all neutral oil fractions. On the basis of boiling point and ultraviolet correlations, it was found that they were predominantly polymethylnaphthalenes. There was no evidence of any long chain or branched alkyl substitution. Infrared bands at 6.25 and 9.67  $\mu$  along with strong out-of-plane hydrogen deformation vibration bands in the 11.0 to 14.0  $\mu$  region were observed. The increasing number of possible isomers with increasing molecular weight of methylnaphthalenes made identification of specific isomers extremely difficult. It was observed from this laboratory's data and a collection of methylnaphthalene spectra from the literature, that in general, for polymethylnaphthalenes the specific absorptivity of the 230  $m\mu$  band decreases regularly in intensity with increasing molecular weight. The values for each carbon number were in a range narrow enough to justify the use of an average. The average specific absorptivity for 14 trimethylnaphthalenes ( $C_{13}$ ) was 530, for 7 tetramethylnaphthalenes ( $C_{14}$ ), 442, for 3 pentamethylnaphthalenes ( $C_{15}$ ), 346, and for 4 hexamethylnaphthalenes ( $C_{16}$ ), 317. An average specific absorptivity of 7 literature ethylmethylnaphthalenes ( $C_{13}$ ) falls very close to the value of trimethylnaphthalenes ( $C_{13}$ ), and an average of 4 diethylmethylnaphthalenes ( $C_{15}$ ) falls very close to that of pentamethylnaphthalenes ( $C_{15}$ ).

Hydroaromatics and Biphenyls. - A broad ultraviolet band at 259  $m\mu$  at a maximum in tubes 11 to 14 FC represented a mixture of biphenyls and hydroaromatics. Biphenyls were indicated by a series of shoulders occurring on this major band and also by an infrared band at 14.30  $\mu$ . The hydroaromatic structure was indicated by the aromatic band at 6.25  $\mu$  which, although present, was relatively weak. Additional evidence to support this class was obtained from ultraviolet quantitative data. From the actual weight of these fractions and the observed absorbances, ultraviolet absorptivities were approximated and found to be low, indicating saturation of aromatic rings.

Fluorenes. - Fluorenes were identified by their distinctly characteristic ultraviolet spectra and their strong out-of-plane hydrogen deformation bands in the infrared. The ultraviolet band at 300  $m\mu$ , which shifts to slightly higher wavelengths for methyl isomers, fortunately occurs in a region where analysis was unhindered by other components. For fluorene and 1-methylfluorene, analysis was straightforward, using specific absorptivity values of 59 and 41 respectively, determined at 300  $m\mu$  from available samples. The amount of the 2- and 3-methylfluorene mixture was determined at 260  $m\mu$  using an average specific absorptivity value of 116 obtained from pure samples.

Phenanthrenes. - Differentiation among the 1-methyl, 2-methyl, and 3-methyl isomers was readily made from strong infrared bands in the out-of-plane hydrogen deformation region at 11 to 14  $\mu$ . The strong ultraviolet band which ranged from 251 to 253.5  $m\mu$  in these CCD fractions indicated monomethyl-substituted phenanthrenes. This band shifts from 250.2  $m\mu$  for phenanthrene to a range of 251 to 254.4  $m\mu$  as observed in spectra of monomethylphenanthrenes. Dimethylphenanthrenes were also identified in the ultraviolet from the position of this strong band with a range of 252 to 256  $m\mu$ . From literature spectra of 12 dimethylphenanthrenes this range was observed to be 252 to 258  $m\mu$ . The shift in peak tubes accompanying the change in range of this ultraviolet band verified methylation. Phenanthrene determination was made in the ultraviolet, using a specific absorptivity value of 359 at 250.2  $m\mu$ . An average specific absorptivity of 322 was determined from pure samples of 1-methyl-, 2-methyl-, and 3-methylphenanthrene. Absorbances were read from the peak of the large band as it shifted from 251 to 253.5  $m\mu$ . The ratios of the individual monomethyl isomers were estimated from their strong infrared out-of-plane hydrogen deformation bands. For dimethylphenanthrenes, using the same intense ultraviolet band, an average specific absorptivity of 293 was determined from ultraviolet spectra of 12 dimethylphenanthrenes.

Anthracenes. - Qualitatively the distinction between anthracene and its monomethyl and dimethyl derivatives can best be made in the ultraviolet region where their longest wavelength bands are highly diagnostic. Neither the monomethyl nor the dimethyl anthracenes were substituted in the 9 or 10 position, as this causes a marked shift to longer wavelengths as compared to other positions. Quantitative analyses for anthracenes were conducted at 375.6  $m\mu$  for anthracene, 377.6  $m\mu$  for monomethylantracenes, and 380.0  $m\mu$  for dimethylantracenes. A specific absorptivity value of 43 for anthracene was determined from a pure sample. A monomethyl specific absorptivity value of 43 was obtained from a sample of 2-methylantracene and a literature spectrum of 1-methylantracene (15). From literature spectra of 7 dimethylantracenes, a value of 30 was determined for specific absorptivity.

Dibenzofurans. - Alkyldibenzofurans can be characterized in the infrared by a sharp, strong band in the 8.2 to 8.5  $\mu$  region (13) assigned to the C-O stretching vibration. The analysis was conducted in the ultraviolet region for dibenzofurans using a strong absorption band near 250  $m\mu$ . For dibenzofuran a value of 115 at 248.8  $m\mu$  for the specific absorptivity was obtained from a pure sample. The monomethyldibenzofurans were determined by using an average specific absorptivity value of 98 at 251 to 253  $m\mu$ , obtained from pure samples of 2-methyl-, 3-methyl-, and 4-methyldibenzofurans, and the spectrum for 1-methyldibenzofuran (14). For dimethyldibenzofurans, an average specific absorptivity value of 81 near 250  $m\mu$  was obtained from spectra of 6 dimethyldibenzofurans (14).

## REFERENCES

1. American Petroleum Institute Research Project 44. Catalog of Infrared Spectra. Carnegie Inst. Technol., Pittsburgh, Pa.
2. Bellamy, L. J. The Infra-red Spectra of Complex Molecules. John Wiley & Sons, Inc., New York, 1960, 2d ed., 425 pp.
3. Chang, Ta-Chuang Lo, and Clarence Karr, Jr. Gas-Liquid Chromatographic Analysis of Aromatic Hydrocarbons Boiling Between 202° and 280° in a Low-Temperature Coal Tar. *Anal. Chim. Acta*, v. 24, No. 4, April 1961, pp. 343-356.
4. \_\_\_\_\_. Gas-Liquid Chromatographic Analysis of Aromatic Hydrocarbons Boiling Up to 218° in a Low-Temperature Coal Tar. *Anal. Chim. Acta*, v. 21, No. 5, November 1959, pp. 474-490.
5. Chang, Yi-Chung, and Robert D. Wotring. Countercurrent Distribution of Some Aromatic Hydrocarbons. *Anal. Chem.*, v. 31, No. 9, September 1959, pp. 1501-1504.
6. Estep, Patricia A., and Clarence Karr, Jr. A Liquid Ultramicrocavity Cell Holder for Use With an Infrared Beam Condenser. *Appl. Spectry.*, v. 16, No. 5, October 1962, pp. 167-168.
7. \_\_\_\_\_. Quantitative Infrared Microanalysis of High-Boiling Aliphatic Neutral Oil Fractions. *Anal. Chem.*, v. 36, No. 11, October 1964, pp. 2215-2218.
8. Golumbic, Calvin. Separation and Analysis of Polynuclear Compounds by Countercurrent Distribution. *Anal. Chem.*, v. 22, No. 4, April 1950, pp. 579-582.
9. Haines, R. E. Bureau of Mines, Laramie Petrol. Res. Center, Laramie, Wyo., private communication, 1962.
10. Lederer, Michael, editor. *Chromatographic Reviews*. Elsevier Publishing Co., New York, v. 5 (covering the year 1962), 1963, 244 pp.
11. Mold, James D., Thomas B. Walker, and Lee G. Veasey. Selective Separation of Polycyclic Aromatic Compounds by Countercurrent Distribution With a Solvent System Containing Tetramethyluric Acid. *Anal. Chem.*, v. 35, No. 13, December 1963, pp. 2071-2074.
12. Richards, R. E. Infra-red Spectrum and Structural Diagnosis: Substituted Carbazoles. *J. Chem. Soc.*, 1947, pp. 978-979.
13. Trippett, S. The Synthesis of Methyl- and Dimethyl-dibenzofurans. *J. Chem. Soc.*, January 1957, pp. 419-421.
14. \_\_\_\_\_. The University, Leeds, England, private communication, November 1959.
15. Wolthuis, Enno. Synthesis of Some Methyl-Substituted Anthracenes. *J. Org. Chem.*, v. 26, No. 7, July 1961, pp. 2215-2220.

## ACKNOWLEDGMENTS

The authors wish to express their appreciation to: Chester Muth, Chemistry Department, West Virginia University, Morgantown, W. Va., for a sample of 4-methyldibenzofuran; A. Ladam, Centre d'Etudes et de Recherches des Charbonnages de France, for samples of 1-, 2-, and 3-methylfluorene and 2- and 3-methyldibenzofuran; S. Trippett, University of Leeds, England, for spectra of a variety of alkyl-dibenzofurans; and W. E. Haines, Laramie Petroleum Research Center, Bureau of Mines, Laramie, Wyo., for a sample of 1-methylcarbazole and an ultraviolet spectrum of 3-methylcarbazole.

TABLE 1. - Fractional distillation of neutral oils

CCD No.	Distillate fraction No.	Boiling range, ° C		Weight, grams
		10 mm	760 mm	
1	9	138 - 139	275 - 276	9.0
	10	139 - 141	276 - 278	9.0
2	11	141 - 143	278 - 280	8.6
	12	143 - 144	280 - 282	9.4
3	13	144 - 146	282 - 284	9.2
	14	146 - 148	284 - 286	9.3
4	15	148 - 149	286 - 287	9.6
	16	149	287	3.6
				<sup>1</sup> 67.7
		3.0 mm	760 mm	
5	1	123 - 125	287 - 290	1.9
	2	125 - 127	290 - 292	2.0
6	3	127 - 128	292 - 293	1.6
	4	128	293	1.7
7	5	128 - 132	293 - 298	1.7
	6	132 - 134	298 - 300	1.9
8	7	134 - 135	300 - 301	1.6
	8	135 - 136	301 - 302	1.9
	9	136 - 137	302 - 303	1.6
9	10	137 - 138	303 - 305	1.9
	11	138 - 143	305 - 310	2.0
10	12	143 - 144	310 - 311	2.1
	13	144 - 145	311 - 313	2.0
11	14	145 - 148	313 - 316	2.2
	15	148 - 150	316 - 318	2.3
	16	150 - 152	318 - 321	2.0
12	17	152 - 153	321 - 322	2.0
	18	153 - 160	322 - 329	1.9
13	19	160 - 167	329 - 337	1.9
14	20	167 - 171	337 - 342	2.0
	21	171 - 173	342 - 344	.5
				<sup>2</sup> 38.7

<sup>1</sup> Fractions 9 through 16 are 9.72 weight-percent of the total neutral oil.

<sup>2</sup> An aliquot representing 23.74 weight-percent of the total neutral oil.

TABLE 2. - Countercurrent distribution of high-boiling neutral oils

No.	Constituent Identity	Peak tube no.
<u>CCD NO. 1</u>		
1	Unknown I	34
2	Aliphatic carbonyl	58 FC
3	Dibenzofuran	44 FC
4	Acenaphthene	34 FC
5	Trimethylnaphthalenes (N <sub>1</sub> , N <sub>2</sub> , N <sub>3</sub> , N <sub>4</sub> )	26 FC
6	Hydroaromatics, Biphenyls	14 FC
7	Alkylnaphthenes (6-membered ring)	10 FC
8	trans-Internal olefin	10.5 FC
9	Terminal olefin	10.5 FC
10	n-Alkane	9.0 FC
11	Branched-terminal olefin	8.5 FC
12	2-Methylalkane	6 FC
<u>CCD NO. 2</u>		
1	Unknown I	34.5
2	Aliphatic carbonyl	58 FC
3	Dibenzofuran	48 FC
13	Fluorene	44 FC
5	Trimethylnaphthalenes (N <sub>1</sub> , N <sub>2</sub> , N <sub>3</sub> , N <sub>4</sub> )	25 FC
14	Tri- or tetramethylnaphthalenes (N <sub>5</sub> , N <sub>6</sub> , N <sub>7</sub> )	25 FC
6	Hydroaromatics, Biphenyls	14 FC
7	Alkylnaphthenes (6-membered ring)	10 FC
8	trans-Internal olefin	9 FC
9	Terminal olefin	9 FC
10	n-Alkane	8 FC
11	Branched terminal olefin	6 FC
12	2-Methylalkane	3.5 FC
<u>CCD NO. 3</u>		
15	o-Dimethylphthalate	4
1	Unknown I	33.5
2	Aliphatic carbonyl	58 FC
16	4-Methyldibenzofuran	48 FC
13	Fluorene	42 FC
14	Tri- or tetramethylnaphthalenes (N <sub>5</sub> , N <sub>6</sub> , N <sub>7</sub> )	26 FC

See footnotes at end of table.

Constituent		Peak tube no.
No.	Identity	
6	Hydroaromatics, Biphenyls	14 FC
7	Alkyl-naphthenes (6-membered ring)	10 FC
8	trans-Internal olefin	8 FC
9	Terminal olefin	8.5 FC
10	n-Alkane	8 FC
11	Branched-terminal olefin	8 FC
12	2-Methylalkane	5 FC
<u>CCD NO. 4</u>		
15	o-Dimethylphthalate	4
1	Unknown I	34
2	Aliphatic carbonyl	56 FC
16	4-Methyldibenzofuran	45 FC
13	Fluorene	42 FC
14	Tri- or tetramethylnaphthalenes (N <sub>5</sub> , N <sub>6</sub> , N <sub>7</sub> )	26 FC
6	Hydroaromatics, Biphenyls	14 FC
8	trans-Internal olefin	8 FC
9	Terminal olefin	8 FC
10	n-Alkane	7.5 FC
11	Branched terminal olefin	7 FC
12	2-Methylalkane	3 FC
<u>CCD NO. 5</u>		
17	Unknown II	34.5
2	Aliphatic carbonyl	56 FC
18	2-Methyldibenzofuran	<sup>2</sup> 36 FC
19	3-Methyldibenzofuran	<sup>2</sup> 36 FC
16	4-Methyldibenzofuran	<sup>2</sup> 36 FC
20	1-Methyldibenzofuran	<sup>2</sup> 36 FC
21	Tetramethylnaphthalenes	23 FC
6	Hydroaromatics, Biphenyls	14 FC
8	trans-Internal olefin	8 FC
9	Terminal olefin	8 FC
10	n-Alkane	8 FC
11	Branched-terminal olefin	7.5, 12 FC
12	2-Methylalkane	5 FC

See footnotes at end of table.

No.	Constituent Identity	Peak tube no.
<u>CCD NO. 6</u>		
17	Unknown II	36
18	2-Methyldibenzofuran	<sup>2</sup> 36 FC
19	3-Methyldibenzofuran	<sup>2</sup> 36 FC
16	4-Methyldibenzofuran	<sup>2</sup> 36 FC
20	1-Methyldibenzofuran	<sup>2</sup> 36 FC
21	Tetramethylnaphthalenes	24 FC
6	Hydroaromatics, Biphenyls	14 FC
8	trans-Internal olefin	8.5 FC
9	Terminal olefin	8.5 FC
10	n-Alkane	8.5 FC
11	Branched-terminal olefin	7.5 FC
12	2-Methylalkane	5 FC
<u>CCD NO. 7</u>		
17	Unknown II	35
22	Aliphatic carbonyl	55 FC
23	Unknown III	55 FC
24	Dimethyldibenzofuran	<sup>2</sup> 41 FC
18	2-Methyldibenzofuran	<sup>2</sup> 41 FC
19	3-Methyldibenzofuran	<sup>2</sup> 41 FC
20	1-Methyldibenzofuran	<sup>2</sup> 41 FC
25	1-Methylfluorene	38 FC
26	2- and/or 3-Methylfluorene	38 FC
27	Dimethyldibenzofurans	24 FC
21	Tetramethylnaphthalenes	23.5 FC
6	Hydroaromatics, Biphenyls	14 FC
8	trans-Internal olefin	8 FC
9	Terminal olefin	8 FC
10	n-Alkane	8 FC
11	Branched-terminal olefin	7 FC
12	2-Methylalkane	5 FC
<u>CCD NO. 8</u>		
17	Unknown II	35
28	Unknown IV	55 FC
29	Phenanthrene	51 FC
30	Unknown V	48 FC
18	2-Methyldibenzofuran	<sup>2</sup> 44 FC
19	3-Methyldibenzofuran	<sup>2</sup> 44 FC
25	1-Methylfluorene	38 FC
26	2- and/or 3-Methylfluorene	38 FC

See footnotes at end of table.

Constituent		Peak tube no.
No.	Identity	
31	2, 4-Dimethyldibenzofuran	31 FC
27	Dimethyldibenzofurans	24 FC
32	Alkylnaphthalenes (N <sub>8</sub> , N <sub>9</sub> )	22.5 FC
6	Hydroaromatics, Biphenyls	14 FC
8	trans-Internal olefin	8 FC
9	Terminal olefin	8 FC
10	n-Alkane	8 FC
11	Branched-terminal olefin	7 FC
12	2-Methylalkane	5 FC
<u>CCD NO. 9</u>		
33	Carbazole	27
34	Unknown VI	37.5
29	Phenanthrene	51 FC
30	Unknown V	48 FC
35	Anthracene	48 FC
26	2- and/or 3-Methylfluorene	38 FC
31	Dimethyldibenzofuran (principally 2, 4-dimethyldibenzofuran)	30 FC
32	Alkylnaphthalenes (N <sub>8</sub> , N <sub>9</sub> )	22 FC
6	Hydroaromatics, Biphenyls	14 FC
8	trans-Internal olefin	7 FC
9	Terminal olefin	7 FC
10	n-Alkane	7 FC
11	Branched-terminal olefin	7 FC
12	2-Methylalkane	4 FC
<u>CCD NO. 10</u>		
33	Carbazole	27
34	Unknown VI	38
29	Phenanthrene	51 FC
30	Unknown V	48 FC
35	Anthracene	47 FC
36	Carbonyl compound	42 FC
31	Dimethyldibenzofurans (principally 2, 4-dimethyldibenzofuran)	32.5 FC
32	Alkylnaphthalenes (N <sub>8</sub> , N <sub>9</sub> )	22 FC
6	Hydroaromatics, Biphenyls	13 FC
8	trans-Internal olefin	7 FC
9	Terminal olefin	7 FC
10	n-Alkane	7 FC
11	Branched-terminal olefin	7, 10 FC
12	2-Methylalkane	4 FC

Constituent		Peak
No.	Identity	tube
		no.
<u>CCD NO. 11</u>		
33	Carbazole	27
34	Unknown VI	39
37	Unknown VII	54 FC
29	Phenanthrene	51 FC
30	Unknown V	48 FC
35	Anthracene	45 FC
38	2-Methylphenanthrene	43 FC
39	3-Methylphenanthrene	41 FC
40	1-Methylphenanthrene	38 FC
41	Dimethyldibenzofurans	30 FC
42	Alkylnaphthalenes (N <sub>11</sub> , N <sub>10</sub> )	21 FC
6	Hydroaromatics, Biphenyls	13 FC
8	trans-Internal olefin	7 FC
9	Terminal olefin	7 FC
10	n-Alkane	7 FC
11	Branched-terminal olefin	7, 10 FC
12	2-Methylalkane	4 FC
<u>CCD NO. 12</u>		
43	1-Methylcarbazole	<sup>2</sup> 26.5
33	Carbazole	<sup>2</sup> 26.5
44	Unknown VIII	42
35	Anthracene	45 FC
38	2-Methylphenanthrene	<sup>2</sup> 40 FC
39	3-Methylphenanthrene	<sup>2</sup> 40 FC
40	1-Methylphenanthrene	<sup>2</sup> 40 FC
45	1- and/or 2-Methylanthracene	40 FC
41	Dimethyldibenzofurans	28 FC
42	Alkylnaphthalenes (N <sub>11</sub> , N <sub>10</sub> )	18.5 FC
6	Hydroaromatics, Biphenyls	11 FC
8	trans-Internal olefin	6, 9.5 FC
9	Terminal olefin	6 FC
10	n-Alkane	7 FC
11	Branched-terminal olefin	6, 9 FC
12	2-Methylalkane	4.5 FC
<u>CCD NO. 13</u>		
46	2- and/or 3-Methylcarbazole	<sup>2</sup> 29
43	1- and/or 4-Methylcarbazole	<sup>2</sup> 29
47	Unknown IX	46
38	2-Methylphenanthrene	<sup>2</sup> 40 FC

See footnotes at end of table.

No.	Constituent Identity	Peak tube no.
39	3-Methylphenanthrene	<sup>2</sup> 40 FC
40	1-Methylphenanthrene	<sup>2</sup> 40 FC
45	1- and/or 2-Methylanthracene	38 FC
48	Alkyldibenzofurans	26 FC
42	Alkyl-naphthalenes (N <sub>11</sub> , N <sub>10</sub> )	18.5 FC
6	Hydroaromatics, Biphenyls	11 FC
8	trans-Internal olefin	7 FC
9	Terminal olefin	7 FC
10	n-Alkane	6 FC
11	Branched-terminal olefin	7 FC
12	2-Methylalkane	4 FC
<u>CCD NO. 14</u>		
46	2- and/or 3-Methylcarbazole	<sup>2</sup> 31
43	1- and/or 4-Methylcarbazole	<sup>2</sup> 31
47	Unknown IX	46
49	Unknown X	57 FC
45	1- and/or 2-Methylanthracene	39 FC
50	Dimethylphenanthrenes	35.5 FC
51	Dimethylantracenes	32 FC
48	Alkyldibenzofurans	25 FC
42	Alkyl-naphthalenes (N <sub>11</sub> , N <sub>10</sub> )	18 FC
6	Hydroaromatics, Biphenyls	11 FC
8	trans-Internal olefin	6 FC
9	Terminal olefin	6 FC
10	n-Alkane	6 FC
11	Branched-terminal olefin	6 FC
12	2-Methylalkane	3 FC

<sup>1</sup> FC = fraction collector.

<sup>2</sup> Peak tube for a mixture of compounds.

TABLE 3. - Quantitative analysis of neutral oils  
boiling from 275° to 344° C

Constituent	Weight-percent in neutral oil <sup>1</sup>
Alkylbinuclear naphthenes	0.15
n-Alkanes	3.16
2-Methylalkanes	1.09
Terminal olefins	2.42
Branched-terminal olefins	.37
trans-Internal olefins	1.29
Aliphatic carbonyl	.21
	8.69
Acenaphthene	.37
Hydroaromatics, biphenyls	3.02
Trimethylnaphthalene, No. 5	1.88
Alkyl-naphthalenes (tetramethyl), No. 14	2.60
Alkyl-naphthalenes, Nos. 21, 32, 42	7.75
	12.23
Fluorene	.20
1-Methylfluorene	.10
2- and/or 3-Methylfluorene	.23
	.53
Phenanthrene	.39
1-Methylphenanthrene	.11
2-Methylphenanthrene	.19
3-Methylphenanthrene	.23
Dimethylphenanthrenes	.23
	1.15
Anthracene	.05
Monomethylantracenes	.04
Dimethylantracenes	.01
	.10

<sup>1</sup> Total neutral oil (distilling up to about 360° C) constituted 16.92 weight-percent of the total tar.

(Continuing)  
**TABLE 3. - Quantitative analysis of neutral oils**  
boiling from 275° to 344° C

Constituent	Weight-percent in neutral oil <sup>1</sup>
Dibenzofuran	0.32
1-Methyldibenzofuran	.19
2-Methyldibenzofuran	.27
3-Methyldibenzofuran	.46
4-Methyldibenzofuran	.34
Dimethyldibenzofurans	3.84
(Approximately 50 percent 2, 4-dimethyldibenzofuran)	
Alkylated dibenzofurans (trimethyl-)	.68
	<hr/> 6.10
o-Dimethylphthalate	.03
Carbazole	.09
1- and/or 4-Methylcarbazole	.08
2- and/or 3-Methylcarbazole	.17
	<hr/>
Unknowns I through X	1.02

<sup>1</sup> Total neutral oil (distilling up to about 360° C) constituted 16.92 weight-percent of the total tar.

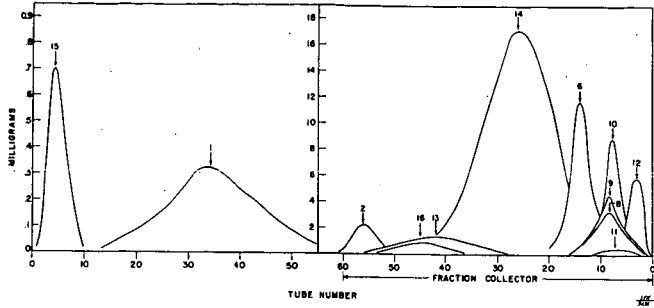


FIGURE 1. - Countercurrent Distribution of Neutral Oil, Run No. 4.

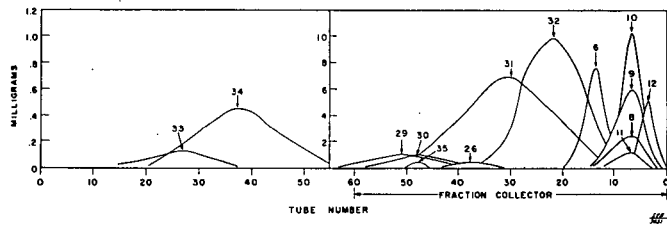


FIGURE 2. - Countercurrent Distribution of Neutral Oil, Run No. 9.

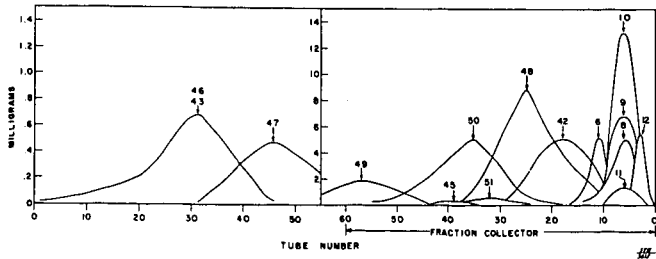


FIGURE 3. - Countercurrent Distribution of Neutral Oil, Run No. 14.

FORMATION AND NATURE OF NITROGENOUS GUM DERIVED FROM  
COKE-OVEN GAS UNDER CRYOGENIC CONDITIONS

by  
W. Kulak  
E. V. Nagle  
J. G. Crist

Applied Research Laboratory  
United States Steel Corporation  
Monroeville, Pennsylvania

Introduction

A type of nitrogenous gum called "vapor-phase gum" has long been known to form in coke-oven gas. It is generally accepted that the formation of this gum is due primarily to the interaction of nitric oxide (NO), oxygen, and organic compounds such as the unsaturated hydrocarbons. Another type of nitrogenous gum is one that is formed in coke-oven gas under cryogenic conditions that also involves the interaction of nitric oxide, oxygen, and hydrocarbons. It is widely recognized<sup>1,2,3,4</sup>\* that NO by itself does not react with gum-forming hydrocarbons; however, under cryogenic conditions the oxidation of NO or its dimer, (NO)<sub>2</sub>, is rapid and the products of the oxidation, nitrogen trioxide (N<sub>2</sub>O<sub>3</sub>) and nitrogen tetroxide (N<sub>2</sub>O<sub>4</sub>), react with gum-forming hydrocarbons. In the liquid phase, ethylene is known to react with N<sub>2</sub>O<sub>3</sub> and N<sub>2</sub>O<sub>4</sub>; however, such reactions are slow at low temperatures.<sup>1,5</sup> Generally it is assumed that nitrogen oxides react primarily with cyclopentadiene and butadiene when present in liquid ethylene. It is the purpose of this paper to present the results of work undertaken to investigate the reactions, and the products of the reactions, of N<sub>2</sub>O<sub>3</sub> and N<sub>2</sub>O<sub>4</sub> with cyclopentadiene and butadiene in liquid ethylene. For comparison, some investigations were made in which liquid ethane was used in place of liquid ethylene.

Materials and Experimental Work

Materials - All materials were obtained from The Matheson Company. Ethylene (99.5% minimum purity) and ethane (99.0% minimum) were purified by passage through activated carbon. Butadiene and N<sub>2</sub>O<sub>3</sub> (both 99.0% minimum purity) and N<sub>2</sub>O<sub>4</sub> (99.5% minimum) were used as received. Cyclopentadiene was freshly distilled as needed; mass-spectrometric analysis of the distilled material showed it to contain 93.8 percent cyclopentadiene, 2.7 percent dicyclopentadiene, 2.9 percent 1,3-cyclohexadiene, 0.5 percent benzene, and less than 0.1 percent toluene.

Apparatus and Procedure - Liquid ethylene (or ethane) for the tests was prepared by passing the Matheson gas through activated

---

\* See References.

carbon and condensing it at atmospheric pressure and, as well as possible, in the absence of air. As the first step in preparing the gums, the Pyrex condenser and receiver were purged with gaseous ethylene (or ethane) and the receiver was cooled with liquid nitrogen. When cyclopentadiene was used, a weighed amount of the diene was injected into the receiver through a septum-covered port by means of a syringe and about 200 cubic centimeters (cc) of liquid ethylene (or ethane) were then condensed into the receiver. When butadiene was used, it was more convenient to condense the liquid ethylene (or ethane) into the receiver first and then inject a measured volume of butadiene gas into the liquid by means of a graduated syringe. With either procedure, the next step was to introduce a measured volume of  $N_2O_3$  or  $N_2O_4$  into the liquid with a graduated syringe. The following procedure was followed to minimize the amount of nitrogen oxide that escaped as vapor during this operation. The syringe tip (a polyethylene tube) was inserted into the liquid and a small portion of liquid was withdrawn into the partially filled syringe containing nitrogen oxide; this liquid vaporized and expelled the nitrogen oxide from the syringe. The operation was repeated several times to ensure that all of the nitrogen oxide was flushed into the receiver. (With ethylene, the temperature of the reaction mixture was about  $-105^\circ C$ ; with ethane, the temperature of the reaction mixture was about  $-90^\circ C$ .) After 15 minutes in the receiver, the mixture was placed in a loosely covered vessel and left to stand until the liquid evaporated (about 1 hour).

For colorimetric examinations, the gums remaining after evaporation of the reaction mixtures were weighed and then dissolved in 20 milliliters (ml) of a 1 percent aqueous solution of sodium hydroxide. The solutions were allowed to stand 20 to 30 minutes for color development, and the spectral absorbance was then measured at a wavelength of 425 millimicrons on a Beckman Model DU spectrophotometer. With some solutions, the optical densities were too high to be measured and dilution with known amounts of additional caustic was necessary.

For infrared measurement, the gum residue was mounted on a sodium chloride plate immediately after it was isolated, and its spectrum from 2 to 15 microns was obtained. Infrared measurements were also repeated after the gum residues had been stored for varying numbers of days on the plates.

For determination of the nitrogen content of a gum residue, the gum was first allowed to stand overnight. On the following day, the weight of the gum was determined and the gum was dissolved by adding dilute (1%) aqueous sodium hydroxide to the vessel. The gum in the caustic solution was then reduced with Devarda's metal and subsequently analyzed for nitrogen by the Kjeldahl method.

### Results and Discussion

Gums were formed rapidly when  $N_2O_3$  and either butadiene or cyclopentadiene were introduced into liquid ethylene; however, the

yields of gum varied considerably with differences in the mole ratio of  $N_2O_3$  to butadiene. In fact, difficulties were encountered in reproducing the yield of gum with any particular mole ratio of reactants. Variations were most noticeable with the reaction mixtures prepared with butadiene. Because of such variations, the reaction mixtures in which this compound had been introduced were divided into aliquots so that multiple determinations of the gum content could be made. The variability in the yield of gum might be explained if the initial products formed from the reactants can either evaporate or polymerize into the non-volatile gum.

In an attempt to develop a method for quantitative determination of the gums, aqueous sodium hydroxide solutions of gums were prepared and examined spectrophotometrically. The absorbance of light of 425-millimicron wavelength (selected from an examination of the absorption spectra of such solutions) was found to be roughly proportional to the concentration of the gum, Figure 1. As the ratio of nitrogen oxide to diene was increased, however, the slopes of the Beer's law plots shifted markedly and irregularly, Figures 1 and 2. The technique therefore could not be used to estimate gum concentrations.

Significantly more gum was obtained from cyclopentadiene than from butadiene. For example, at a ratio of about 0.75 moles of  $N_2O_3$  per mole of diene (in liquid ethylene) cyclopentadiene yielded about 0.5 grams of gum per gram of diene whereas butadiene yielded only about 0.1 grams. One possible reason for this difference may be that the products of the reaction with cyclopentadiene are less volatile and tend to remain as residue upon evaporation of the ethylene.

As shown in Figure 3, air appeared to retard the gum formation when  $N_2O_3$  and cyclopentadiene were introduced into liquid ethylene, since greater yields of gum were obtained when air was excluded from the reaction mixtures. It may be that air oxidizes the  $N_2O_3$  to  $N_2O_4$ , which is less reactive as a gum former.

#### Participation of Ethylene in Gum Formation

Under the conditions of the described tests, no gums were formed when only  $N_2O_3$  was added to liquid ethylene. Nevertheless, ethylene was found to take part in the gum formation when both  $N_2O_3$  and cyclopentadiene were introduced into liquid ethylene.

When the amount of  $N_2O_3$  charged was in considerable excess of the amount of cyclopentadiene, the yield of gum was considerably greater than the amount of cyclopentadiene charged, Figure 4. The nitrogen content of such gums was only 6.7 to 7.8 percent, however, indicating that  $N_2O_3$  did not comprise the major portion of the gum. It was therefore apparent that the gum contained ethylene, and because of the participation of ethylene, the yields of gum were not limited by the amounts of dienes available.

Because ethane was not expected to react with the gum-formers

at the temperatures employed (about  $-100^{\circ}\text{C}$ ), several tests were made in which the nitrogen oxide and diene were mixed with liquid ethane instead of liquid ethylene. Comparison of the results of these tests with the results obtained with ethylene gave further evidence that ethylene participated in gum formation.

Plots of the yields of gum per gram of cyclopentadiene charged against the starting reactant ratios are shown in Figure 5. In liquid ethane, the highest yield of gum per gram of cyclopentadiene was obtained when near equimolecular amounts of  $\text{N}_2\text{O}_3$  and cyclopentadiene were used, and in contrast to the results obtained with liquid ethylene, the yield of gum per gram of cyclopentadiene subsequently decreased as the proportion of cyclopentadiene charged was decreased. Thus, the divergence of the curves for the gum yields per gram of cyclopentadiene in the two liquids indicates that ethylene was incorporated in the gum. As illustrated by the curves presented in Figure 6, the gum yields per gram of  $\text{N}_2\text{O}_3$  charged also appeared to differ somewhat in the two media.

#### Gum Formation From the Addition of $\text{N}_2\text{O}_4$ and Cyclopentadiene to Liquid Ethylene

Gums were also formed when  $\text{N}_2\text{O}_4$  and cyclopentadiene were added to liquid ethylene, Figure 7. The gum-forming reaction was similar to that obtained with  $\text{N}_2\text{O}_3$  in that gum of about the same nitrogen content was produced and at least some and probably all, of the gums contained ethylene; however, the gum yields were somewhat smaller.

The gum produced from  $\text{N}_2\text{O}_4$  and cyclopentadiene in ethylene contained 5.8 to 7.1 weight percent nitrogen, which was about the same as for the gums produced from  $\text{N}_2\text{O}_3$  and cyclopentadiene in ethylene (6.7 to 7.8 wt %). That the gum formed from  $\text{N}_2\text{O}_4$  contained ethylene was evident from the fact that the yields of gum at the higher  $\text{N}_2\text{O}_4$ -to-cyclopentadiene ratios tested were unusually high for the amounts of cyclopentadiene charged and, as shown by the nitrogen content of the gums, these unusually high yields could not be accounted for by the proportion of  $\text{N}_2\text{O}_4$  incorporated in the gum. Regardless of the ratios of  $\text{N}_2\text{O}_4$  to cyclopentadiene, the gums all contained about the same percentage of nitrogen.

The gum yields with  $\text{N}_2\text{O}_4$  were somewhat less than with  $\text{N}_2\text{O}_3$ , as indicated by experiments in which gums were produced with the two nitrogen oxides by procedures made as identical as possible. By starting with 1.5 moles of the nitrogen oxide per mole of cyclopentadiene, the yield of gum per gram of cyclopentadiene was about 1.5 grams with  $\text{N}_2\text{O}_3$  and about 1.2 grams with  $\text{N}_2\text{O}_4$ .

#### Infrared Examination of Gums

Infrared spectra were obtained for 13 samples of gum produced

by mixing cyclopentadiene and  $N_2O_3$  with liquid ethylene. That the spectra are those of a highly unstable gum was confirmed when one of the freshly isolated samples "fumed-off" after it was placed on a sodium chloride plate for infrared examination. Typical spectra are shown in Figures 8, 9, and 10 for gums produced from  $N_2O_3$ -to-cyclopentadiene mole ratios of 0.52, 2.3, and 7.7, respectively.

In the spectra of the gum, characteristic absorptions were noted for several groups of atoms. Evidence of the following groups was obtained in all gum samples:

- (1) -OH or -NH (possibly representing hydrogen bonding).
- (2) -CH (merely indicating carbon-hydrogen linkages in general).
- (3) C=O (shifted in concentration and structure during storage of samples).
- (4) -ONO<sub>2</sub> (definitely organic nitrate).
- (5) -CNO<sub>2</sub> (organic nitro groups).
- (6) NaNO<sub>3</sub>.

The same identifications were also made in samples prepared by passing  $N_2O_3$  through cyclopentadiene in the absence of ethylene; however, the residue from the evaporation of ethylene treated with  $N_2O_3$  in the absence of cyclopentadiene showed only the NaNO<sub>3</sub> absorption. NaNO<sub>3</sub> is probably present in all of the samples because of a reaction of nitrogen oxides with the salt plate in the presence of moisture.

The functional groups whose presence was detected (carbonyl, nitro, and nitrate) or suspected (hydroxyl) in the gum were among those found by Levy and co-workers<sup>5)</sup> in the products of the reaction of  $N_2O_3$  and  $N_2O_4$  with simple olefins at 0 C. According to Levy, when  $N_2O_3$  and an unsaturated compound are reacted, the primary reaction is a simple addition to yield products (usually several) containing nitro (-NO<sub>2</sub>), nitrite (-ONO), and nitroso (-NO) groups. Products containing nitrite and nitroso groups are seldom isolated, apparently because of their instability (if isolated from solution they usually explode) and ensuing secondary reactions. Nitrite groups are frequently oxidized by  $N_2O_4$  to nitrate groups; however, they may also be hydrolyzed (for example, by water produced by oxidation) to produce hydroxyl groups and nitric or nitrous acid. The fate of nitroso groups is not known. Carbonyl groups might be expected to result from the nitrogen oxide oxidation of carbons having nitro groups.

\* \* \*

In summary, the experimental investigations have confirmed that nitrogenous gums are formed when  $N_2O_3$  or  $N_2O_4$  and cyclopentadiene or butadiene are introduced into liquid ethylene. Indications were obtained that ethylene is readily incorporated in the gum. Some of the reaction products are apparently volatile; however, other material formed remains as a gummy residue when the solvent ethylene is evaporated. Whereas the yields of gum per unit weight of diene increase

with an increase in the ratio of  $N_2O_3$  to diene, the nitrogen content of the gum prepared from  $N_2O_3$  and cyclopentadiene in ethylene was 5.8 to 7.1 weight percent, regardless of the starting reactant ratio. Furthermore, the yields were not limited by the amount of diene present but only by the amount of nitrogen oxide available. The yields of gum residue were greater with cyclopentadiene than with butadiene and the yields appeared to be favored by the absence of air. It may be that air oxidizes  $N_2O_3$  to  $N_2O_4$ , which is less reactive as a gum former. Infrared studies have shown what functional groups are present in the gum, and the spectra obtained should be useful as references in examining materials formed under similar conditions.

#### Acknowledgement

The authors wish to acknowledge the assistance of A. J. Miskalis, who measured and interpreted the infrared spectra of the gum samples, R. W. Baudoux, who determined their nitrogen content, and Dr. M. H. Wilt, for helpful suggestions during the work and for reviewing the manuscript.

#### References

1. F. Rottmayr, Linde Berichte aus Technik und Wissenschaft, No. 7 (1959).
2. N. V. Sidgwick, The Organic Chemistry of Nitrogen, Clarendon Press, Oxford, 1949, p. 213.
3. J. F. Brown, Jr., J. Am. Chem. Soc., 79, 2480 (1957).
4. Whytelaw-Gray, Gas Journal, November 11, 1936, p. 465.
5. N. Levy, et al., J. Chem. Soc. (London), 1946, 1093-1104.

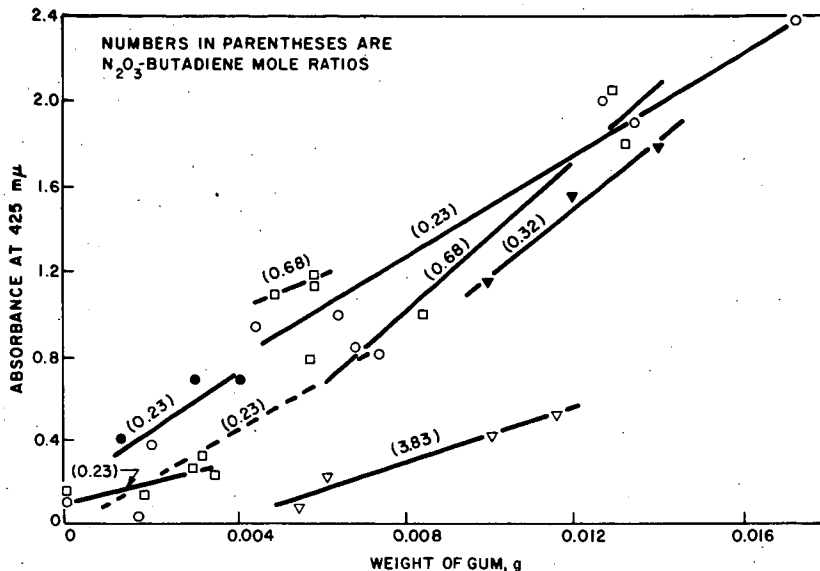


Fig. 1.-SPECTRAL ABSORBENCE OF CAUSTIC SOLUTIONS OF GUMS PREPARED FROM NITROGEN TRIOXIDE AND BUTADIENE IN LIQUID ETHYLENE

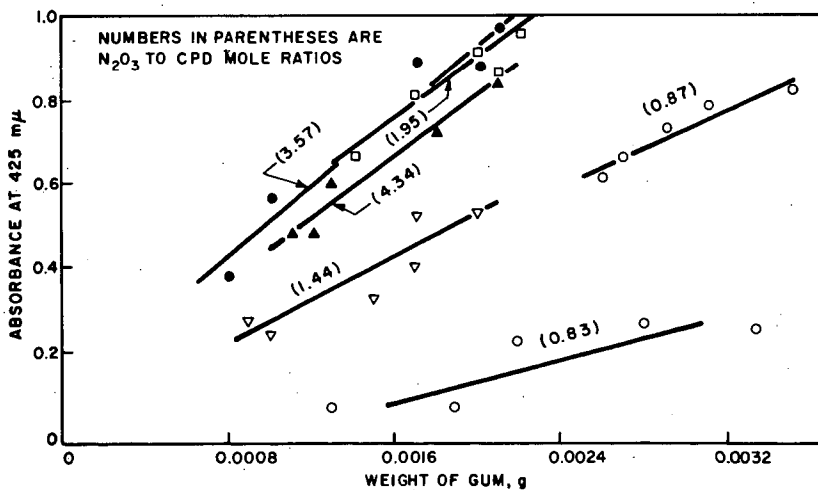


Fig. 2.-SPECTRAL ABSORBENCE OF CAUSTIC SOLUTIONS OF GUMS PREPARED FROM CYCLOPENTADIENE AND  $N_2O_3$  IN ETHYLENE

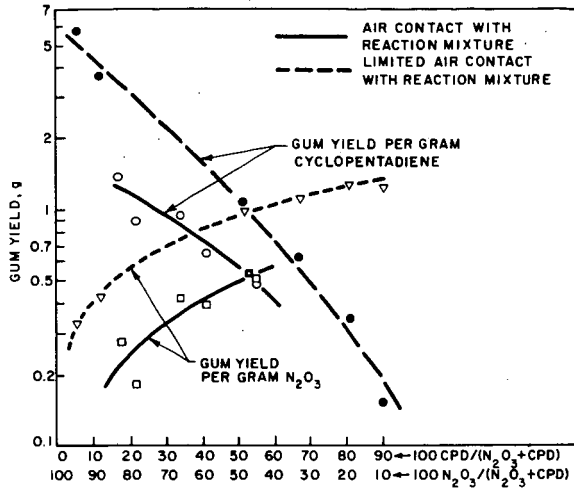


Fig. 3.-YIELDS OF GUM FROM DIFFERENT N<sub>2</sub>O<sub>3</sub> TO CYCLOPENTADIENE RATIOS (IN LIQUID ETHYLENE)

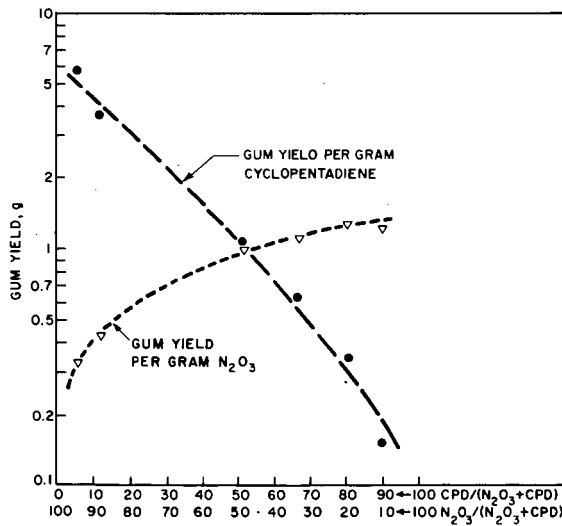


Fig. 4.-YIELDS OF GUM FROM DIFFERENT N<sub>2</sub>O<sub>3</sub> TO CYCLOPENTADIENE RATIOS (IN LIQUID ETHYLENE)

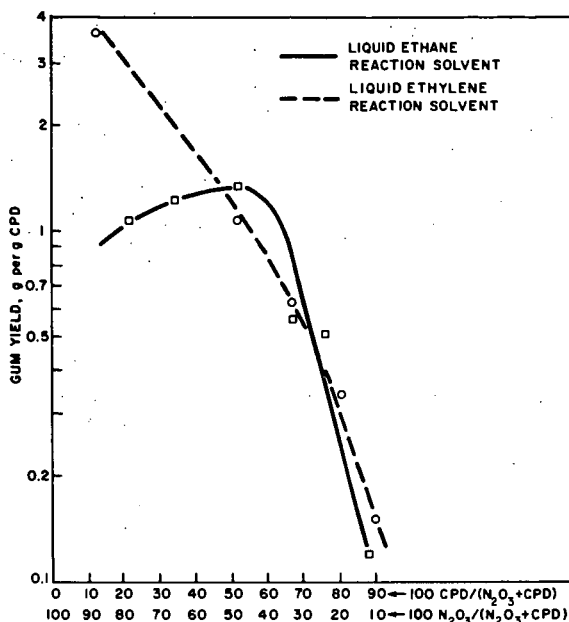


Fig. 5.-YIELDS OF GUM FROM DIFFERENT  $N_2O_3$  TO CYCLOPENTADIENE RATIOS

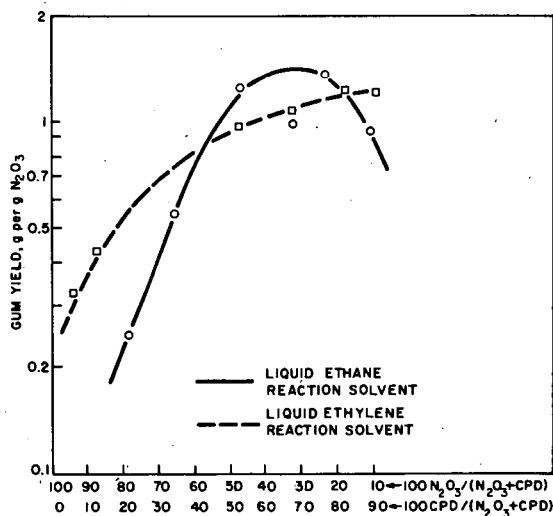


Fig. 6.-YIELDS OF GUM FROM DIFFERENT  $N_2O_3$  TO CYCLOPENTADIENE RATIOS

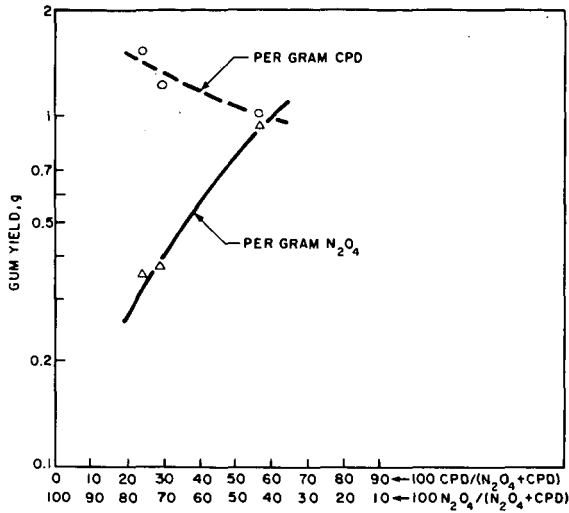


Fig. 7.-YIELDS OF GUM FROM DIFFERENT N<sub>2</sub>O<sub>4</sub> TO CYCLOPENTADIENE RATIOS

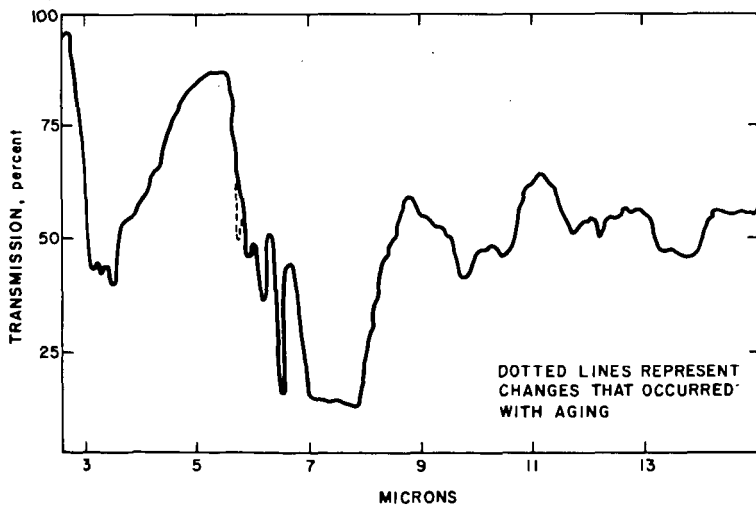


Fig. 8.-INFRARED SPECTRUM OF GUM PRODUCED FROM THE REACTION OF N<sub>2</sub>O<sub>3</sub> AND CYCLOPENTADIENE IN ETHYLENE (0.52 MOLE N<sub>2</sub>O<sub>3</sub> PER MOLE OF CYCLOPENTADIENE)

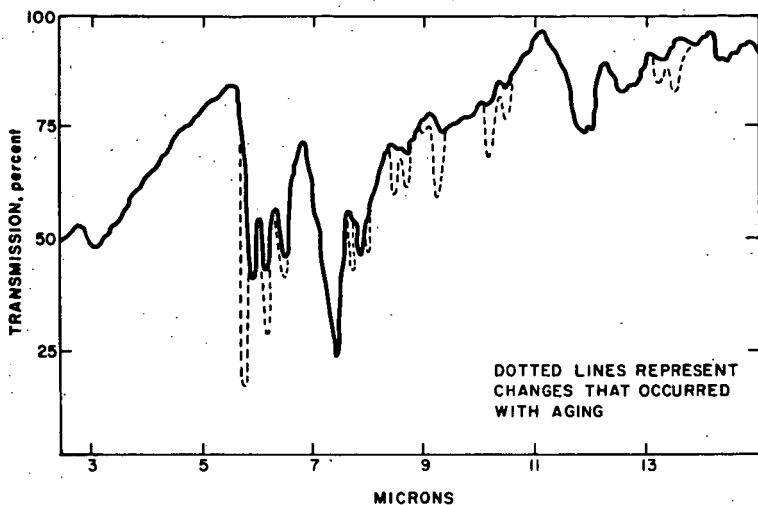


Fig. 9.-INFRARED SPECTRUM OF GUM PRODUCED FROM THE REACTION OF  $N_2O_3$  AND CYCLOPENTADIENE IN ETHYLENE (2.30 MOLES  $N_2O_3$  PER MOLE OF CYCLOPENTADIENE)

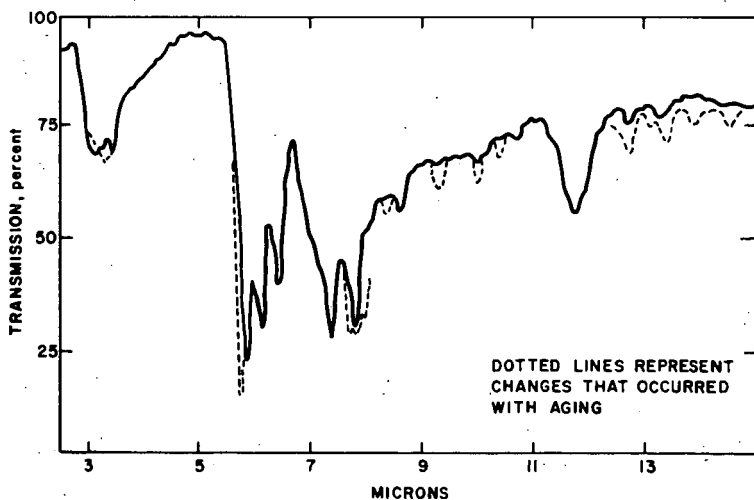


Fig. 10.-INFRARED SPECTRUM OF GUM PRODUCED FROM THE REACTION OF  $N_2O_3$  AND CYCLOPENTADIENE IN ETHYLENE (7.73 MOLES  $N_2O_3$  PER MOLE OF CYCLOPENTADIENE)

## HOT GAS IGNITION TEMPERATURES OF HYDROCARBON FUEL VAPOR-AIR MIXTURES

Ralph J. Cato, and Joseph M. Kuchta

Explosives Research Center, Bureau of Mines  
U.S. Department of the Interior, Pittsburgh, Pa.

### ABSTRACT

Laminar hot air jets of 1/4 to 3/4-inch diameter were employed to determine the hot gas ignition temperatures of various combustible vapor-air mixtures. The combustibles were n-hexane, n-octane, n-decane, a hydrocarbon jet fuel (JP-6) and an adipate ester aircraft engine oil (MIL-L-7808). Minimum ignition temperatures occurred at a fuel-air weight ratio of about 0.5 and were not greatly sensitive to variations of fuel concentration. Moderate variations of jet velocity also had little influence on these ignition temperatures. However, these temperatures decreased with an increase in heat source dimensions (jet diameter) similar to that observed in the hot surface ignition of the hydrocarbon combustibles. Furthermore, it was noted that the hot gas ignition temperatures of the combustibles tended to approximate corresponding auto-ignition and wire ignition temperatures when the size of the heat source and the ignition criterion were the same. Temperature profiles obtained for 1/2-inch diameter hot air jets indicated that the jet temperatures required to produce "hot" flame ignitions and luminous or "cool" flame reactions with these combustibles are of greater significance than the corresponding heat flux values.

### INTRODUCTION

Most of the ignition temperature data available for combustible fluids have been obtained using heated vessels, wires, or tubes as the sources of ignition. A jet of heated air or other gas, if sufficiently hot, can also produce ignition when it comes into contact with combustible gases or vapors. Such an ignition source may be a problem during the rupture of an oil seal in a jet engine or during blasting operations in a coal mine where hot gases are released from the explosives employed. The temperatures at which combustible gas mixtures can be ignited by laminar jets of hot air and inert gases have been determined only in recent years by Wolfhard and others (5,6,7) for hydrogen, carbon monoxide, and various low molecular weight hydrocarbons. The present work was conducted to investigate the hot gas (air) ignition temperature characteristics of several high molecular weight hydrocarbon combustibles mixed with air.

Hot gas ignitions differ from wire ignitions and autoignitions in heated vessels primarily in that surface effects are absent with a hot gas heat source, providing the reaction chamber is relatively large. The hot gas ignition temperatures of hydrocarbon combustible mixtures have been reported to agree generally with corresponding wire ignition temperatures but to be much higher than the autoignition temperatures (AIT's) of the mixtures (7). However, according to our hot surface ignition studies (2) and to the preliminary findings of the present study (3) which are included here, the variation between such ignition temperatures can depend greatly on the size of the heat source and on the ignition criterion used. The hot gas ignition temperature data of this work were obtained with laminar jets of hot air injected into combustible vapor-air mixtures under near-stagnant flow conditions. Data are included on the effects of combustible concentration, jet diameter, and jet velocity for a given size of reaction chamber. Since a relatively stable luminous jet is ordinarily observed prior to these ignitions, temperature profiles of the jets were obtained to compare the heat requirements for the initial luminous or "cool" flame reactions and the

subsequent "hot" flame ignitions with each combustible. The combustibles included n-hexane, n-octane, n-decane, a hydrocarbon jet fuel (JP-6), and an adipate ester aircraft engine oil (MIL-L-7808).

#### EXPERIMENTAL APPARATUS AND PROCEDURES

The apparatus used for the hot gas ignition temperature determinations is shown in figure 1 and, except for some minor modifications, is similar to that employed by Wolfhard (7). Basically, the apparatus consisted of a tubular ceramic furnace that was used to heat the air stream, a cylindrical reaction chamber into which was fed the hot air jet and the combustible vapor-air mixture, and the feed assemblies that provided the desired mixture at a uniform rate. The tubular furnace was wound externally with platinum-rhodium wire and was enclosed in a cylindrical Nichrome\*-wound furnace (3-inch ID). The reaction chamber consisted of a 4-inch diameter Pyrex pipe (26 inches long) that was also heated to maintain the combustible mixture at a given temperature. Narrow slits were located on both sides of the enclosed pipe along its longitudinal axis to permit visual observation of flame propagation. The combustible mixture was fed to the reaction chamber through a "mixing ring" (perforated coil of tubing) located just below the base of the hot jet; a water jacket between the ring and the ceramic tubular furnace helped maintain the mixture at a uniform initial temperature.

The temperatures of the hot air jets were measured with a 33-B&S gage platinum/platinum-10 percent rhodium thermocouple at a point of about 1/4 inch above the jet base; the temperature decreased progressively with the height above the jet base at a rate that was determined in part by the jet diameter and velocity. The temperatures of the combustible mixtures were measured with three thermocouples spaced 3 inches apart as shown in figure 1; recorded temperature differences were usually not in excess of  $\pm 25^\circ$ . A mixture temperature of  $600^\circ$  F was used for the engine oil which contained higher boiling point constituents than did the fuels. The mixture flow rate was  $365 \text{ in}^3/\text{min}$  ( $\sim 1 \text{ in}/\text{sec}$ ), and the jet flow rate was  $185 \text{ in}^3/\text{min}$  ( $\geq 50 \text{ in}/\text{sec}$ ), both at N.T.P. conditions, in the experiments with 1/4, 3/8, and 1/2-inch diameter jets; a jet flow rate of  $365 \text{ in}^3/\text{min}$  ( $\sim 50 \text{ in}/\text{sec}$ ) was used with a 3/4-inch size jet. These jet flow rates were used since they appeared to be optimum for ignition of the mixtures in the 4-inch diameter reaction chamber.

To conduct an experiment, the temperatures of the hot air jet and ambient atmosphere in the reaction chamber were measured initially. The thermocouples were then removed and the combustible mixture was introduced, flowing coaxially with the hot jet. If ignition did not occur, the jet temperature was increased in successive increments until ignition was evidenced by the propagation of flame throughout the combustible mixture. Normally, a small precursor flame or luminous column was faintly visible above the base of the jet prior to ignition (figure 2); this flame extended to a height of 6 inches or less above the jet base and resembled a pale blue "cool" flame. Fuel residence time and fuel-air ratio were also varied to obtain the minimum ignition temperatures with each size of hot air jet. Generally, ignitions occurred in 10 to 60 seconds, although a few took place after as much as 180 seconds from the time the combustible mixture was admitted. The minimum ignition temperature values were repeatable to within  $\pm 25^\circ$ .

Temperature profiles of 1/2-inch diameter jets of hot air were determined with the jets flowing into preheated air and into preheated combustible vapor-air mixtures. For this purpose, the cylindrical reaction chamber was equipped with a probe which

\* Reference to trade names is for information only and endorsement by the Bureau of Mines is not implied.

could be adjusted to make axial and radial temperature measurements at various heights within the hot gas jet. Adjustment of the temperature probe was made by rotating a micrometer in contact with a movable plate supporting the probe. The thermocouple bead of this probe was made with 36-gage platinum/platinum-rhodium wire and was coated with a ceramic material recommended by the Bureau of Standards; addition of the coating resulted in slightly lower ( $\leq 25^\circ$ ) jet temperatures. In making these measurements, jet base temperatures were selected to produce the initial luminous reactions and the subsequent "hot" flame ignitions under the given flow conditions. However, the ignition reactions were usually quenched when the temperature probe was inserted at a distance between 0 and 4 inches above the jet base; under such conditions, ignitions were obtained only when the probe was positioned at distances in excess of about 4 inches above the base of the jet.

All of the neat hydrocarbon fuels used in this work were of chemically pure grade, at least 99 percent pure. The MIL-L-7808 engine oil consisted primarily of adipate diesters which vaporized at temperatures between  $480^\circ$  and  $780^\circ$  F; its flash point was  $435^\circ$  F. The JP-6 jet fuel contained about 85 percent saturated hydrocarbons and 14 percent aromatic hydrocarbons; its flash point was  $100^\circ$  F.

## RESULTS AND DISCUSSION

### Hot Gas Ignition Temperatures

The temperature required to ignite a combustible vapor-air mixture with a jet of hot gas depends on the dimensions of the jet as well as on the composition and velocity of the jet and combustible mixture. Since jets of hot air were used in the present work, the combustible vapor-air mixture was diluted by the air jet, particularly along the interface between the two moving fluids. Accordingly, relatively high fuel concentrations and low jet flow rates should be the most optimum for ignition; low flow rates provide low air dilution rates and long contact times with the combustible which are highly favorable for ignition. The results presented here for n-hexane, n-octane, n-decane, JP-6 jet fuel, and MIL-L-7808 engine oil vapor-air mixtures were consistent in this connection.

Figure 3 shows the variation of the hot gas ignition temperatures with fuel-air weight ratio (F/A) employing 1/2-inch diameter air jets flowing concurrently into the combustible vapor-air mixtures; jet flow rate was  $185 \text{ in}^3/\text{min}$ , and the mixture flow rate was  $365 \text{ in}^3/\text{min}$ . As in hot surface ignition temperature determinations (2), the effect of F/A ratio is seen to be slight except at low ratio values ( $\sim 0.30$ ) where the ignition temperatures tend to increase noticeably as the F/A ratio is decreased. Similar behavior was also noted in the ignition temperature determinations made with 1/4, 3/8 and 3/4-inch diameter hot air jets; figure 4 shows the data obtained for n-decane with the various sized jets. Generally, a F/A ratio of approximately 0.5 was required to obtain the minimum temperatures for ignition. Since uniform mixtures of these combustibles in air usually would not be expected to propagate flame at such high F/A ratios, the observed behavior is probably attributed to the dilution of the mixtures and the elevation of the mixture temperatures ( $\geq 350^\circ$  F) by the hot air jet.

In the above experiments, with the 1/2-inch diameter jet the jet velocity was about  $50 \text{ in}/\text{sec}$  ( $185 \text{ in}^3/\text{min}$ ) and the mixture velocity  $1 \text{ in}/\text{sec}$  ( $365 \text{ in}^3/\text{min}$ ). Data obtained under other flow conditions are summarized in table 1 from experiments conducted with 1/2-inch diameter jets of hot air and MIL-L-7808 engine oil vapor-air mixtures. It is evident from these data that the influence of jet velocity on minimum ignition temperature was not great for the range of velocities used in these experiments; this behavior is consistent with that reported by other investigators (5). The ignition temperature increased only slightly when the jet velocity was varied from  $36.5$  to  $81.0 \text{ in}/\text{sec}$  with a constant mixture velocity of  $1.0 \text{ in}/\text{sec}$ . They also

increased slightly when the mixture velocity was varied between 0.7 and 1.5 in/sec; here, the jet velocity/mixture velocity ratio was maintained at a constant value slightly above 50. Although a jet velocity of approximately 50 in/sec was near optimum for ignition of the mixtures with 1/2-inch and 3/4-inch size jets, higher jet velocities were required with 1/4-inch and 3/8-inch diameter jets to provide ideal heat inputs for ignition.

TABLE 1. - Effect of jet and mixture velocity on the minimum hot gas ignition temperature of MIL-L-7808 engine oil with a 1/2-inch diameter hot air jet.  
Fuel-air Weight Ratio - 0.55

Jet Velocity/ Mixture Velocity Ratio	36.5	52.1	52.5	52.7	54.7	81.0
Mixture Velocity, in/sec	1.0	0.7	1.0	1.3	1.5	1.0
Ignition Temperature, °F	1240	1255	1250	1270	1315	1300

Table 2 lists the minimum hot gas ignition temperatures obtained for the hydrocarbon fuel and engine oil vapor-air mixtures with the 1/4, 3/8, 1/2 and 3/4-inch diameter jets of hot air. These data are also shown graphically in figure 5 where the minimum ignition temperature values are plotted against the reciprocal of jet diameter (1/d); a similar plot including hot surface ignition temperatures is shown for the data found with n-decane vapor-air mixtures in figure 6, which is discussed later. As expected, the ignition temperatures of these combustibles decreased consistently as the heat source diameter was increased. However, for n-octane, the decrease was only 30° in varying the jet diameter from 1/2-inch to 3/4-inch. The use of larger size jets was not investigated because dilution effects could be great for the size of reaction chamber employed. For a given jet diameter, the ignition temperature values for the paraffin hydrocarbons increased only slightly with decreasing molecular weight. Also, the values for the JP-6 fuel tend to be the highest, and those for the MIL-L-7808 engine oil tend to be the lowest for jet diameters ≤ 0.5-inch. These results are unusual since the engine oil is a high AIT (~750° F) combustible, whereas the jet fuel is a low AIT (~450° F) combustible like the above paraffin hydrocarbons. However, the trend is consistent with that observed for these materials in autoignition and wire ignition temperature determinations with varying heat source diameters (2). Since the thermal stability of the combustibles at the pertinent temperatures may account for such observations, decomposition studies would be interesting to pursue, particularly with the adipate diesters which largely make up the engine oil.

TABLE 2. - Minimum hot gas ignition temperatures of the hydrocarbon fuels and engine oil (fuel vapor-air mixtures) with various hot air jets.  
Mixture Flow Rate - 365 in<sup>3</sup>/min (N.T.P.)  
Fuel-air Weight Ratio - Optimum for ignition (~ 0.5)

Diameter of Jet, inch	Jet Flow Rate, in <sup>3</sup> /min	Ignition Temperature, °F				
		n-Hexane	n-Octane	n-Decane	JP-6	Engine Oil MIL-L-7808
1/4	185	1630	1610	1600	1670	1530
3/8	185	1450	1440	1440	1500	1410
1/2	185	1280	1250	1220	1410	1250
3/4	365	1210	1220	1170	1290	1210

### Comparison of Hot Gas and Hot Surface Ignition Temperatures

A comparison was made of the autoignition, wire ignition, and hot gas ignition temperatures of various paraffin hydrocarbon and JP-6 fuel vapor-air mixtures for cylindrical heat sources of about 0.4-inch diameter. Figure 7 shows the variation of these ignition temperatures with the number of carbon atoms present in each combustible; 12 carbon atoms were assumed for JP-6. The hot gas ignition data for the low molecular weight hydrocarbons are those of Vanpee and Wolfhard (6). They were obtained by injecting hot air jets at 365 in<sup>3</sup>/min, as compared to 185 in<sup>3</sup>/min for the data from the present study, into pure fuel under near stagnant conditions ( $\sim 1$  in/sec). According to the data in table 1, the difference in jet flow rates should not be serious. The autoignition temperatures (2) were determined in a quiescent air atmosphere by injecting liquid fuel into a heated cylindrical Pyrex vessel, 6 inches long. The wire ignition temperatures (2) were also obtained under near stagnant conditions (0.15 in/sec) where the combustible mixture was passed over a heated Inconel wire (2 inches long) mounted perpendicular to the axis of flow. Fuel-air weight ratio (0.3-0.5) and fuel residence time (> 1 second) were optimum for ignition for the data shown.

It is seen in figure 7 that the ignition temperatures generally decrease with increasing number of carbon atoms or molecular weight of the combustible, although all of the data are not consistent. In addition, the hot gas ignition temperatures are about 200° higher than the corresponding wire ignition temperatures and at least 300° higher than the AIT's. Somewhat the same behavior is found in comparing these ignition temperatures at various heat source diameters. Figure 6 shows such a comparison for n-decane vapor-air mixtures. Here, the hot gas ignition temperatures again are the highest, and their variation with the reciprocal of heat source diameter (1/d) resembles most closely that displayed by the autoignition temperatures; the wire ignition temperatures tend to display the least variation for 1/d values greater than 2-inch<sup>-1</sup>. Such correlations may improve if the diameter as well as the length of the heat source are considered. The criterion of ignition is also important. For example, table 3 shows that luminous or "cool" flame reactions were observed at jet temperatures between 100° and 200° below those required for "hot" flame ignition. In the above correlations, the hot surface ignition temperatures referred to any visible flame whereas the hot gas ignition temperatures referred only to "hot" flame ignitions. Furthermore, the latter temperatures were measured near the jet base and were at least 200° higher than those at the plane where ignition occurred above the jet base (see table 3). Thus, the hot gas ignition temperatures of the given combustibles probably do not differ greatly from their hot surface ignition temperatures when the ignition criterion and the heat source dimensions are the same.

Considering that heterogeneous surface reactions are absent in hot gas ignitions, some variation probably exists between the hot gas and hot surface ignition temperatures of the given combustibles. At the same time, these hot gas ignition temperatures appear to vary somewhat the same as the autoignition or wire ignition temperatures with heat source diameter and with combustible concentration and composition. Even the anomalous hot gas ignition behavior displayed by the ethane and JP-6 fuels in figure 7 was also observed in the autoignition or wire ignition experiments. Apparently, the temperature dependency of the reactions controlling these hot gas and surface ignitions at atmospheric pressure did not vary greatly with the nature of the heat source.

Thermal Considerations of Hot Gas Ignition

Hot gas ignitions are unique in that the heat source is essentially free of surfaces and the pre-ignition reactions may be observed at relatively high temperatures and long duration (several seconds). Reaction kinetics involving hot gas ignitions of combustible mixtures may be studied by an analysis of rates of heat production within the hot jet (1,4,7). Such information should also be useful in the study of the heat requirements for the formation of "hot" and "cool" flames.

Thermal ignition of a combustible mixture by a hot gas jet should occur at a point in the jet stream where the heat generated by chemical reaction is greater than the heat lost from the system. If radial convection is assumed to be negligible and axial convection to be most important, the heat balance equation can be reduced to the following expression according to other investigators (1):

$$Q = \rho C_p v_y \left[ \frac{\partial T}{\partial y} - \left( \frac{\partial T}{\partial y} \right)_{Q=0} \right] \quad (1)$$

where Q is rate of heat release by chemical reaction,  $\rho$  is density of the gas jet,  $C_p$  is specific heat,  $v_y$  is axial velocity, and T is jet temperature. Since  $\rho C_p v_y$  varies slightly with temperature, the heat release can be determined by measuring the axial jet temperature profiles with combustible  $\left( \frac{\partial T}{\partial y} \right)_{Q=0}$  and without combustible present  $\left( \frac{\partial T}{\partial y} \right)_{Q=0}$ . Such measurements were made here with the 1/2-inch diameter hot air jet flowing into preheated air or preheated fuel vapor-air mixtures at 350° F; a mixture temperature of 600° F was used with the MIL-L-7808 engine oil. The jet flow rate was 185 in<sup>3</sup>/min, the mixture flow rate was 365 in<sup>3</sup>/min, and the fuel-air weight ratio was about 0.25. Since the low jet flow rate produced steep axial temperature gradients, the use of equation (1) was only applicable to low jet heights. Furthermore, the Q values which were determined here should be considered only as relative values because of experimental uncertainties.

The above measurements were made in the center of the hot air jet where the radial temperature gradient was minimum. Figure 8 shows that the radial temperature profiles for the 1/2-inch diameter air jet ( $T_{base} = 1265^\circ \text{ F}$ ) are reasonably symmetrical and are essentially flat up to a radial distance of about 0.05 inch for distances up to 2 inches above the jet base. In comparison, the corresponding axial temperature gradients are much greater because of the low jet flow rates employed here to obtain minimum ignition temperatures.

Figure 9 shows the axial temperature profiles obtained with preheated air and n-decane vapor-air mixtures at jet base temperatures of 1060° and 1265° F. At the lower temperature, heat evolution is not evident, and the curve describing the data with combustible present is below or coincides with the one found without combustible. Jet base temperatures in excess of 1060° F were required to form luminous reactions or "cool" flames. At 1265° F, the curve with combustible present is noticeably above the corresponding one without combustible at distances equal to and greater than 1-1/2 inches above the jet base. Here, a slight increase of jet temperature would be expected to overcome the thermal losses and produce "hot" flame ignition; a jet base temperature of about 1280° F produced ignition without the temperature probe present. Although sampling data of reaction products were incomplete, these data also indicated that the extent of reaction became noticeable at jet heights of about 1-1/2 inches for jet temperatures near critical for ignition. Similar axial temperature profiles were obtained with n-hexane, n-octane, JP-6 fuel, and MIL-L-7808 engine oil vapor-air

mixtures. In all cases, the temperature differences observed with and without combustible became significant at heights equal to or greater than about 1-1/2 inches above the jet base. Motion picture records of the ignition of n-octane vapor-air mixtures indicated that ignition of these mixtures occurs about 3 inches above the jet base with the 1/2-inch diameter jet at 1400° F (figure 10); the height at which ignition occurs can be expected to increase with decreasing temperature.

From the axial temperature profiles, the critical jet temperature and heat flux which may produce "hot" and "cool" flame reactions were determined for each of the combustibles. The reference temperature was taken at 1-1/2 inches above the jet base where initial reaction was noticeable; a higher level was avoided since the jet tended to be less coherent, in which case radial convection could be as important as axial convection. The gas velocity required in equation (1) was determined from photographs of dust particle tracks of dust entrained in the jet stream and illuminated at selected time intervals. A particle velocity of 73 in/sec was obtained near the center of the jet at distances between 1 and 2 inches above the jet base. In table 3, one observes significant differences between the temperatures which define the two ignition conditions for each combustible. However, the axial heat flux values ( $A_{Q=0}$ ) vary little since the terms  $\rho C_p v_y$  and  $T/y$  in equation (1) were not sensitive to moderate temperature changes. Thus temperature controls the hot gas ignitions to a greater extent than the rate of heat input; this behavior is not unusual for a heat source of relatively large diameter.

TABLE 3. - Critical temperature and heat flux for "cool" flame or luminous reactions and "hot" flame ignitions with 1/2-inch diameter hot air jet flowing into various combustible vapor-air mixtures.

Jet Flow Rate - 185 in<sup>3</sup>/min  
 Mixture Flow Rate - 365 in<sup>3</sup>/min  
 Fuel-air Weight Ratio - 0.25 to 0.30

Combustible	T <sub>base</sub> °F	T <sub>1</sub> <sup>1/</sup> °F	A <sub>Q=0</sub> × 100 Btu/in <sup>3</sup> -sec	T <sub>base</sub> °F	T <sub>2</sub> <sup>1/</sup> °F	A <sub>Q=0</sub> × 100 Btu/in <sup>3</sup> -sec	Q <sub>2</sub> <sup>2/</sup> Btu/in <sup>3</sup> -sec
n-Hexane	1350	1100	5.55	1455	1190	5.60	1.25
n-Octane	1150	900	5.35	1330	1085	5.50	1.25
n-Decane	1060	750	5.30	1265	1065	5.50	2.15
JP-6 Fuel	1265	1035	5.45	1415	1195	5.55	2.45
MIL-L-7808							
Engine Oil	1320	1130	5.55	1415	1155	5.55	0.60

1/ Jet temperatures above which "cool" (T<sub>1</sub>) and "hot" (T<sub>2</sub>) flame ignitions can occur; measured at 1-1/2 inches above jet base.

2/ Heat release determined from axial convection with and without combustible ( $A_{Q \neq 0} - A_{Q=0}$ ) at T<sub>2</sub>.

The rates of heat release (Q<sub>2</sub>) in table 3 correspond to temperature rises between 10° and 40° F which were observed at the jet height of 1-1/2 inches. If equation (1) is applicable, a temperature rise of about 160° to 180° F would be required to obtain a heat balance between the heat release rates and the axial convective heat losses (A) and thereby produce ignition. Indeed, temperature rises as high as about 140° have been observed in other similar experiments conducted at temperature conditions near optimum for ignition. Ordinarily, ignitions resulted before temperature rises of this magnitude were realized. Although such axial temperature measurements can be utilized to indicate the possibility of ignition, the use of equation (1) in this connection is more

applicable at relatively high jet flow rates which tend to produce uniform jets and small axial temperature gradients. Accordingly, similar data are presently being obtained at a jet flow rate of 365 in<sup>3</sup>/min to examine the reaction kinetics involved in the hot gas ignitions of the given combustibles.

#### CONCLUSIONS

The hot gas ignition temperatures of various hydrocarbon fuel and engine oil vapor-air mixtures decreased with increasing diameter of the hot air jet. These temperatures are not greatly dependent on fuel-air ratio and jet flow rate. They also do not differ greatly from hot surface ignition temperatures for comparable heat source diameters. The formation of "hot" flames and luminous reaction zones or "cool" flames in these hot gas ignitions appear to depend more on jet temperature than on rate of heat input.

#### REFERENCES

1. Bruszak, A. E., D. Burgess, and M. H. J. Wijnen, Reaction Kinetics in Hot Gas Ignition of Ethane Air. *Combustion and Flame*, v. 7, September 1963, p. 245.
2. Kuchta, J. M., A. Bartkowiak, and M. G. Zabetakis, Hot Surface Ignition Temperatures of Hydrocarbon Fuel Vapor-Air Mixtures. Presented at the 148th Meeting of American Chemical Society, Chicago, Ill., September 2, 1964.
3. Kuchta, J. M., R. J. Cato, and M. G. Zabetakis, Comparison of Hot Surface and Hot Gas Ignition Temperatures. *Combustion and Flame*, (Letter to Editor), v. 8, December 1964, p. 348.
4. Marble, F. E., and T. C. Adamson, Jr., Ignition and Combustion in a Laminar Mixing Zone. *Selected Combustion Problems*, v. 1, Butterworths Scientific, Inc., London, 1954, p. 111.
5. Vanpee, M., and A. E. Bruszak, The Ignition of Combustible Mixtures by Laminar Jets of Hot Gases. *BuMines Rept. of Inv. 6293*, 1963, 84 pp.
6. Vanpee, M., and H. G. Wolfhard, Comparison Between Hot Gas Ignition and Limit Flame Temperatures. *ARS Jour.*, v. 29, July 1959, p. 517.
7. Wolfhard, H. G., The Ignition of Combustible Mixtures by Hot Gases. *Jet Propulsion*, December 1958, p. 798.
8. Zabetakis, M. G., A. L. Furno, and G. W. Jones, Minimum Spontaneous Ignition Temperatures of Combustibles in Air. *Ind. and Eng. Chem.*, v. 46, October 1954, p. 2173.

This research was sponsored by the USAF Aero Propulsion Laboratory, Research and Technology Division, Wright-Patterson Air Force Base, under Delivery Order 33(657)-63-376, Task 304801.

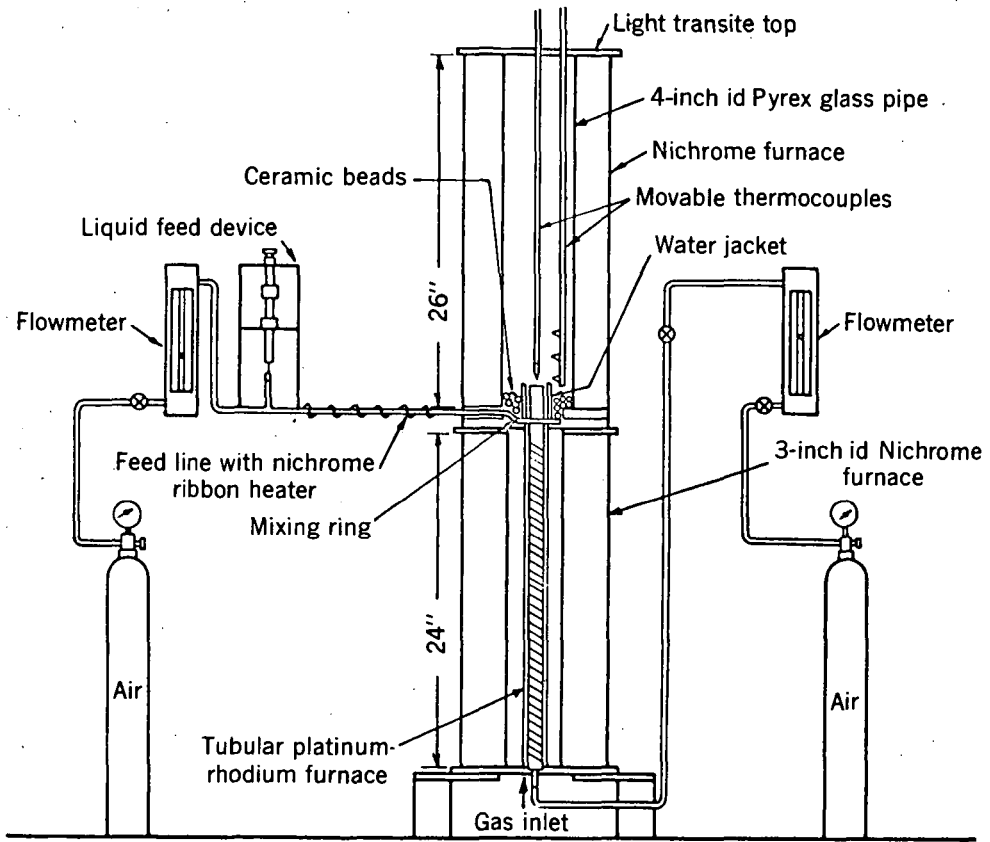


Figure 1. - Hot gas ignition temperature apparatus.

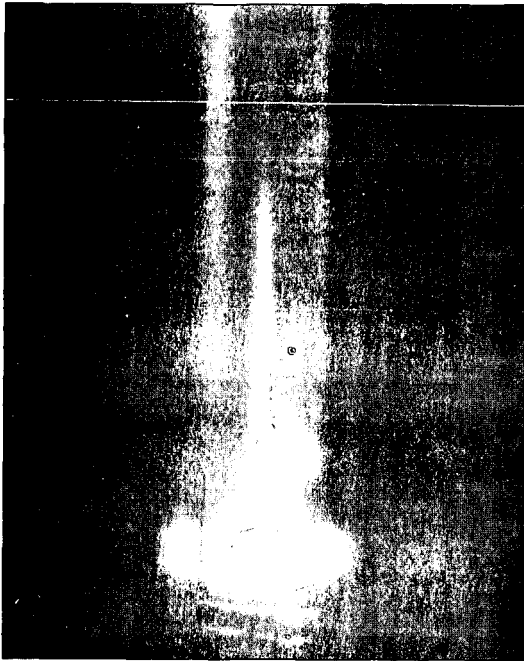


Figure 2. - Precursory flame formed in pre-ignition reaction of 1/4-inch diameter hot air jet (1670° F) with a uniform octane-vapor-air mixture at 350° F.  
Jet flow rate - 185 in<sup>3</sup>/min      Fuel-air weight ratio - 0.14  
Mixture flow rate - 365 in<sup>3</sup>/min      Scale: 1 inch = 0.935 inch

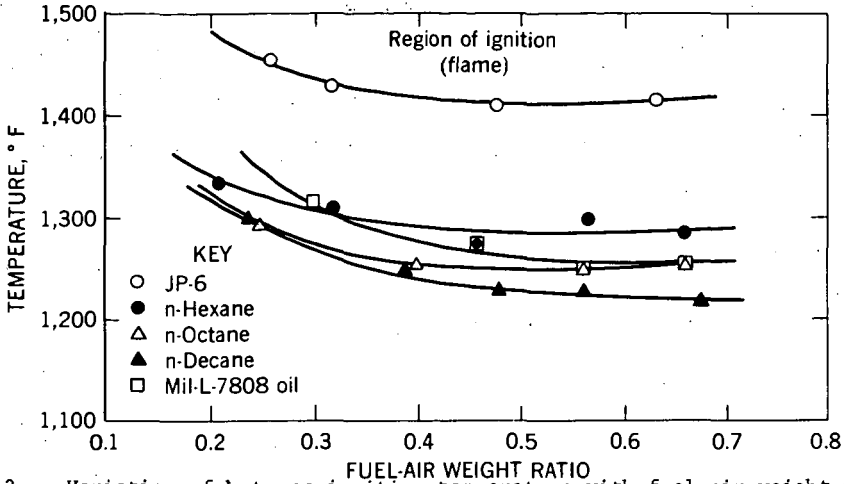


Figure 3. - Variation of hot gas ignition temperature with fuel-air weight ratio for various hydrocarbon combustible vapor-air mixtures with 1/2-inch diameter jets of hot air (Mixture flow rate - 365 in<sup>3</sup>/min).

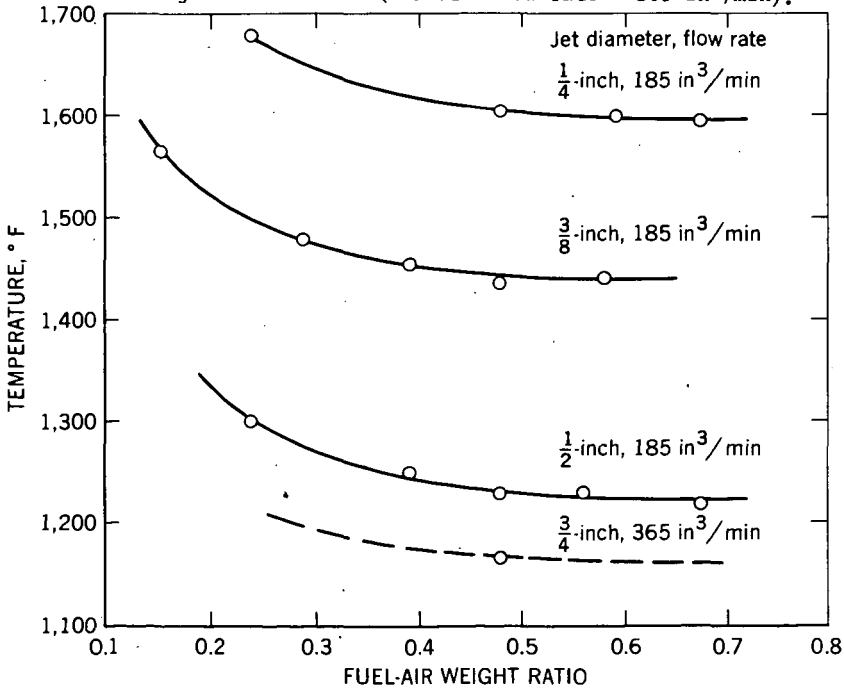


Figure 4. - Variation of hot gas ignition temperature with fuel-air weight ratio and diameter of hot air jet for n-decane vapor-air mixtures (Mixture flow rate 365 in<sup>3</sup>/min, N.T.P.)

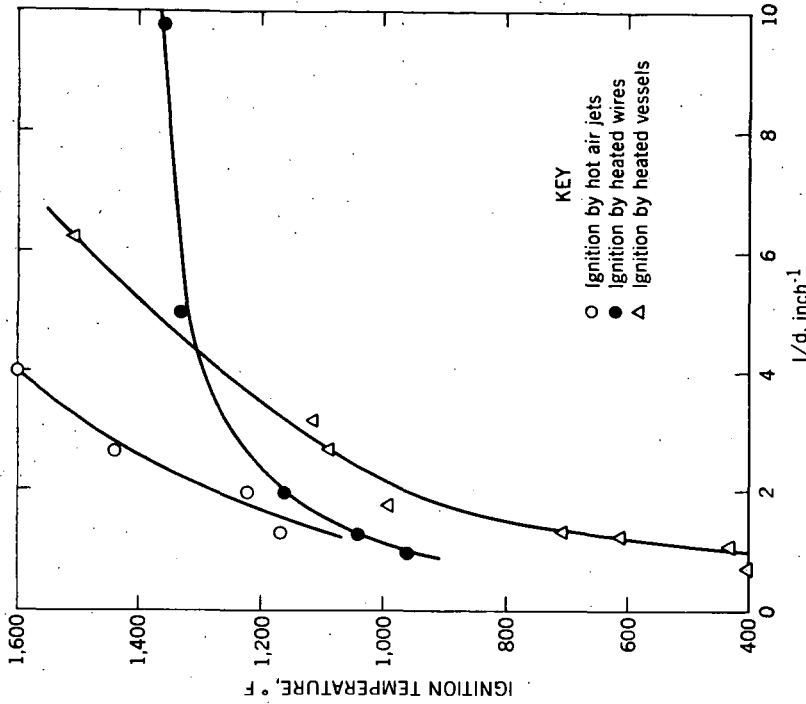


Figure 6. - Variation of hot gas and hot surface ignition temperatures with reciprocal diameter of heat source for n-decane vapor-air mixtures.

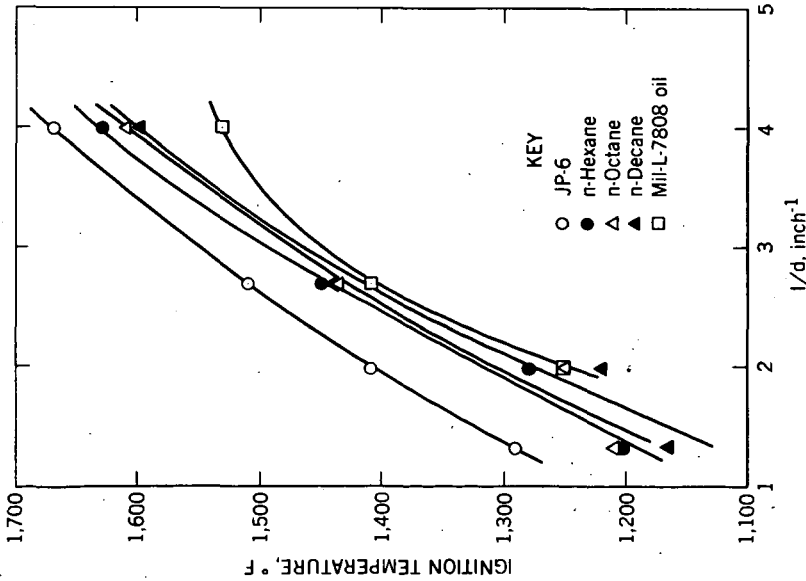


Figure 5. - Variation of hot gas ignition temperature with reciprocal diameter of hot air jet for various hydrocarbon combustible vapor-air mixtures (Flow conditions in figure 4 and table 2).

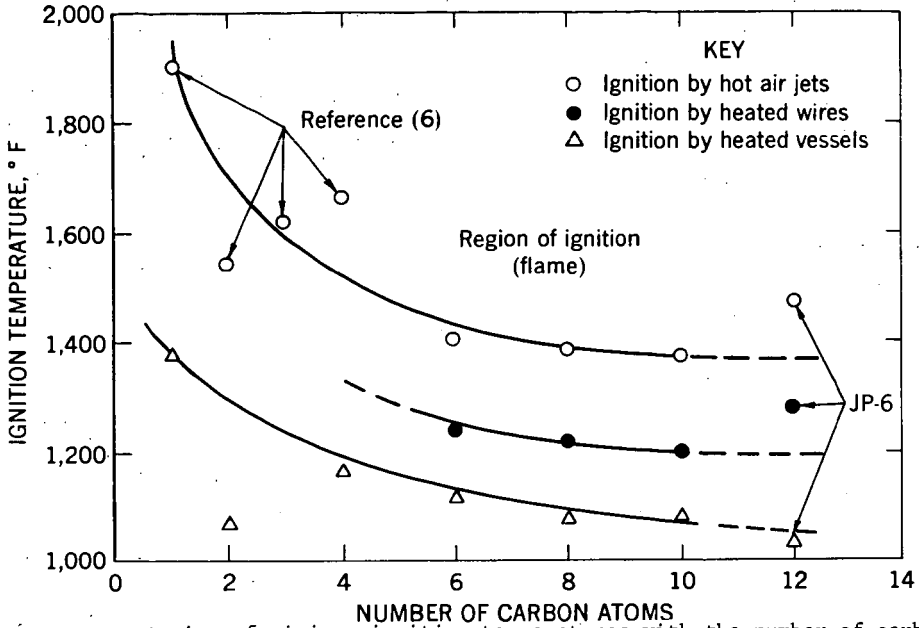


Figure 7. - Variation of minimum ignition temperatures with the number of carbon atoms for hydrocarbon (paraffin) and JP-6 vapor-air mixtures ignited with 0.4-inch diameter cylindrical heat sources.

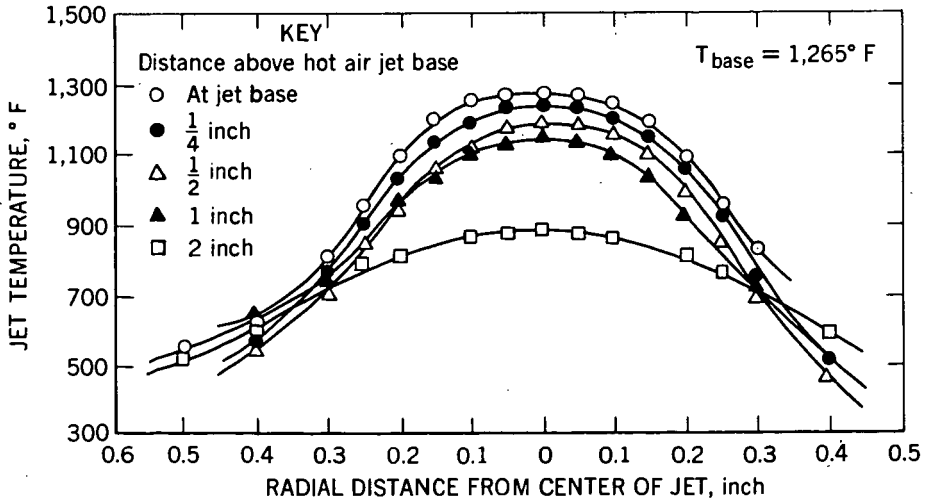


Figure 8. - Radial temperature profiles for 1/2-inch diameter jets of hot air flowing at  $185 \text{ in}^3/\text{min}$ , (N.T.P.) into preheated air at  $350^{\circ}F$ .

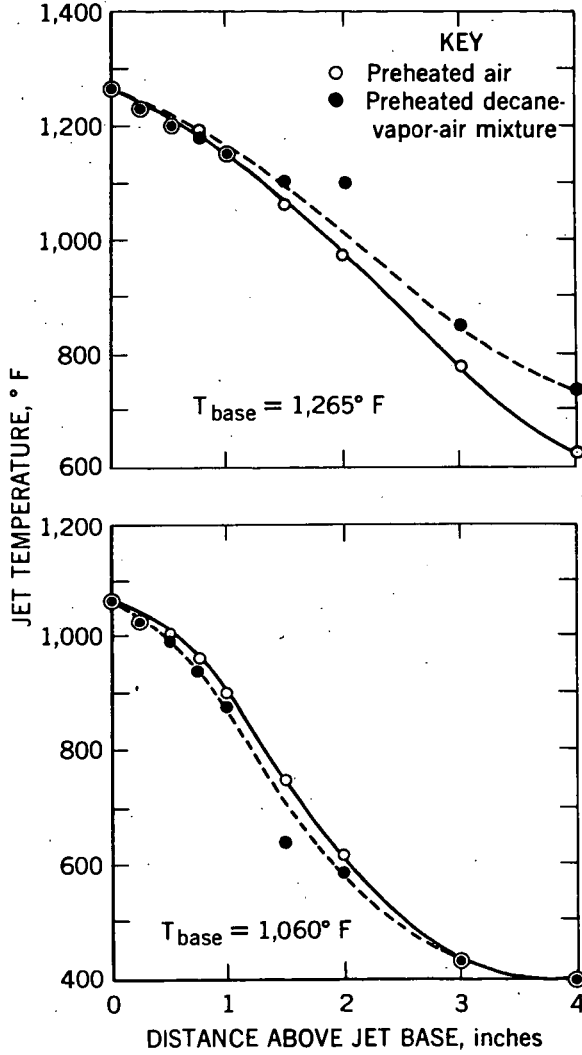


Figure 9. - Axial temperature profiles for 1/2-inch diameter jets of hot air flowing at 185 in /min, (N.T.P.) into preheated air and n-decane vapor-air mixtures at 350° F.

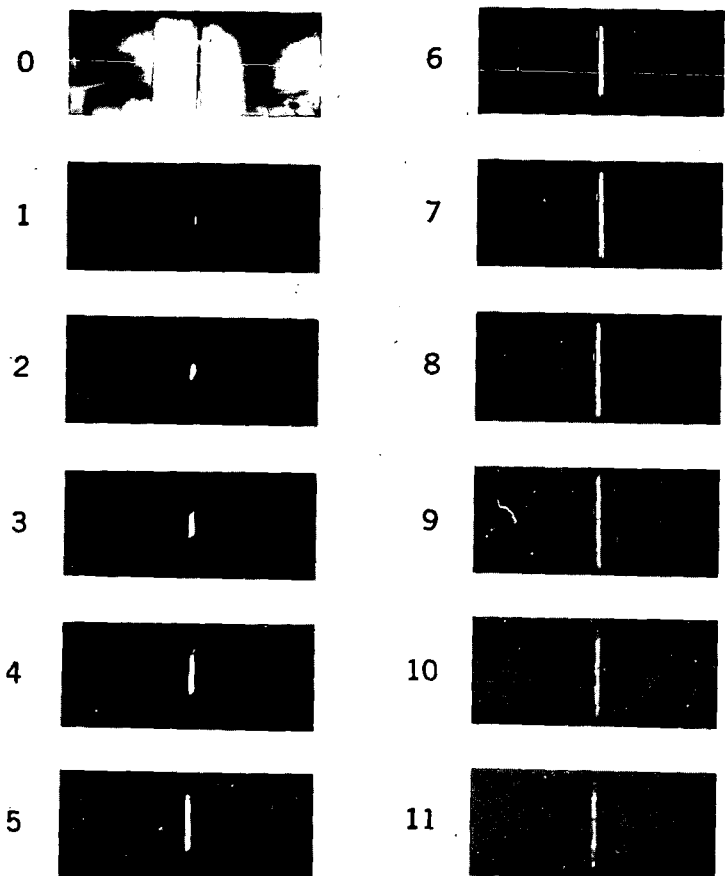


Figure 10. - Motion picture records showing the ignition of an n-octane vapor-air mixture with a 1/2-inch diameter hot air jet at 1400° F.

Jet flow rate - 185 in<sup>3</sup>/min (N.T.P.)

Mixture flow rate - 365 in<sup>3</sup>/min (N.T.P.)

Camera speed - 360 frames/sec

Scale: 1/4-inch = 5.4 inches for frames 1-11.

ELECTRICAL AUGMENTATION OF NATURAL GAS FLAMES

C. Marynowski

Stanford Research Institute  
Menlo Park, California

B. Karlovitz

Combustion and Explosives Research, Inc.  
Pittsburgh, Pennsylvania

T. Hirt

Northern Natural Gas Company  
(at Stanford Research Institute, Menlo Park, California)

I INTRODUCTION

Many industrial processes could make advantageous use of an economical source of heat at temperatures intermediate between those of combustion flames and those of electric arcs. This need has provided the incentive for numerous attempts to combine electrical energy with the heat released by combustion.

Combustion flames are, of course, limited in their heat release rate by reaction kinetics, and are limited in their ultimate temperature by the partial dissociation of the products of combustion.

The electric arc is not thus limited, but it has its own disadvantages. It is inherently a device characterized by extreme temperature gradients; that is, the electrically conducting path in the working fluid tends to contract into a very narrow, superheated channel, while the parallel surrounding paths carry little or no current and are relatively cold. The arc is further characterized by a relatively low voltage gradient along the conducting path; hence, it requires a high current if it is to dissipate substantial power in the gas. The high current, in turn, creates serious electrode maintenance problems, because the area of attachment of the arc at the electrodes is extremely small at any given instant. With a low voltage gradient through the gas, the energy dissipated as electrode losses (which are primarily a function of current density) is a relatively high proportion of the total energy input, thus tending to make the arc an inefficient means for heating the gas. In addition, the higher unit cost of electrical energy (versus combustion energy) puts the arc at an economic disadvantage.

Past research on electrical augmentation of flames, such as that of Southgate,<sup>1</sup> has utilized an electric arc in conjunction with the flame. Materials problems associated with the arc put a severe limitation on this technique, and interest in electrical augmentation of flames virtually disappeared until recently.

Renewed interest in the subject was initiated by a patent issued to Karlovitz<sup>2</sup> and by the preliminary development work on the patent concepts, by A. D. Little, Inc.<sup>3,4</sup> This work demonstrated that large amounts of electrical energy could be imparted to a flame, in the form of a high-voltage, low-current discharge that was dispersed throughout the flame volume. Subsequently, several other publications<sup>5,6</sup> have dealt with this subject. This paper will attempt to describe some of the performance characteristics obtained with the improved burner design.

## II DISCUSSION OF THE DIFFUSE ELECTRICAL DISCHARGE

Gases at ordinary temperatures are very poor electrical conductors, because they have a very low concentration of free electrons and positive ions. As the temperature is raised, polyatomic gases tend to become more and more unstable and to dissociate into their constituent atoms. However, in most cases the constituent atoms are themselves highly resistant to further dissociation into ions and electrons. Only at extremely high temperatures (above 5000°K) do such elements as oxygen, nitrogen, hydrogen, and carbon begin to ionize to an extent sufficient to impart significant electrical conductivity to the gas.

In the region between 5000°K and 20,000°K, the extent of ionization of common gases is an extremely sensitive function of temperature, and the electrical conductivity rises by many orders of magnitude as the temperature rises. The gases are said to have a large "positive temperature coefficient of electrical conductivity."

Because of this large positive coefficient, an ordinary gaseous conductor is an inherently unstable resistive load, and cannot be placed directly across a constant-voltage source without degenerating into a virtual short circuit. (As the gas is heated by the electrical discharge passing through it, its conductivity rises almost without limit.) A "ballast," consisting of an appropriately large auxiliary resistance or inductance, must be placed in series with the usual gaseous conductor in order to achieve control of the current drawn by the latter. This is the usual method employed to stabilize an electric arc.

A large positive temperature coefficient of conductivity also results in a second effect within the gaseous conductor. The flow of current naturally takes the path of least resistance. If there are even minor local nonuniformities among various alternative paths, the most conducting path will be heated most rapidly and will therefore increase in conductivity most rapidly. Unless this process is somehow opposed, the flow of current will very rapidly contract into a single, very narrow channel.

Two main strategies are available to counteract filament formation. The first is to reduce the positive temperature coefficient of electrical conductivity of the gas to the minimum possible value. (If it could be reduced to zero, or made negative, no further strategy would be necessary.) The second is to reduce or eliminate random local nonuniformities in conductivity before they grow too large.

To implement the first strategy, the familiar tactic of "seeding" the flame is employed. Alkali metals (and their compounds) are much more easily ionized than are the constituents of the common gases. For example, as shown in Fig. 1, potassium chloride (added in low concentration to a flame) can approach complete ionization of the outer electron of the potassium atom at temperatures several thousand degrees Kelvin lower than those at which any significant ionization of the bulk flame gases occurs. Thus, the conductivity of such a seeded flame is provided almost entirely by the additive, and once the latter reaches a state of essentially complete ionization, the temperature coefficient of conductivity of the flame assumes a relatively low value. Only a few parts per million of "seed" material is required to furnish adequate conductivity for the flame to be able to dissipate a large amount of power at relatively modest voltages.

Implementation of the second strategy is possible in principle because the overheating of a conducting path (relative to its surroundings) and the contraction of that path into a narrow filament are both time-dependent phenomena; therefore, it should be possible to oppose them by means of the powerful mixing action that can be provided by turbulence. Such mixing would tend to level out any local nonuniformities in temperature and conductivity before they could develop too far.

A mathematical treatment of the condition required for prevention of filament formation has been described by Karlovitz.<sup>4</sup> This treatment leads to the concept of a "critical voltage gradient," above which the rate of mixing provided by turbulence is inadequate to prevent the intensification of local inequalities in heating rate. Below the critical voltage gradient, the theory predicts that turbulence can act within a time interval comparable to that required for filament formation; this prediction has been verified experimentally. Thus, the two main tactics required for reduction of the diffuse discharge principle to practice are both available.

The initial mathematical model of Karlovitz is admittedly simplified, and will have to be refined to take into account such perturbing effects as dissociation of the working gas, nonequilibrium ionization (particularly during exothermic chemical reactions), and nonequilibrium electron capture (reported to be important during endothermic chemical reactions).<sup>7</sup> Nevertheless, the simple theory has been found to provide a very useful guide for design.

### III DESCRIPTION OF EXPERIMENTAL DEVICE

The work described here was conducted with a burner designed to operate on natural gas and air, at flow rates up to those corresponding to a maximum combustion heat release rate of 342,000 Btu per hour (equivalent to 100 kw of combustion energy).

The fuel and air were premixed and seeded with a dilute aerosol of potassium chloride. Combustion occurred in a constant-area duct and the diffuse electrical discharge was established in the fully combusted gases, immediately downstream of the combustion zone.

Figure 2 is a schematic representation of only the final stage of the device (in which the diffuse discharge takes place). This stage consists of a tube of refractory, electrically insulating material, bounded at both ends by metal electrodes. Provisions for cooling the tube and the electrodes are not shown in the diagram.

The electrodes are connected to a single-phase, 60-cycle power supply nominally designed for a power output of 100 kw, and actually capable of providing up to 150 kva at output voltages variable between about 2 and 8 kv. Inductive ballasting is provided, with the amount of inductance variable up to a maximum value sufficient to limit the short-circuit current to about twice rated current.

#### IV EXPERIMENTAL RESULTS

The initial burner configuration was similar to the original design described by Karlovitz, in that the discharge zone coincided with the combustion zone. Visually, the discharge did appear to be reasonably uniformly dispersed throughout the burner volume, and photographs taken with exposure times of the order of  $1/50$  second, such as that in Fig. 3, confirmed this impression. However, when high-speed photographs were taken, such as that in Fig. 4, the discharge was shown to consist of one (or at most a few) rapidly wandering, contracted arc filaments. Regardless of the concentration of ionizing additive or the degree of approach stream turbulence employed, the contracted nature of the discharge persisted if more than 10% electrical augmentation was attempted.

At this point, the possibility had to be considered that the zone in which turbulent combustion was in process did not have the properties necessary to sustain a powerful diffuse discharge. Especially near the gas inlet end of the discharge tube, the ionizing additive could not be expected to be fully vaporized and uniformly dispersed, and severe local temperature and electrical conductivity gradients were likely to be present.

The nature of the discharge changed drastically when another section of the duct was added downstream of the combustion zone, and when the discharge was established in this final stage. Figure 5 is a frame from a high-speed movie (3000 frames per second), showing such a discharge at that point in a single half-cycle of a.c. corresponding to peak power. The average electrical power per cycle dissipated by the discharge during this movie was 100 kw, and the peak electrical power at the instant of the frame shown in Fig. 5 was over 200 kw, on the basis of simultaneous oscilloscopic records of discharge current and voltage. Stoichiometric proportions of natural gas and air were employed, at a total flow rate equivalent to 100 kw of combustion power.

The photograph shows that, under these conditions, no filamentary structure can be discerned in the discharge column. Other frames from the same film (such as that shown in Fig. 6) occasionally show a short length of arc filament immediately adjacent to the electrode (mainly next to the upstream electrode, during that half-cycle when it has negative polarity); however, this is not surprising, because the discharge generally anchors at a relatively small spot on the electrode, thus necessitating a very high current density in the relatively cool and nonconductive boundary layer surrounding the electrode. With proper preconditioning of the working gas, the main portion of the discharge column remains completely diffuse.

By permitting combustion to proceed to completion prior to the superposition of the electrical discharge, any undesirable nonequilibrium ionization due to exothermic chemical reactions during the

discharge is avoided. In fact, the combustion products have the desirable property of being able to undergo endothermic dissociation, thus providing a self-contained heat sink that should tend to help avoid localized overheating of the gas by the discharge. Another way of stating this is that the slope of the conductivity versus enthalpy curve is reduced by dissociation. This slope may be regarded as an even more direct criterion of the susceptibility of the gas to filament formation than is the slope of the conductivity versus temperature curve.

Further confirmatory evidence of the diffuse nature of the discharge in a well preconditioned gas is provided by oscilloscopic traces of current and voltage, such as those shown in Fig. 7. These may be contrasted with the traces shown in Fig. 8, obtained from a contracted arc superimposed on a seeded, turbulent, combusting gas stream, like that illustrated in Fig. 4. Several important differences between the two cases may be pointed out. First, during each half-cycle at a given average power level, the ratio of voltage to current (representing the instantaneous ohmic resistance of the discharge) fluctuates between much wider limits, and drops to much lower values at peak current, in the arcing case than in the diffuse case. Second, there is no pronounced rise in voltage during the extinction period in the case of the diffuse discharge. Third, the arcing case exhibits a rapid, high amplitude fluctuation in voltage that does not appear in the diffuse case. (In an inductively ballasted circuit, the current is prevented from undergoing rapid changes by the reactive back--emf developed across the inductance; therefore, any rapid fluctuations in discharge conductivity are exhibited as voltage fluctuations to a much greater degree than as current fluctuations.) An arc in a highly turbulent medium is stretched and distorted in a random fashion so that it would be expected to exhibit just the sort of random fluctuations in conductance as are observed. A diffuse discharge, on the other hand, has a cross-section that is large compared with the scale of turbulence, so that its average conductance is less easily perturbed by turbulent mixing.

One further observation may be cited in support of the conclusion that the discharge illustrated in Fig. 5 is truly diffuse. At a given power level, the total luminosity of the discharge region is remarkably low, compared to that of the arcing discharge. This low luminosity is consistent with the absence of superheated filaments. We have not quantitatively examined either the absolute intensity or the spectral distribution of the emitted radiation.

The theoretical enthalpy of the augmented stoichiometric, natural gas-air flame (referred to 298°K) is shown in Fig. 9, plotted against the augmentation ratio (the ratio of electrical power to nominal combustion power). The discharge has been successfully maintained in the

diffuse mode at average augmentation ratios up to, and even slightly in excess of unity, and at peak ratios more than twice as high as the average. At peak power in each half-cycle of a.c., the total enthalpy of the gas is so high that only the dissociation of the initial combustion products prevents the temperature from rising to a level at which the conductivity would rise excessively because of ionization of the bulk gas.

The theoretical equilibrium temperature and composition of a stoichiometric methane-air mixture are shown plotted versus total enthalpy, in Fig. 10. These data were obtained with the aid of a machine computation program developed in the course of this study, with the assistance of Dr. Stuart Brinkley of Combustion and Explosives Research, Inc. Experimental gas compositions for the effluent gases from the augmented burner indicate a close approach to equilibrium, after allowance is made for recombination reactions occurring in the sampling probe.

The experimentally determined rate of heat transfer from the augmented flame to a transient-type flux probe is shown in Fig. 11, as a function of total enthalpy and of distance from the burner exit plane. It may be seen that the over-all heat transfer coefficient is considerably higher than that typical of unaugmented flames, a result attributable to the effect of recombination reactions on the probe surface.

#### V SUMMARY

An improved version of an electrically augmented burner has been described in which a powerful, 60-cycle electrical discharge can be maintained in the combustion products from a natural gas-air flame, and in which the discharge can be maintained in a completely diffuse mode.

Proper preconditioning of the gas appears to be the most essential factor tending to oppose contraction of the discharge into an arc filament. A high degree of turbulence, both in the discharge zone and in the approach stream, also assists in combating filament formation, the effect being most noticeable at high electrical power levels.

The diffusely augmented flame has potential technical and economic advantages over other sources of high temperature heat, that are expected to be significant to chemical, metallurgical, and other industrial uses. Experimental work with respect to various such applications is continuing.

REFERENCES

1. Southgate, G. T., "Boosting Flame Temperatures with the Electric Arc." Chem. Metallurgical Eng. 31, 16 (1924)
2. Karlovitz, B., U. S. Patent 3,004,137 October 10, 1961
3. A. D. Little, Inc., "Investigation of the Thermodynamic Properties of the Combex-ADL Natural Gas Burner," June 1961
4. Karlovitz, B., "Flames Augmented by Electrical Power," Pure and Appl. Chem. 5, 557 (1962)
5. Lawton, J., K. G. Payne, and F. J. Weinberg, "Flame-Arc Combination," Nature 193, 746 (1962)
6. "Proceedings of the Tenth Symposium (International) on Combustion," London, Butterworth, 1965
7. Atallah, S. and W. A. Sanborn, "The reduction of the electron density of a plasma by endothermic reactions," XV International Astronautical Congress, Warsaw, Poland, September 1964

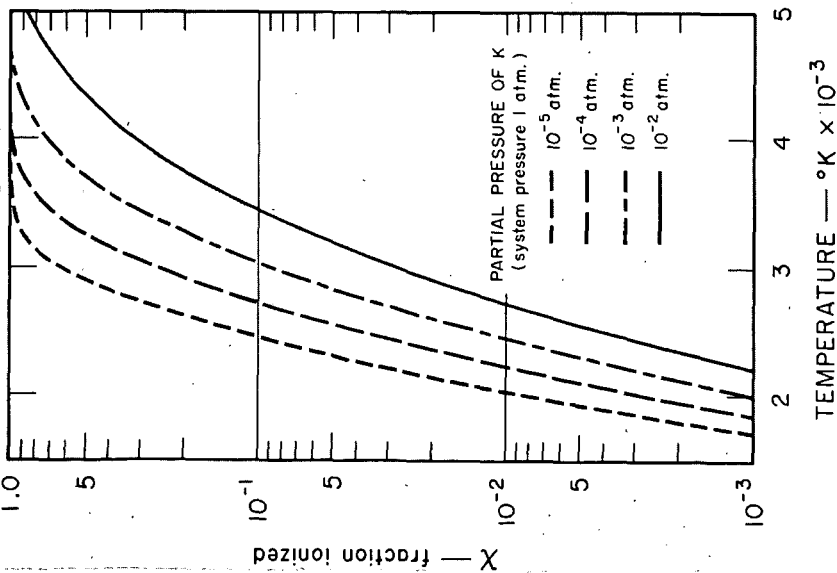


Fig. 1.-TEMPERATURE DEPENDENCE OF EXTENT OF IONIZATION

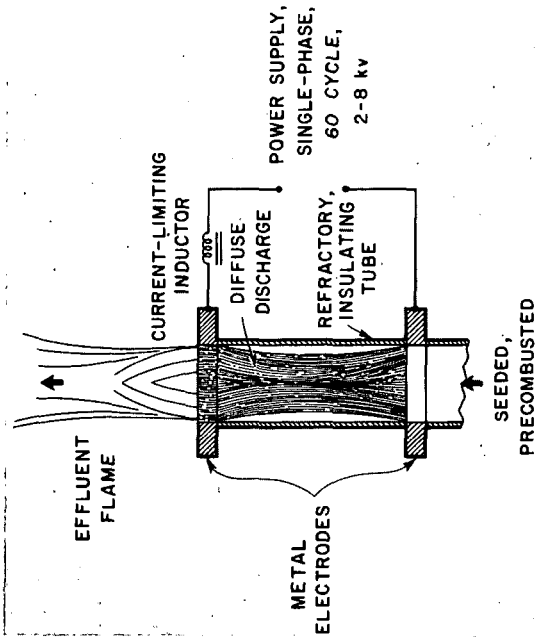


Fig. 2.-SCHEMATIC DIAGRAM OF FINAL STAGE OF ELECTRICALLY AUGMENTED BURNER

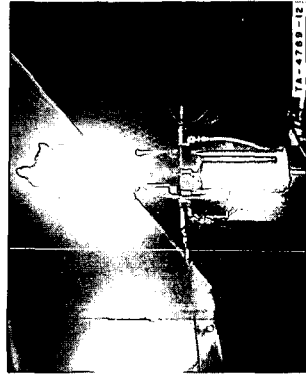


Fig. 3 -DIFFUSE APPEARANCE OF FILAMENTARY DISCHARGE AT SLOW SHUTTER SPEED

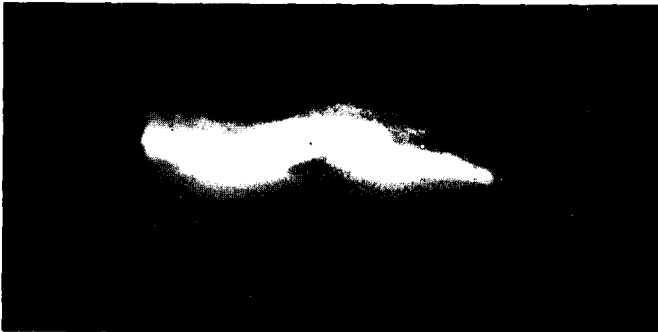


Fig. 4.-APPEARANCE OF  
FILAMENTARY DISCHARGE  
AT FAST SHUTTER SPEED

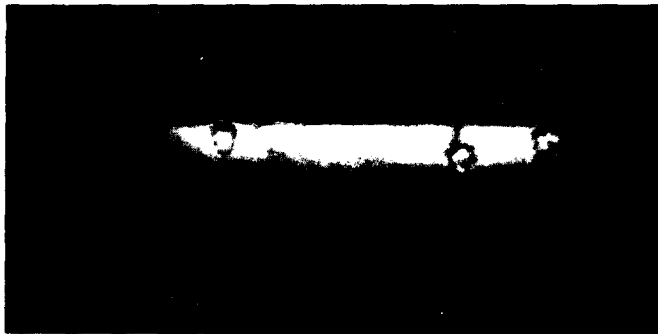
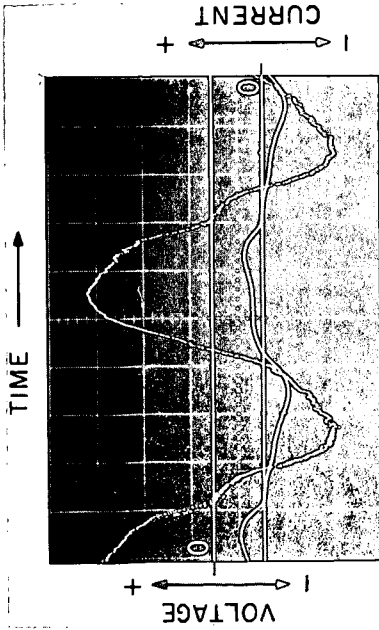


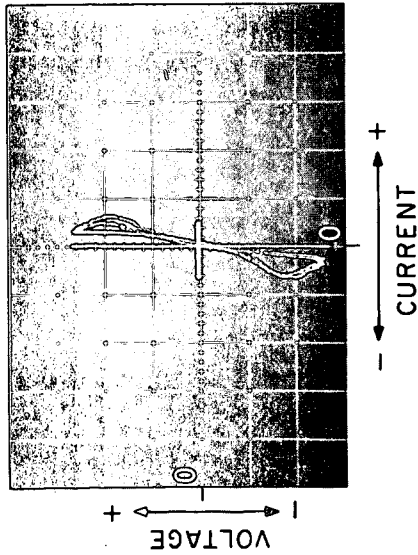
Fig. 5.-APPEARANCE OF  
DIFFUSE DISCHARGE AT  
FAST SHUTTER SPEED



Fig. 6.-MAXIMUM EXTENT  
OF FILAMENT FORMATION  
NORMALLY OBSERVED WITH  
DIFFUSE DISCHARGE

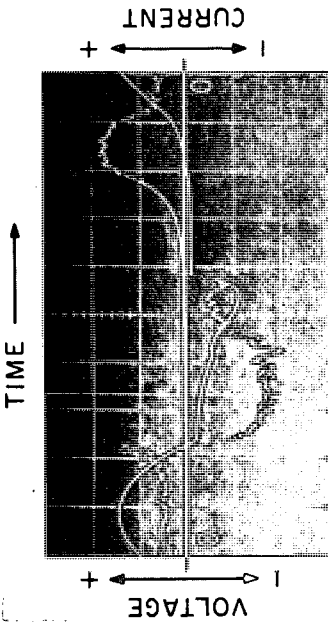


(a)

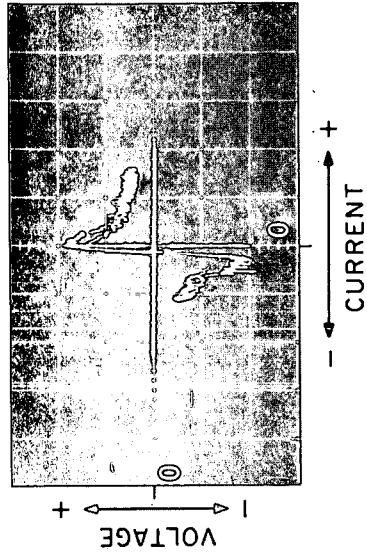


(b)

Fig. 7. -VOLT-AMPERE CHARACTERISTIC OF DIFFUSE DISCHARGE



(a)



(b)

Fig. 8. -VOLT-AMPERE CHARACTERISTIC OF FILAMENTARY DISCHARGE (at the same average power as that of Fig. 7)

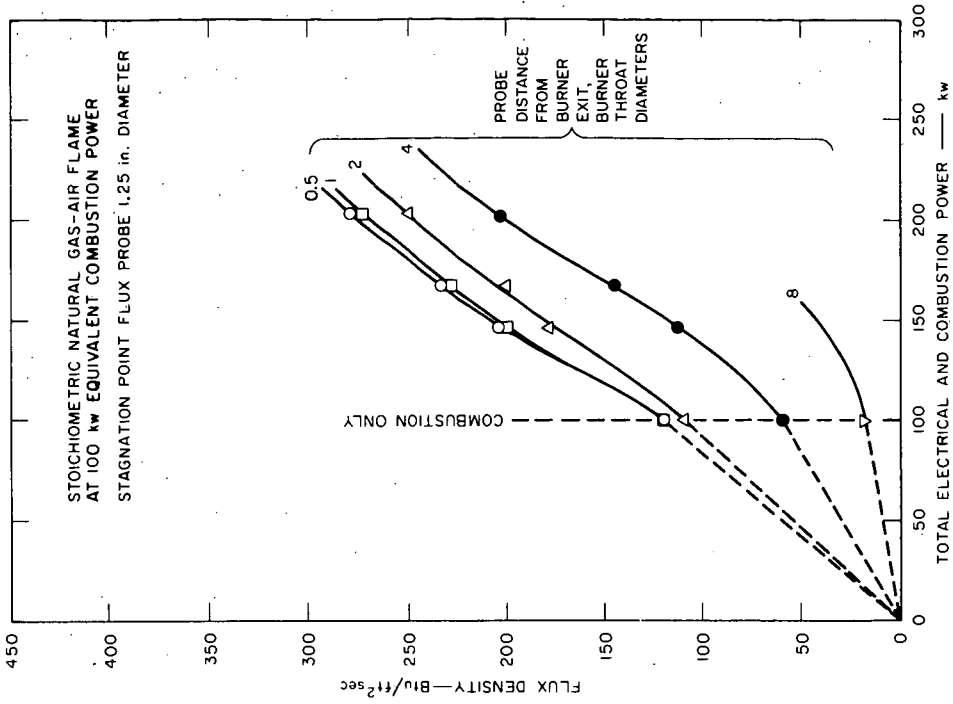


Fig. 11.—HEAT TRANSFER FROM ELECTRICALLY AUGMENTED BURNER TO A COLD-WALL, STAGNATION-POINT PROBE

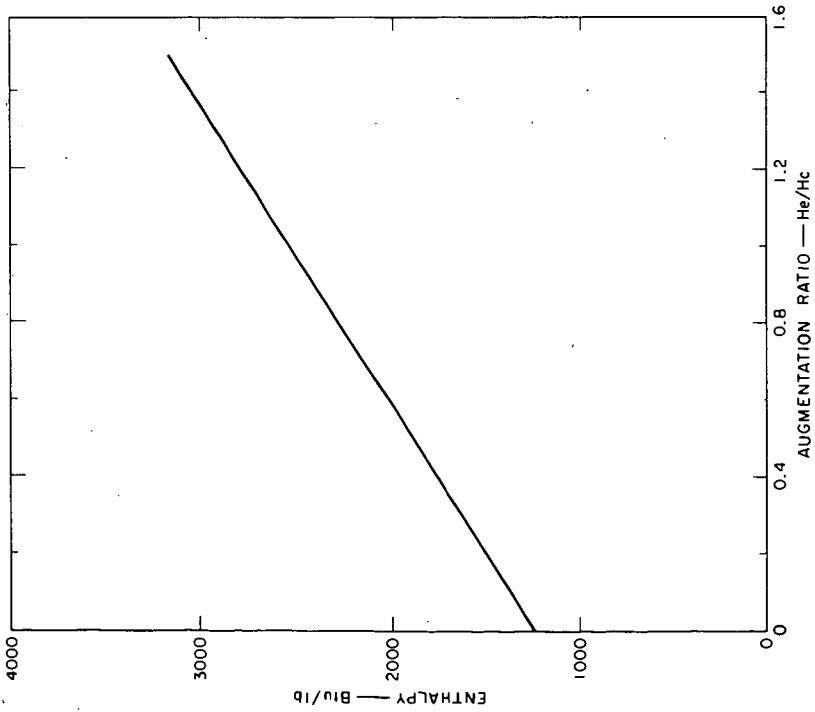


Fig. 9.—THEORETICAL ENTHALPY AS A FUNCTION OF ELECTRICAL AUGMENTATION RATIO

Figure to be distributed at meeting

Fig. 10.—THEORETICAL EQUILIBRIUM TEMPERATURE AND COMPOSITION AS A FUNCTION OF TOTAL ENTHALPY

## MICROBIAL SYNTHESIS OF FOOD FROM COAL-DERIVED MATERIALS

Melvin P. Silverman, Joan M. Novak, and Irving Wender

U. S. Bureau of Mines, Pittsburgh Coal Research Center  
4800 Forbes Avenue, Pittsburgh, Pennsylvania 15213

### ABSTRACT

Recent reports on the microbial production of protein from petroleum fractions for use as human or animal food supplements prompted studies on the feasibility of producing microbial protein from coal-derived materials. Growth yields of four species of the yeast *Candida* on several low temperature lignite tar and Fischer-Tropsch synthetic liquid fuel fractions were compared with yields obtained on a normal paraffin fraction derived from petroleum. It was found just as feasible technically to produce microbial food material from low temperature tar and Fischer-Tropsch fractions as from petroleum-derived paraffins. Growth yields were as high as 99.8% (Fischer-Tropsch fraction), 95.2% and 84.2% (two low temperature lignite tar fractions) of the yields obtained on the petroleum-derived paraffin fraction. Similar studies on producing microbial food from coal acids, nitric acid-oxidized anthracite, and a mixture of polynuclear hydrocarbons found in relatively large amounts in high temperature coal tar revealed that these substrates did not support the growth of yeasts. However, a number of bacterial cultures grow at the expense of these materials. Determinations of growth yields are in progress.

### INTRODUCTION

The problem of the world's population explosion is further compounded by an overall global food shortage. New or unusual sources of food, especially high quality protein, are needed as animal feed supplements or for human consumption. The Permanent Section on Food Microbiology and Hygiene, International Association of Microbiological Societies, in an unanimous resolution calling for an increased contribution of microbiology to world food supplies, outlined several research areas, including hydrocarbon microbiology, which might lead to increased world food production.<sup>1/</sup> Recently, reports have appeared dealing with the microbial conversion of petroleum hydrocarbons to protein, vitamins or amino acids. High yields of yeast cells rich in protein and vitamins have been obtained at the expense of the n-alkanes (preferably C<sub>10</sub> or higher) in crude petroleum fractions,<sup>2-6/</sup> feed stocks,<sup>7,8/</sup> or with the pure hydrocarbons themselves.<sup>9-11/</sup> Microbial synthesis of amino acids from petroleum products has also been reported.<sup>12,13/</sup>

The rate of microbial protein synthesis far exceeds the rate at which animals synthesize protein. One 500 kg. cow fed by grazing can synthesize 0.5 kg. of protein per day,<sup>15/</sup> whereas 500 kg. of microorganisms growing on paraffinic hydrocarbons could synthesize 1250 kg. of protein per day.<sup>3/</sup> It has been estimated that 3 million tons of protein per year (equal to the world's present protein deficit) could be produced by microorganisms at the expense of only 1% of the world's annual production of 700 million tons of crude paraffinic petroleum.<sup>3/</sup>

Coal, in addition to petroleum and natural gas, is one of the world's cheapest sources of fixed carbon and energy. The present paper reports the results of our studies on the feasibility of growing microorganisms for their food value at the expense of materials derived from coal.

EXPERIMENTAL

**Materials.** Three fractions of Bureau of Mines Fischer-Tropsch synthetic liquid fuel (iron catalyst) were used; fraction FTL (boiling range 0° to 204°), fraction FTD (boiling range 204° to 316°), and fraction FTW (boiling range > 316°).

Two fractions of hexane-soluble material from Rockdale lignite low temperature tar were obtained from the Texas Power and Light Company; the hexane solubles forerun (HSF) and the hexane solubles distillate (HSD). The HSF fraction constituted 7% and the HSD fraction 46% of the primary tar. The composition of fractions HSF and HSD are given in table 1. Phenolic compounds were removed by chromatographing fractions HSF and HSD on alumina with petroleum ether as the eluent to yield phenol-free fractions HSF $\emptyset$  and HSD $\emptyset$ . Approximately 20% by weight of starting material was removed by this procedure.

Table 1. Approximate composition of Rockdale lignite low temperature tar fractions, volume percent

Type of constituent	HSF	HSD
Caustic solubles	6-8	10-15
Acid solubles	2-4	1-3
Neutral oil	88-92	80-90
Paraffins	13-15	15-20
Olefins	40-55	40-50
Alpha-olefins	17-20	17-20
Aromatics	30-47	35-45

A paraffin-rich fraction (CTP) and a linear paraffin-olefin fraction (CTPO), both derived from the neutral oil of low temperature tar, were supplied by the Bureau of Mines' Morgantown Coal Research Center. Their analyses are given in table 2. The normal paraffin fraction derived from petroleum (PET) was a product of the Olefins Division of the Union Carbide Corporation. Our mass spectrometric analysis of this fraction is given in table 3.

Table 2. Analyses of paraffin-rich (CTP) and paraffin-olefin (CTPO) fractions from Rockdale lignite low temperature tar, weight percent

Carbon No.	CTP		CTPO	
	n-Paraffin	n-Olefin	n-Paraffin	n-Olefin
C <sub>8</sub>	0.2	--	--	--
C <sub>9</sub>	3.2	--	0.1	0.2
C <sub>10</sub>	11.7	0.7	1.3	1.6
C <sub>11</sub>	18.2	1.5	3.6	5.3
C <sub>12</sub>	22.4	3.3	5.8	7.6
C <sub>13</sub>	20.7	2.8	7.8	9.5
C <sub>14</sub>	10.8	3.7	7.5	10.9
C <sub>15</sub>	0.8	--	6.7	9.4
C <sub>16</sub>	--	--	4.6	5.6
C <sub>17</sub>	--	--	2.3	2.9
C <sub>18</sub>	--	--	4.2	3.1
	88.0	12.0	43.9	56.1

Table 3. Mass spectrometric analysis of n-paraffin fraction (FT) from petroleum

<u>Carbon No.</u>	<u>Volume percent</u>
C <sub>9</sub>	0.5
C <sub>10</sub>	7.2
C <sub>11</sub>	37.9
C <sub>12</sub>	29.1
C <sub>13</sub>	23.4
C <sub>14</sub>	1.9

**Microorganisms.** Cultures were obtained from soil by standard enrichment culture techniques or from the culture collections of the University of Pittsburgh, Syracuse University, and the University of Iowa.

**Measurement of Growth Yields.** Basal medium NX was prepared by adding  $\text{NH}_4\text{NO}_3$  (5.0 g.),  $\text{K}_2\text{HPO}_4$  (2.5 g.), and  $\text{MgSO}_4 \cdot 7\text{H}_2\text{O}$  (1.0 g.) to one liter of tap water. The pH was adjusted to 7.0 and any insoluble salts were removed by filtration. After sterilization by autoclaving, filter-sterilized yeast extract was added to a final concentration of 0.01%.

Inocula were prepared from cultures grown overnight in 50 ml. of Mycophil broth. The resultant growth was collected by centrifugation, washed twice in the sterile mineral salts solution of medium NX and resuspended in 20 ml. of the same solution. One ml. of washed cell suspension served as standard inoculum for all experiments.

For growth yield studies inocula prepared as above were added to 50 ml. of medium NX in 300-ml. Erlenmeyer flasks in triplicate. A quantity of substrate equivalent to 0.3 ml. was weighed into each flask. Triplicate controls consisted of inoculated flasks without added substrate. Cultures were incubated at 30° C. on a rotary shaker (225 r.p.m.) for six days. The resultant growth was collected on tared 2-inch diameter solvent resistant membrane filters (0.20  $\mu$  pore size), washed with 10-ml. volumes of acetone and n-hexane, dried overnight in air, and then weighed. All data are corrected for growth of controls.

## RESULTS

More than 200 cultures of bacteria, yeasts, and fungi were screened for their ability to grow on Fischer-Tropsch and low temperature tar fractions. The yeasts *Candida lipolytica* strains 409, 409A, 409B, and *Candida tropicalis* strain 410 were selected as the most promising cultures with respect to total cell yield, ability to utilize diverse substrates, and resistance to reasonably high substrate concentrations. These preliminary studies also indicated that growth yields on Fischer-Tropsch fraction FTL and low temperature tar fractions HSF and HSF $\emptyset$  were negligible. No further studies were made with these fractions.

**Comparative Growth Studies. Pure Compounds vs. Coal-Derived Material.** Absolute growth yields, in mg. dry weight per gram of substrate added, are given in table 4. The highest growth yields for all cultures (ranging from 433 to 719 mg. dry weight) were obtained with n-hexadecane as substrate; *C. lipolytica* 409 and 409A gave the best yields. Growth yields of 300 mg. or higher were obtained when 1-octadecene (*C. lipolytica* 409 and *C. tropicalis* 410) and Fischer-Tropsch fraction FTW (*C. lipolytica* 409B) served as growth substrates. Other substrates yielding

more than 200 mg. dry weight were paraffin-rich low temperature coal tar fraction CTP (all cultures), and Fischer-Tropsch fractions FTD (*C. lipolytica* 409B) and FTW (*C. lipolytica* 409). All cultures yielded less than 100 mg. dry weight on low temperature tar fraction HSDØ.

Table 4. Growth yields on pure compounds, low temperature tar, and Fischer-Tropsch fractions<sup>1/</sup>

Substrate	<i>C. lipolytica</i>			<i>C. tropicalis</i>
	409	409A	409B	410
Low temperature tar				
HSDØ <sup>2/</sup>	83	43	0	62
CTP	272	276	294	208
Fischer-Tropsch				
FTD	134	115	280	-
FTW	287	127	344	200
Pure compounds				
1-Octadecene	357	295	244	344
n-Hexadecane	719	628	433	453

1/ Average of triplicate cultures. Data in mg. dry weight per gram substrate added, corrected for growth in controls.

2/ Phenols removed by two passes on alumina column.

Figures 1 and 2 illustrate comparative growth yields relative to n-hexadecane using the data in table 4. On all substrates tested, with the exception of low temperature tar fraction HSDØ, *C. lipolytica* 409B consistently gave yields greater than 50% relative to n-hexadecane and appears to be the most versatile culture. *C. tropicalis* 410 is noteworthy for its ability to utilize the terminal olefin 1-octadecene (75% relative to n-hexadecane).

Comparative Growth Studies. Petroleum-Derived Paraffin Fraction vs. Coal-Derived Material. Table 5 compares absolute growth yields on coal-derived material with yields on a normal paraffin fraction derived from petroleum (PET). The three *C. lipolytica* cultures yielded over 300 mg. dry weight on petroleum fraction PET. Yields greater than 300 mg. dry weight were also obtained on Fischer-Tropsch fraction FTW with *C. lipolytica* 409 and 409B. All cultures gave yields greater than 200 mg. dry weight on low temperature tar fraction CTP. *C. lipolytica* 409B and *C. tropicalis* 410 both produced more than 200 mg. of dry cells on low temperature tar fraction CTPO. *C. lipolytica* 409B also yielded more than 200 mg. dry weight on Fischer-Tropsch fraction FTD. All cultures yielded negligible or no growth on low temperature tar fraction HSD; however, upon removal of the phenolic constituents from this fraction, *C. lipolytica* 409B and *C. tropicalis* 410 produced more than 100 mg. of dry cell material.

Figures 3 and 4 illustrate comparative yields relative to petroleum fraction PET using the data in table 5. *C. lipolytica* 409 was outstanding on Fischer-Tropsch fraction FTW and low temperature tar fraction CTP, yielding 99.8% and 84.5%, respectively, of the growth obtained on PET. *C. lipolytica* 409A gave a relative growth yield of 70.5% on fraction CTP. The versatility of *C. lipolytica* 409B is again illustrated by relative yields ranging from 60.4% (fraction CTPO) to 85.3% (fraction FTW) on all substrates except fractions HSD and HSDØ. *C. tropicalis* 410 was outstanding in its relative ability to grow on low temperature tar fractions

CTP (95.2%) and CTPO (84.2%), although absolute yields were below those obtained with *C. lipolytica* 409B on the same substrates (see table 5). Also interesting is the apparent correlation between the abilities of *C. lipolytica* 409B and *C. tropicalis* 410 to use a terminal olefin (table 4) and their ability to grow on low temperature tar fraction CTPO which contains 56% of olefinic compounds (table 2). The *C. lipolytica* 409 and 409A cultures, which gave lower yields on 1-octadecene relative to n-hexadecane (figure 1), reflected this in their lower absolute and relative yields on CTPO compared with CTP (figure 3, table 5).

Table 5. Growth yields on low temperature tar, Fischer-Tropsch, and petroleum fractions<sup>1/</sup>

Substrate	<i>C. lipolytica</i>			<i>C. tropicalis</i>
	409	409A	409B	410
Low temperature tar				
HSD <sup>2/</sup>	14	6	0	0
HSD <sup>3/</sup>	73	72	106	102
CTP	259	235	287	232
CTPO	113	124	233	205
Fischer-Tropsch				
FTD	114	150	243	0
FTW	306	167	329	161
Petroleum				
PET	307	333	385	244

1/ Average of triplicate cultures. Data in mg. dry weight per gram substrate added, corrected for growth in controls.

2/ Phenols not removed.

3/ Phenols removed by three passes on alumina column.

Growth Studies on Other Coal-Derived Materials. Studies were begun to investigate the feasibility of producing microbial food from other materials derived from coal, such as acids obtained by oxidizing coal with air, nitric acid-oxidized anthracite, and a mixture of polynuclear hydrocarbons found in high temperature coal tar.

A 56% aqueous solution of coal acids (obtained from the Dow Chemical Co.) and a water-soluble mixture of aromatic acids from the alkaline oxidation of coal (obtained from the Carnegie Institute of Technology) were tested as growth substrates for all of our yeast cultures. No growth was obtained. Similarly, soil enrichment culture procedures designed to favor the isolation of yeasts gave negative results. However, a number of bacterial cultures capable of growing on the coal acids were isolated; quantitative studies on growth yields are in progress.

A series of oxidation products from the nitric acid oxidation of anthracite was obtained from the Bureau of Mines Anthracite Research Center.<sup>14/</sup> The acid-soluble residue of the 1000-hour oxidation time supports the growth of a bacterial culture previously isolated on one of the coal acids. Growth yield studies and enrichment culture procedures are in progress.

A mixture of polynuclear hydrocarbons found in relatively large amounts in high temperature coal tar was prepared. It was composed of (by weight percent) 1-methylnaphthalene, 59.2; 2-methylnaphthalene, 16.3; naphthalene, 11.9; phenanthrene, 12.5. A number of bacterial cultures, but no yeasts, capable of growing on this material have been isolated from soil. Growth yield studies are in progress.

## DISCUSSION

In practice, over 80% conversion of hydrocarbon substrates to cell material has been obtained.<sup>3,6,9-11/</sup> Although our absolute growth yields on pure hydrocarbons, petroleum, Fischer-Tropsch, and low temperature tar fractions were somewhat lower, it must be remembered that our experiments were designed solely to test the feasibility of using these substrates for microbial food production. Improvements in the nutritional quality of the growth medium, closer control of pH, more efficient aeration, and other practices of the fermentation microbiologist's art will undoubtedly result in higher cell yields.

It is clear that some of the substrates derived from coal which were tested are closely comparable to petroleum-derived normal paraffins in their ability to support microbial growth with the concomitant production of cell material (food). Paraffin-rich low temperature tar fraction CTP and Fischer-Tropsch fraction FTW were outstanding in this regard.

Oxidized coals and polynuclear aromatic hydrocarbons may be suitable for the growth of bacteria, rather than yeasts, for use as food material. Further experiments along this line are in progress.

## REFERENCES

1. The Contribution of Microbiology to World Food Supplies. In *Recent Progress in Microbiology*. VIII International Congress for Microbiology, Montreal, (1962). N. E. Gibbons, ed., pp. 719-720, University of Toronto Press.
2. Champagnat, A. and Filosa, J. Procédé de production de levures a partir de fractions du pétrole. French Patent 1,297,619, May 21, 1962.
3. Champagnat, A., Vernet, C., Laine, B., and Filosa, J. Biosynthesis of Protein-Vitamin Concentrates from Petroleum. *Nature*, 197, pp. 13-14 (1963).
4. New Aims for Biosynthesis. *Chem. & Eng. News*, pp. 49-51, Feb. 2, 1963.
5. British Petroleum Expands Protein-from-Oil Research. *Chem. & Eng. News*, p. 41, Jan. 20, 1964.
6. Gatellier, C. Make Food from Crude Oil. *Hydrocarbon Processing & Petroleum Refiner*, 43, pp. 143-145 (1964).
7. Takahashi, J., Kobayashi, K., Kawabata, Y., and Yamada, K. Studies on the Utilization of Hydrocarbons by Microorganisms. Part III. Production of Bacterial Cell from Hydrocarbons. *Agric. Biol. Chem.* 27, pp. 836-842 (1963).
8. Komagata, K., Nakase, T., Katsuya, N. Assimilation of Hydrocarbons by Yeasts. I. Preliminary Screening. *J. Gen. Appl. Microbiol.*, 10, pp. 313-321 (1964).
9. Johnson, M. J. Utilisation of Hydrocarbons by Micro-organisms. *Chem. & Ind.*, pp. 1532-1537, Sept. 5, 1964.
10. Miller, T. L., Lie, L., and Johnson, M. J. Growth of a Yeast on Normal Alkanes. *Biotechnol. Bioeng.*, 6, pp. 299-307 (1964).

11. Azouley, E., Couchoud-Beaumont, P., and Senez, J. C. Croissance de Candida lipolytica à partir des Hydrocarbures Paraffiniques. Ann. Inst. Pasteur, 107, pp. 520-533 (1964).
12. Yamada, K., Takahashi, J., Kobayashi, K., and Imada, Y. Studies on the Utilization of Hydrocarbons by Microorganisms. Part I. Isolation of Amino Acids Producing Bacteria from Soil. Agric. Biol. Chem., 27, pp. 390-395 (1963).
13. Takahashi, J., Kobayashi, K., Imada, Y., and Yamada, K. Effects of Corn Steep Liquor and Thiamine on L-Glutamic Acid Fermentation of Hydrocarbons. IV. Utilization of Hydrocarbons by Microorganisms. Appl. Microbiol., 13, pp. 1-4 (1965).
14. Hammer, M. A., Brady, G. A., and Eckerd, J. W. Oxidation of Anthracite with Concentrated Nitric Acid. BuMines Rept. of Inv. 5782, 18 pp. (1961).
15. Thaysen, A. C. In Yeasts (1957), W. Roman, Ed., p. 155, W. Junk, Hague.

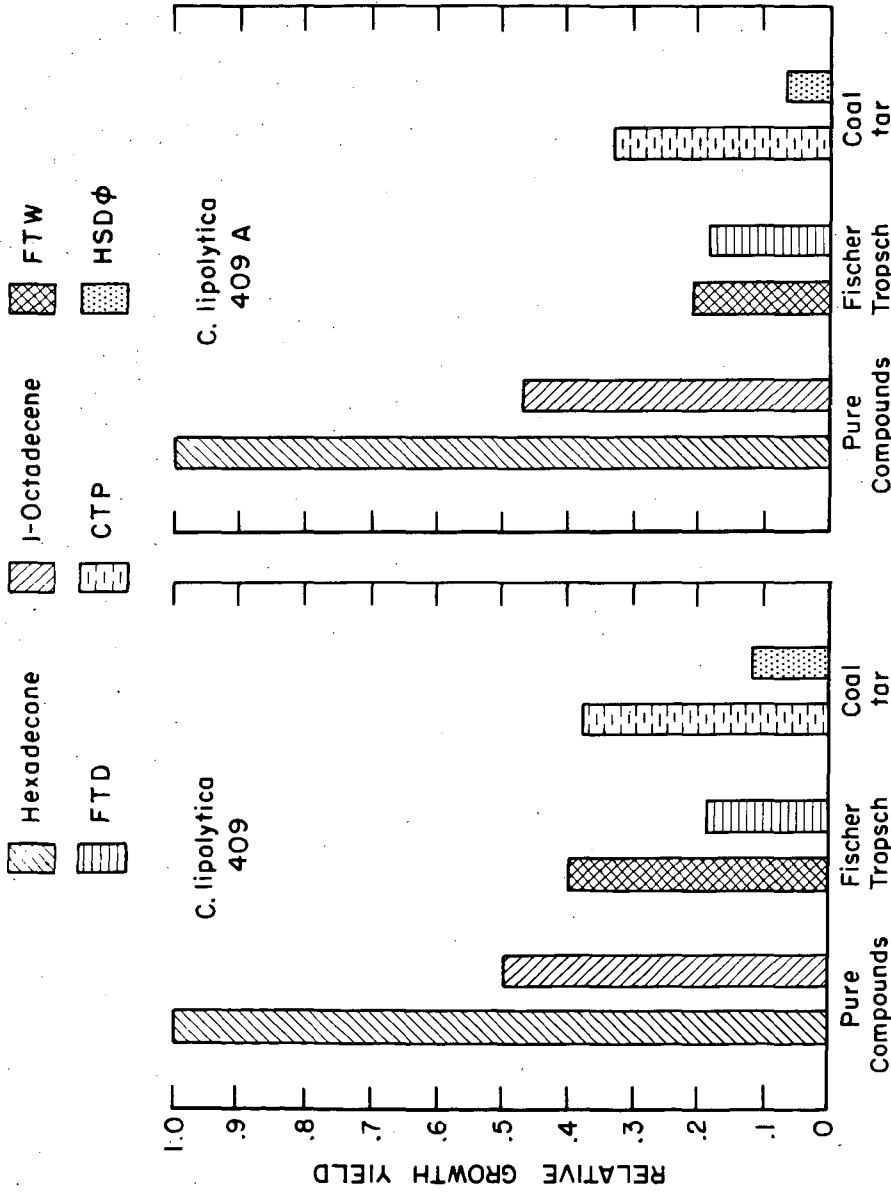


Figure 1.- Growth yields relative to n-hexadecane.

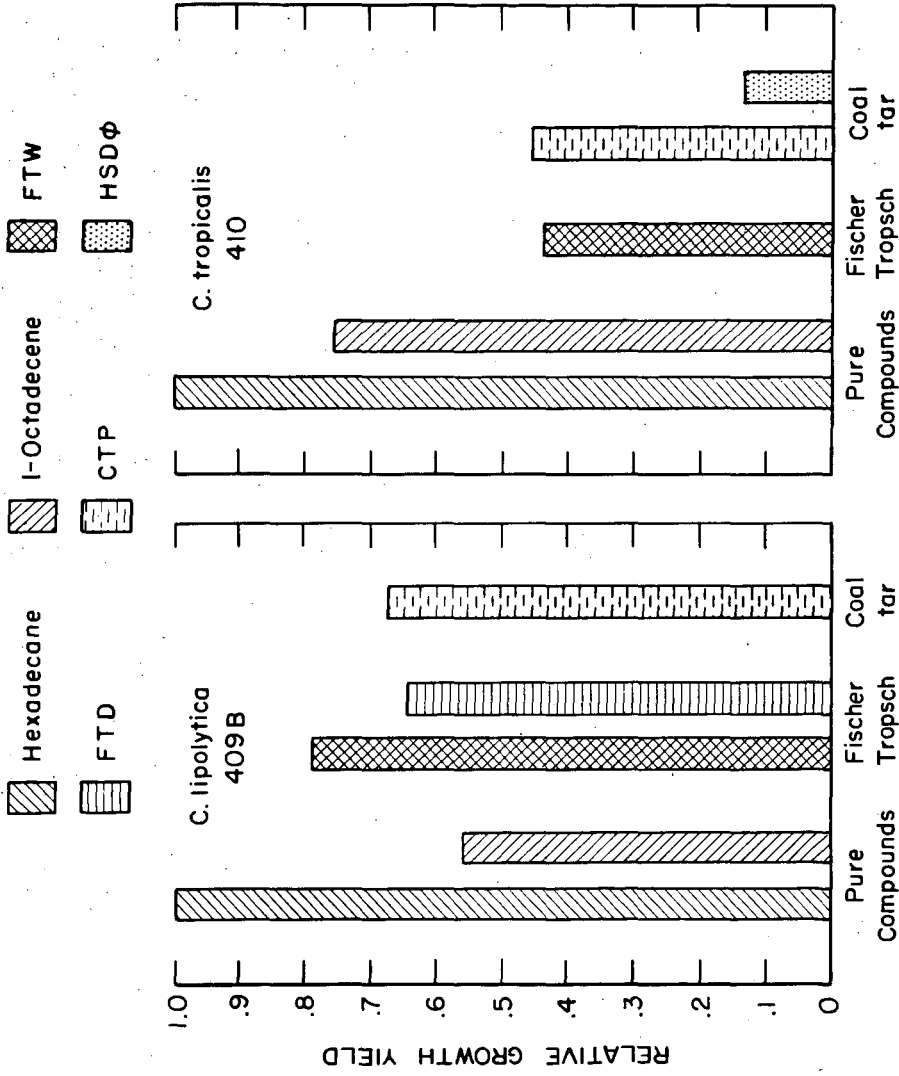


Figure 2.-Growth yields relative to n-hexadecane.

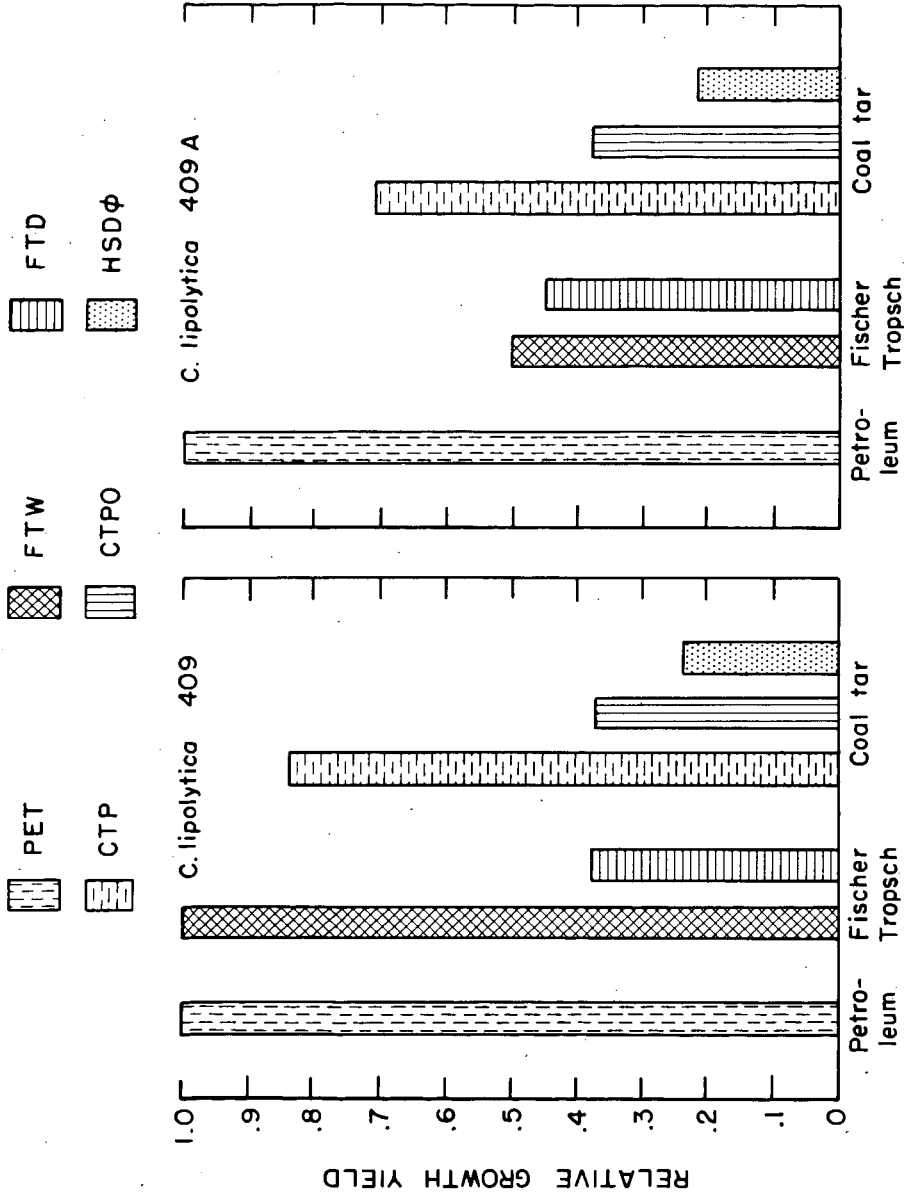


Figure 3.- Growth yields relative to petroleum.

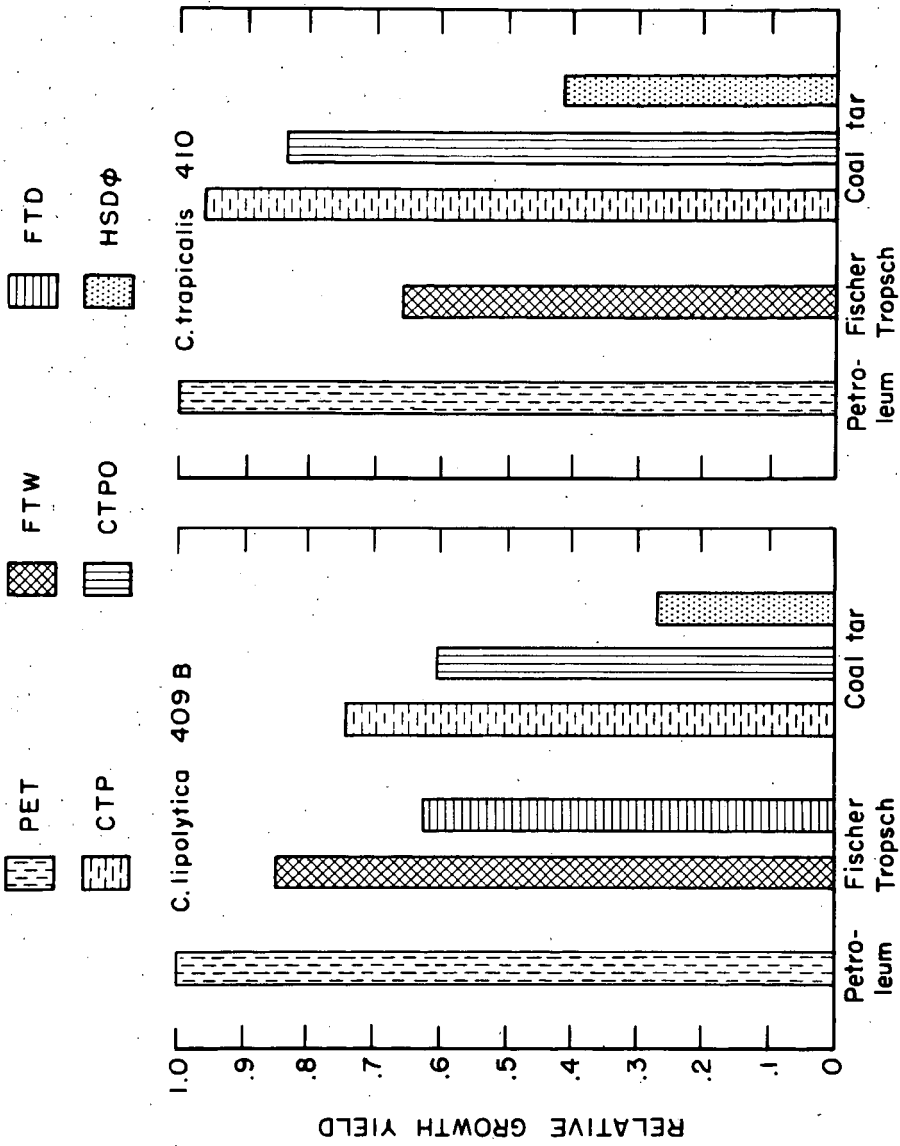


Figure 4.-Growth yields relative to petroleum.

The Effect of Air Oxidation on the Caking Properties of  
Pittsburgh-Seam Coal

A. J. Forney, R. F. Kenny, and J. H. Field  
U. S. Bureau of Mines, 4800 Forbes Avenue  
Pittsburgh, Pennsylvania 15213

INTRODUCTION

Production of synthetic liquid and gas fuels is a potential means for increasing the market for coal. The demand for fuel is high in the East and Midwest, but unfortunately most coals in these sections become sticky and agglomerate or cake when they are heated through the range of 300°-400° C. If they could be made noncaking, they would be suitable for fluidized-bed gasification, hydrogenation, and carbonization.

Nathan<sup>7/</sup> destroyed the caking property of coal (10 to 400 mesh) by pre-treating it in air at 316°-441° C. Channabasappa<sup>1/</sup> treated coal of 88 to 98 percent through 100 mesh with air as well as other gases at a temperature range of 200°-382° C. Schmidt<sup>8/</sup> decaked Pittsburgh-seam coal of 0 to 1/4-inch size with air at 99.3° C. He also noted that the agglutinating value of the coals decreased as the oxidation of the coals increased. Minet<sup>6/</sup> oxidized coal with steam plus air at 370°-430° C in the first stage of a carbonization process, and Williams<sup>9/</sup> treated coal (80 percent through 1/8 inch screen) with an oxygen-containing gas at 80°-300° C.

Pittsburgh-seam coal is highly caking. In earlier work at the Bureau<sup>2/</sup> it was made nonagglomerating, and with only slight variation the treatment was successfully applied to other caking coals. In this previous work the caking property of Pittsburgh-seam coal was destroyed by treating it in both static<sup>4/</sup> and fluidized<sup>2,3/</sup> beds with steam plus oxygen or air. To extend this study the present program was to treat Pittsburgh-seam coal with air only, to study the effect of operating variables such as mesh size, temperature, residence time and pressure, and to deduce the changes that may take place in the coal during treatment by carbonizing the treated coal.

Decaking was considered successful if the free-swelling index (FSI) of the treated coal (char) did not exceed 1-1/2 and the treated coal did not agglomerate when it was heated in a hydrogen atmosphere to 900° C.

#### STATIC-BED EXPERIMENTATION AND RESULTS

In the static-bed experiments fine particles of Pittsburgh-seam coal were spread in 100 x 50 ml dishes to a 1/2-inch depth, placed in a large drying oven, and heated in air to 95°-100° C. To decake these coals, using an FSI of 1-1/2 or less as indicating satisfactory decaking, required about 16 hours treatment under these conditions for 150-200 mesh<sup>a/</sup> coal, 24 hours for 100-150 mesh, and 50 hours for 48-100 mesh (figure 1). At the end of 64 hours the 18-48 mesh coal had an FSI of 3-1/2. The oxygen content of all coals increased with time; with the finer coals the increase was more rapid. The loss in volatile matter averaged about 3 percentage points (a change from 40 percent volatile matter in the raw to 37 percent in the treated coal). About 6 months after the original data were collected, additional tests were made on different batches of coal of 18-48 and 48-100 mesh sizes. These results are shown on figure 1 as larger squares and dots. While the later data with the 18-48 mesh coals correlate with the earlier results, data from the 48-100 mesh size show some discrepancies. These results, although not exact due to the method of operation, demonstrate that treating fine coal in air at 100° C will decake the coal, but at least 16 hours time will be needed. These tests also indicate that it is not safe to assume that there is no change in the properties of fine coal dried in air at this temperature.

#### FLUIDIZED-BED EXPERIMENTATION AND RESULTS

Apparatus for the fluid-bed experiments is shown in figure 2. The reactor is a stainless steel tube of 1-inch diameter with an expanded section of 2-inch diameter at the top. The 29-inch section containing the fluidized bed of coal is heated electrically. Thermocouples are inserted inside a well placed down through the center of the reactor. Raw coal from the continuous feeder is entrained in the air stream and carried into the bottom of the reactor. The oxygen in the air renders the coal noncaking at specified temperatures, and the treated coal overflows into a collection vessel. Gases, tars, and dusts are discharged from the top of the reactor.

Because the height of the fluidized bed is constant, the rate that the coal is fed determines the residence time of the coal in the reactor. Only 40 minutes were required to decake Pittsburgh-seam coal in the fluid bed at 200° C for the 150-200 mesh size and 400° C for the 18-48 and 48-100 mesh size (figure 3). The results are more relative than absolute, but the trends are realistic. The oxygen content of the coals reached a maximum between 300° and 400° C and was less at the higher temperatures. The

---

<sup>a/</sup> All mesh sizes are Tyler Standard Screen Series.

temperature at which it reached a maximum depended on the mesh size. As the temperature was raised to 300° C, the volatile-matter content decreased gradually, and then precipitously at higher temperatures. The minimum loss in volatile matter was about 3 percentage points at 300° C.

With the same 40-minute residence time the 150-200 mesh coal was treated at pressures of 1, 2, 5, and 10 atmospheres and 100° to 450° C (figure 4). At atmospheric pressure the coal became noncaking at 200° C; at 5 atmospheres it became noncaking at about 175° C, and at 10 atmospheres the coal burned above 150° C. At 150° C there was little change in the FSI. The oxygen content increased at higher pressures, the maximum being about 13 percent at 2 atmospheres and 300° C.

The volatile matter decreased at higher temperatures, but the change in volatile matter was insignificant at higher pressures. The least volatile matter was removed (3 percentage points) when the coal was treated at 200° C and atmospheric pressure.

Shortening the residence time to 20 minutes had little effect on the volatile matter and the FSI of the treated coal (figure 5) when compared with 40 minutes (figure 4). The amount of oxygen absorbed was the same as in the previous test at 2 atmospheres and 300° C. As the same results were obtained with the shorter residence times, the controlling variable seems to be temperature. Residence time might be shortened even more, but the limit of operability had been reached and the coal feed could not be increased to make such a test.

Also at the 20-minute residence time it was possible to continue the treatment at 5 atmospheres to 400° C, whereas at the 40-minute residence time the coal burned uncontrollably above 200° C. Thus the maximum oxygen content of the coal became 17 percent. Why coal could be treated at higher temperature with shorter residence time is not clear.

These curves show that the FSI is substantially independent of pressure, but highly dependent on coal size. More oxygen is absorbed by the coal at higher pressures and no more volatile matter is lost. The decrease in volatile matter is primarily a function of temperature, at least in the pressure range up to 10 atmospheres. Of course, when the pressure is increased, the air flow must also be increased to maintain fluidization; however, the oxygen/coal ratio at the different pressures indicates that pressure has more effect than air flow.

When the tests were made at 5 atmospheres, two samples of treated coal were taken at each temperature. One sample was evacuated to 30 mm absolute pressure to determine if oxygen taken up during treatment could be removed. Comparison with the nonevacuated sample showed that it could not. Consequently the additional oxygen must have chemically reacted in the coal to form a coal-oxygen complex.

CARBONIZATION TESTS: EXPERIMENTATION AND RESULTS

Comparing the results of low-temperature carbonization of coal fluidized in air at 230° C with raw coal gives a clue as to what changes take place in the volatile matter during the air treatment (table 1). The carbonization unit has a charging vessel at the top (figure 6)<sup>2</sup>. After the reactor reached the desired temperature, the valve below the charging vessel was opened to allow the coal to drop into the heated zone.

TABLE 1.- Batch carbonization tests at 538° C (1,000° F) and 427° C (800° F) at 30-minute residence time

Type of coal	Raw	Treated <sup>1/</sup>	
Temperature, °C	538	538	427
Gas analysis, vol-pct			
H <sub>2</sub>	13	10	2
N <sub>2</sub>	0	0	1
CO	6	16	19
CH <sub>4</sub>	53	39	17
C <sub>2</sub> +	22	13	9
CO <sub>2</sub>	6	22	52
HV	1060	750	410
Cubic feet tail gas per ton feed coal	1100	1600	400
Solids feed analysis, wt-pct, MAF			
Volatile matter	40.2	35.6	36.4
Fixed carbon	59.8	64.4	63.6
Hydrogen	5.6	4.8	4.9
Carbon	83.6	80.1	80.3
Nitrogen	2.3	2.2	1.6
Oxygen	6.6	11.1	11.2
Sulfur	1.9	1.8	2.0

<sup>1/</sup> Made by fluidizing coal in air at 230° C for 30 minutes.

Proximate analysis (table 1) shows that treated and raw coals differ mainly in their volatile matter and oxygen content, the treated coal containing the more oxygen. The higher the oxygen content in the feed, the more carbon oxides in the gas produced by carbonization at 538°--12 percent for raw and 38 percent for treated coal. The heating value of the gas decreased as the carbon oxide yield increased, dropping from 1,060 to 750 Btu per cubic foot.<sup>5</sup> This observation<sup>8</sup> on carbon oxides is in agreement with the data of Juntgen<sup>7</sup> and of Schmidt<sup>8</sup>.

The quality of the volatile matter differs for raw and treated coal. The treated coal carbonized at 427° C yielded primarily carbon oxides (table 1), indicating that the additional oxygenated compounds in the treated coals are reacted faster than the volatile matter in the raw coal. At 538° C the percentage of carbon oxides is less because after the supply of oxygenated compounds is depleted, the usual pyrolytic reactions predominate.

Table 1 gives the volatile matter of the raw coal as 40.2 percent and that of the treated coal as 35.6 percent. The larger quantities of carbon oxides given off during carbonization of the treated coal indicate that its volatile matter has been supplemented by the oxygenated compounds formed during treatment.

#### CONCLUSION

Tests show that Pittsburgh-seam coal, a highly caking coal, can be made nonagglomerating by heating in air in a static bed at 100° C for about 16 hours (150-200 mesh) or 50 hours (48-100 mesh).

In a fluid-bed reactor the finer mesh coal (150-200 mesh) can be made noncaking in 40 minutes by treating and fluidizing it with air at 200° C. As the temperature is increased, more oxygen combines with the coal until at about 350° C (depending on the coal size) the burning of the coal becomes uncontrollable. The percentage of oxygen in the coal increased from about 8 percent in the raw coal to as high as 17 percent when the coal was treated at 5 atmospheres pressure. Satisfactory decaking (as indicated by an FSI of 1-1/2 or less) was obtained with a volatile loss of 3 percentage points (10 percent of the volatile matter).

Carbonization tests indicate by the greatly increased yield of carbon oxides from the treated over the raw coal that a large amount of oxygenated compounds is included in the volatile matter of the treated coal. These additional compounds had to come from the treatment.

REFERENCES

1. Channabasappa, K. G., and H. R. Linden. Fluid-Bed Pretreatment of Bituminous Coals and Lignite. *Ind. and Eng. Chem.*, v. 50, 1958, pp. 637-644.
2. Forney, A. J., R. F. Kenny, S. J. Gasior, and J. H. Field. Destruction of Caking Properties of Coal by Pretreatment in a Fluidized Bed. *Ind. and Eng. Chem. Research and Development*, v. 3, March 1964, pp. 48-53.
3. \_\_\_\_\_. The Production of Nonagglomerating Char from Caking Coal in a Continuous Fluid-Bed Reactor. Symposium on Pyrolysis and Carbonization of Coal. Division of Fuel Chemistry, American Chemical Society, Chicago, Ill., Aug. 31-Sept. 4, 1964.
4. Gasior, S. J., A. J. Forney, and J. H. Field. Destruction of the Caking Quality of Bituminous Coal in a Fixed Bed. *Ind. and Eng. Chem. Research and Development*, v. 3, March 1964, pp. 43-47.
5. Juntgen, Harold, and Kurt-Christian Traenckner. Degassing of Oxidized Bituminous Coal. Contribution to the Reaction Kinetics of Coal Pyrolysis. *Brenstoff-Chemie*, v. 45 (4), 1964, pp. 105-114.
6. Minet, R. G. Continuous Carbonization of Bituminous Coal. *Utilization*, February 1956, pp. 33-35.
7. Nathan, M. F. U. S. Patent 3,032,477, May 1, 1962.
8. Schmidt, L. D., J. L. Elder, and J. D. Davis. Atmospheric Oxidation of Coal at Moderate Temperatures. Effect of Oxidation on the Carbonizing properties of Representative Caking Coals. *Ind. and Eng. Chem.*, v. 32, No. 4, April 1940.
9. Williams, O. E. U. S. Patent 2,805,189, Sept. 3, 1957.

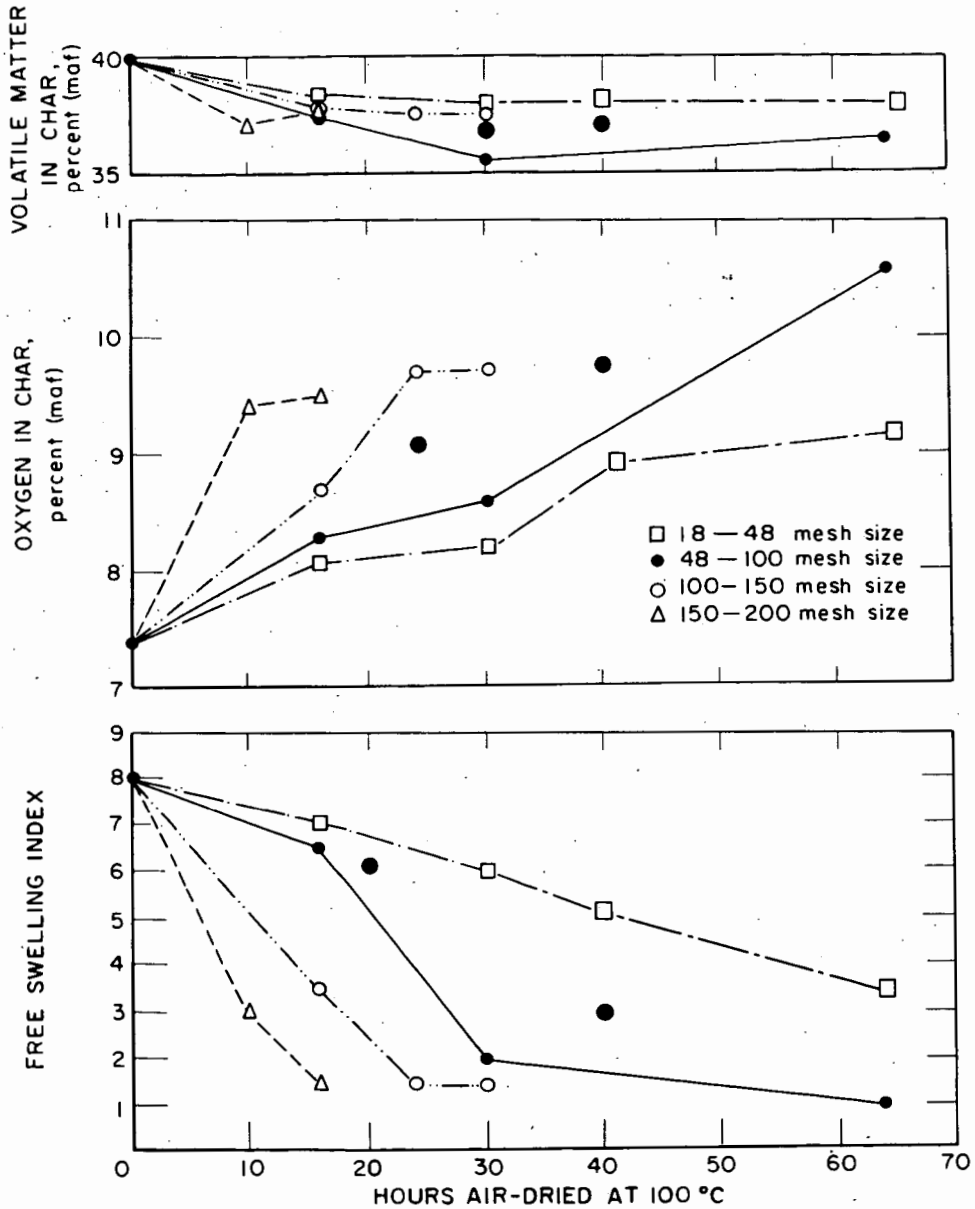


Fig. 1.-EFFECT OF RESIDENCE TIME ON THE FSI, VOLATILE MATTER, AND OXYGEN CONTENT OF CHAR OF PITTSBURGH-SEAM COAL TREATED IN AIR AT 100°C IN A STATIC BED

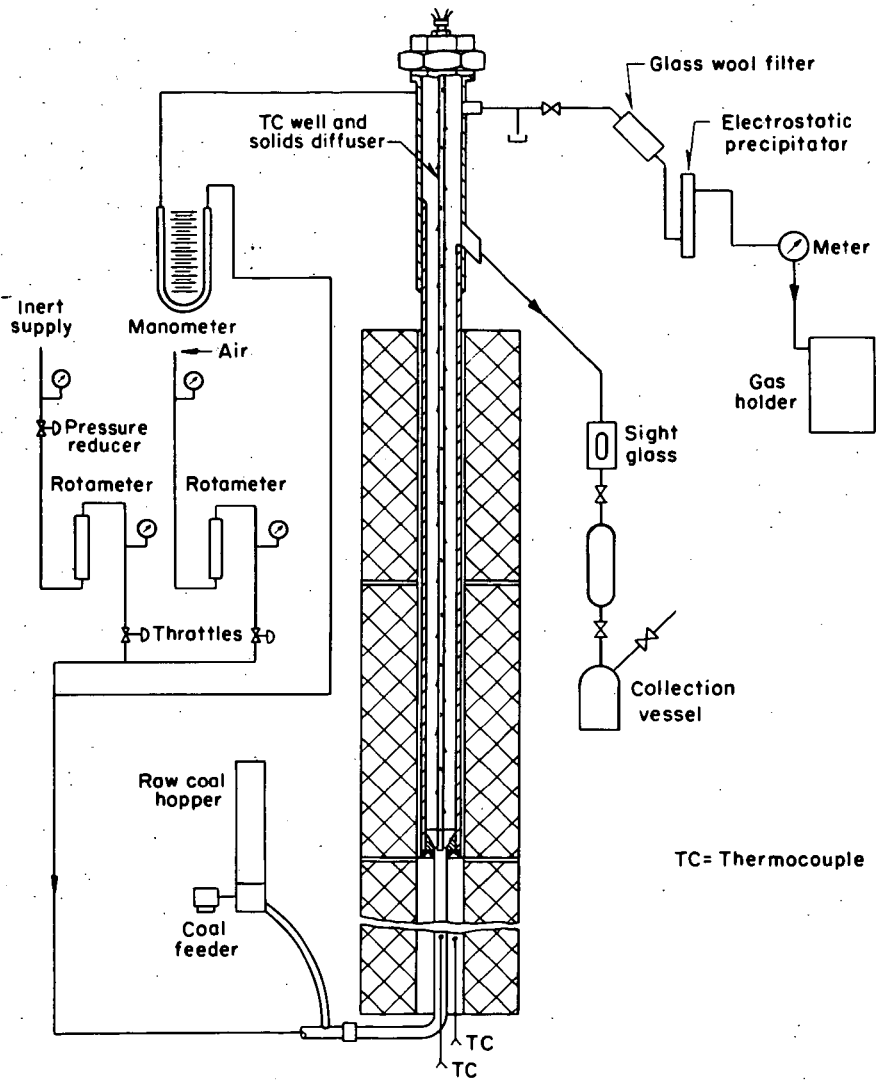


Fig. 2.-CONTINUOUS FLUIDIZED-BED COAL PRETREATER

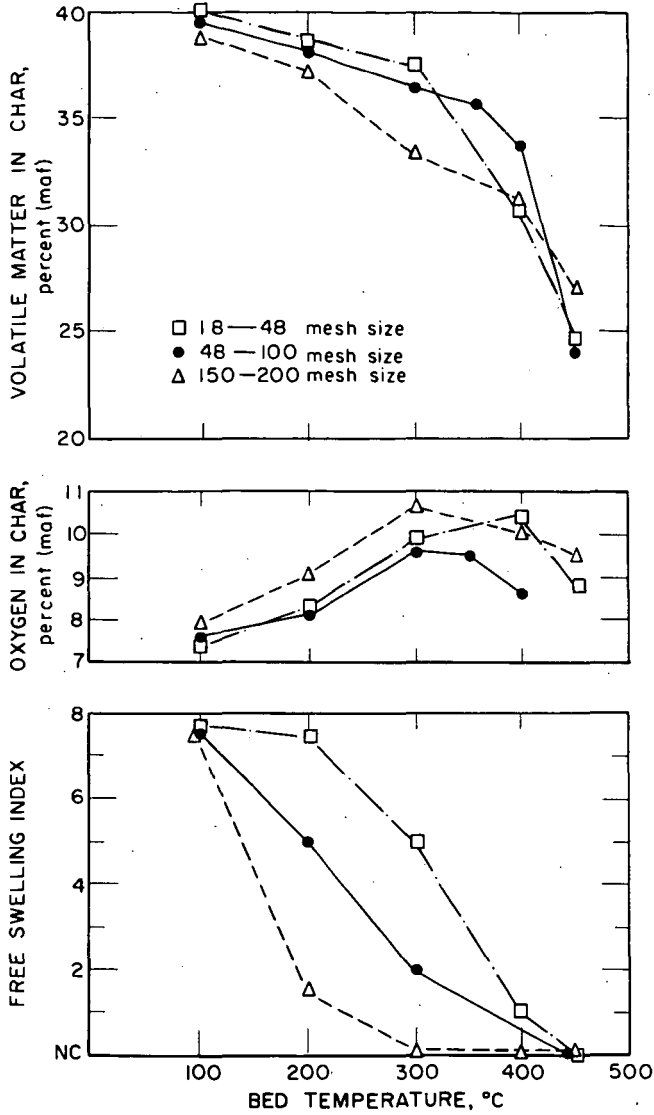


Fig. 3.-EFFECT OF TEMPERATURE DURING AIR TREATMENT IN A FLUID BED ON THE FSI, VOLATILE MATTER, AND OXYGEN CONTENT OF CHARS OF PITTSBURGH-SEAM COAL. RESIDENCE TIME IS ABOUT 40 MINUTES.

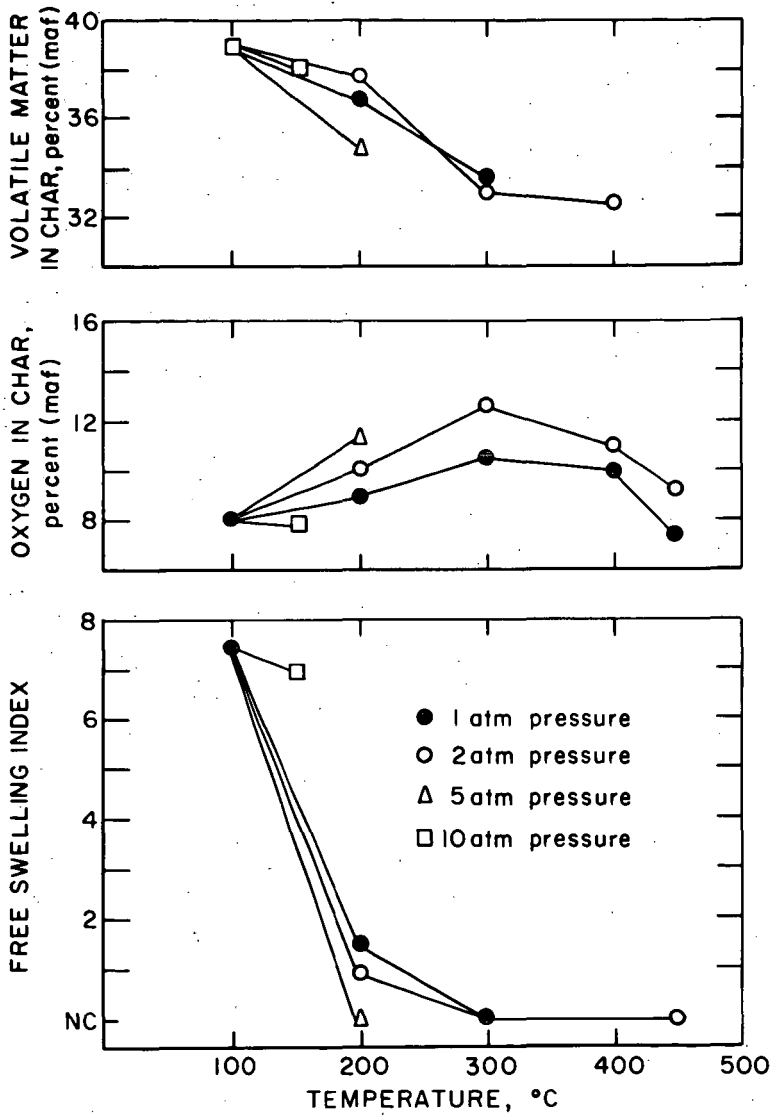


Fig. 4.-EFFECT OF PRESSURE DURING AIR OXIDATION IN A FLUID BED OF PITTSBURGH-SEAM COAL (150-200 MESH) ON FSI, VOLATILE MATTER, AND OXYGEN CONTENT OF CHAR. RESIDENCE TIME IS 40 MINUTES.

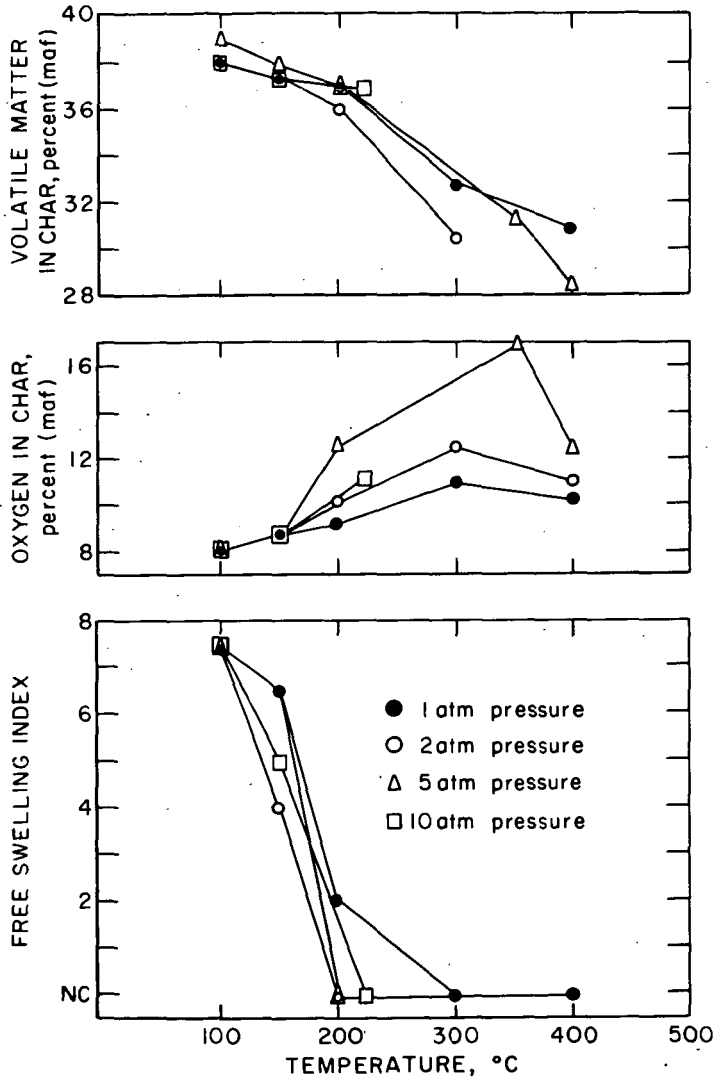


Fig. 5.-EFFECT OF PRESSURE DURING AIR OXIDATION IN A FLUID BED OF PITTSBURGH-SEAM COAL (150-200 MESH) ON FSI, VOLATILE MATTER, AND OXYGEN CONTENT OF CHAR. RESIDENCE TIME IS 20 MINUTES.

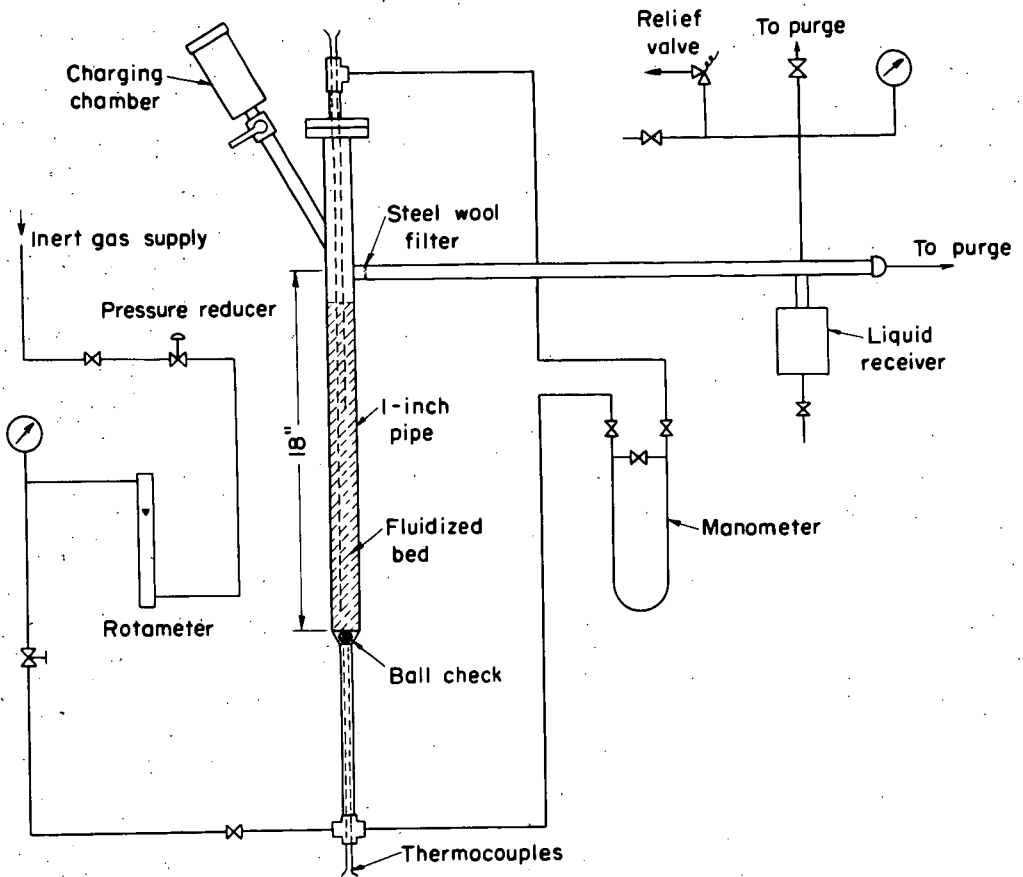


Fig. 6.-ONE-INCH REACTOR FOR CARBONIZATION TESTS

MOLTEN SALT CATALYSTS FOR HYDROCRACKING OF POLYNUCLEAR HYDROCARBONS

C. W. Zielke, R. T. Struck, J. M. Evans, C. P. Costanza, and E. Gorin

Research Division  
Consolidation Coal Company  
Library, Pennsylvania

INTRODUCTION

Intensive investigation has been underway for some time in the laboratories of Consolidation Coal Co. of various catalytic systems for the hydrocracking of coal "extract" to distillate oils. The extraction process and its integration with subsequent hydrocracking operations is described in several recent patents.<sup>(8)</sup>

Contact catalysts for hydrocracking of the extract have been extensively investigated in our laboratories both in batch and in small continuous hydrocracking units. The hydrocracking of coal extract using a contact catalyst in a three-phase fluidized system will be demonstrated on a 50 barrel/day pilot plant now being constructed at Cresap, W. Va.

Sulfur-resistant catalysts of the hydrofining type have given the most satisfactory results. These usually comprise a combination of the sulfides of Mo, Ni and Co on alumina gel support. Best results are obtained with large-pore alumina supports.

Rapid and efficient hydrogenolysis of the coal extract is effected at temperatures in the range of 800-825°F and at conversion levels up to about 60%.

The hydrogenated non-distillable residue from this operation, however, is much more refractory than the feed extract, and can be converted at practical rates only by raising the operating temperature. Although this is practical to do, the yield of the more valuable liquid products is lowered since the gas yield rises with increasing operating temperatures.

The limiting kinetic factor in the use of the "hydrofining" type catalyst is their very low cracking activity.

Dual function contact catalysts promoted by the use of acidic cracking agents were investigated to determine if they would be useful in conversion of the hydro residue. As the work to be reported below shows, this type of catalyst does not actually give improved performance since the acid sites are rapidly poisoned by the nitrogen content of the feed.

Attention was therefore turned to the development of a fused metal halide catalyst system.

The use of massive quantities of the catalyst was found to be desirable not only to develop the maximum hydrocracking activity but to "overwhelm" any nitrogen poisons in the feedstock. Fused salts were emphasized since the process under development visualizes continuous circulation of melt between hydrocracking and a regeneration operation where the nitrogen poisons would be removed.

The development of the massive fused salt catalyst system was initiated by a study of their activity in comparison with contact catalysts in the hydrocracking of hydro residue and a model polynuclear hydrocarbon: pyrene.

A voluminous literature exists on the use of metal halide catalysts in the hydrocracking of coal and coal tar. In many cases, the metal halide was not introduced directly as such but in all likelihood was generated in part in situ by reaction of a halogen promoter with the free metal or with a metal salt.

Excellent review articles<sup>(17,18)</sup> and books<sup>(8,11)</sup> are available summarizing this work so that there is no need to extensively discuss the original references.

In all of this work relatively small amounts of catalyst, i.e., less than 5 wt. % of the feed and generally of the order of 1 wt. % or less were employed. Under these conditions most investigators<sup>(13,14,20)</sup> agree that halogen promoted tin catalysts are the most active of this class. The superiority of tin catalysts over zinc catalysts when used in small concentrations is further illustrated by the fact that there have been no commercial coal hydrogenation operations using zinc catalyst while there were commercial operations in both England<sup>(4,7)</sup> and Germany<sup>(11)</sup> which used tin catalysts.

In addition, excellent results equal or superior to those with  $ZnCl_2$  have been obtained with 1% nickelous chloride<sup>(19)</sup> catalyst when proper methods of distribution of the catalyst on the substrate were used.

The above order of activity has no relationship to the cracking activity of these catalysts. Zinc chloride is well known as a Lewis acid type catalyst<sup>(3)</sup> which has fairly good catalytic activity for most Friedel Crafts type reactions such as polymerization of olefins, alkylation of aromatic compounds with olefins, etc. It also is well known as a cracking catalyst and has been used, for example, for the catalytic cracking of shale oil.<sup>(6)</sup>

Stannous chloride, however, is not well known as an active Lewis acid although it does have electron accepting properties as evidenced by its formation of ammoniate complexes such as  $SnCl_2 \cdot NH_3$ . It is reported to have some catalytic activity of the Friedel Crafts type for reactions such as the polymerization of certain unsaturated compounds such as vinyl ethers,<sup>(12)</sup> and the acetylation of olefins, i.e., reaction of acetic anhydride with 2,4,4-trimethyl pentene-1.<sup>(1)</sup> However, in general, it must be regarded as a very weak Friedel Crafts type catalyst with very little cracking activity as compared with  $ZnCl_2$ .

There is little or no evidence likewise that nickelous chloride has any substantial cracking or Friedel Crafts activity.

Weller<sup>(18)</sup> has pointed out that there is sufficient sulfur in most of the feedstocks to decompose the metal halides, in the small quantities used, by the reaction



and therefore concludes that the halide is not the true catalyst. Rather he proposes that the catalyst is really a dual function one in that the HCl is a splitting or cracking catalyst while the tin acts as a hydrogenating component to stabilize the reactive fragments by reaction with hydrogen. In this respect, the point of view is quite similar to the commonly accepted mechanism of the action of dual function contact catalysts used for hydrocracking of petroleum feedstocks. In this latter case, the role of the hydrogenating metal is regarded<sup>(13)</sup> as one of prevention of coke deposits by hydrogenation of highly unsaturated intermediates formed by catalytic cracking on the acid sites of the catalyst.

The above theory in the case of tin, however, is difficult to accept since there are no experimental facts with pure organic compounds which show that either tin metal or tin sulfide per se has any substantial hydrogenating activity.

It may be, as a matter of fact, that the unique position of tin chloride in the hydrogenolysis of coal is due to its known better thermodynamic stability towards decomposition by hydrogen sulfide as compared with zinc chloride, for example,

Equilibrium constants at 700°K for reaction (1) of SnCl<sub>2</sub> and ZnCl<sub>2</sub> with H<sub>2</sub>S were calculated from available thermodynamic data with the results shown below:

$$K_M = \frac{P_{HCl}^2}{P_{H_2S}} \quad K_{Zn} = 400 \quad K_{Sn} = 1.5$$

It is thus clear that tin chloride is much more stable than zinc chloride and that under equivalent operating conditions with the same quantity of promoter, etc., that a much higher percentage of the tin will be present as tin chloride.

Thus, it appears possible that in contradistinction to the opinion expressed by Weller,<sup>(18)</sup> the true catalyst is the small amount of undecomposed metal halide and that no dual function catalysis is involved.

Another object of the present investigation therefore was to obtain a better understanding of the catalytic activity of molten metal halides in hydrocracking processes. A pure compound, i.e., pyrene, was used to eliminate complications due to the interaction of the metal halide with hetero atom impurities and also to simplify analytical interpretation of the results. Massive quantities were used to insure the presence of a definite molten halide phase and because of the greater catalytic activity when massive quantities are used.

One of the points that was felt desirable to clarify was to what extent satisfactory operation and activation of hydrogen could be achieved with a molten halide catalyst without the addition of a separate hydrogenating component. The prior hydrocracking literature is not wholly clear on this point. There are, however, some references which showed that AlCl<sub>3</sub> and FeCl<sub>3</sub><sup>(10)</sup> have definite catalytic activity for the hydrocracking of naphthalene. Only a small percent of catalyst was used such that no molten halide was likely present and rather severe conditions, i.e., 460°C for 3 hours were employed. Sixty percent conversion to single ring aromatic hydrocarbons was reported.

Similar results were obtained with anthracene although a lower yield of low boiling aromatics was obtained.

Winter and Free<sup>(21)</sup> subsequently investigated the hydrocracking of naphthalene, anthracene and phenanthrene with FeCl<sub>3</sub> and AlCl<sub>3</sub> catalysts at hydrogen pressures of 190-250 atms. and temperatures in the range of 350-490°C. They observed the formation of significant quantities of pitchy condensation products as well as lower boiling aromatic liquids. Again, small quantities of catalyst were used.

Another pertinent reference is that of Schmerling and Ipatieff<sup>(16)</sup> who showed that aqueous zinc chloride impregnated on alumina was an active catalyst for the hydrocracking of naphthalene.

#### Materials Used

Pyrene - Obtained from Gesellschaft Fur Teerverwertung MBH, m.p. = 149-151°C, b.p. = 393.5°C, purity = 98%. Typical analysis of the feedstock is shown in Table I.

Hydro Residue - The hydro residue used for runs in Table III was produced by hydrocracking a coal extract in a continuous fluidized bed unit using a nickel molybdate catalyst described below. The residue represents 29% of the extract fed and is free of material boiling below 400°C. The extract was obtained by extracting a high volatile bituminous coal from the Pittsburgh Seam, Ireland Mine, with tetralin, and amounted to 57% of the moisture- and ash-free coal. Some properties of the hydro residue are given in Table I.

Benzene - Fischer Scientific Co. Certified Reagent, Thiophene-free.

### Catalysts

1. Nickel Molybdate on Alumina - A commercial hydrofining catalyst, containing 6.8% molybdenum, 3.8% nickel, and 0.1% cobalt supported on alumina gel. Unless otherwise noted, this catalyst was presulfided with 15% H<sub>2</sub>S - 85% H<sub>2</sub> at 500°F. It has a surface area of 200 m<sup>2</sup>/g, a porosity of 77%, and an average pore diameter of 200 Å.
2. Fluorided Nickel Molybdate on Alumina - The above sulfided catalyst which was treated with 4 mole percent HF in nitrogen at 300°C until it consumed HF corresponding to 10% of its weight.
3. Nickel Molybdate on Silica-Alumina - Active metals corresponding to those in Catalyst No. 1 (6.8% Mo, 3.8% Ni, and 0.1% Co) were locally impregnated on Houdry S-90, a 12.5% alumina cracking catalyst with a surface area of 430 m<sup>2</sup>/g, a porosity of 65%, and an average pore diameter of 70 Å.
4. Zinc Chloride - Fisher Scientific Co. Certified Reagent, various lots 96.2 to 98.8% pure, dried before use by heating in a vacuum at 110°C. After this treatment, it contained 1 to 1.5% water and up to 1.8% ZnO.
5. Stannous Chloride - Fisher Scientific Co. Certified Reagent, SnCl<sub>2</sub>·2 H<sub>2</sub>O, heated before use at 150°C and 1 mm Hg pressure for 2 hours to remove water.
6. Aluminum Bromide - Fisher Scientific Co. Certified Reagent, Anhydrous, 99% pure.
7. Nickel Molybdate Catalyst Impregnated with Zinc Chloride - A solution of zinc chloride in methyl ethyl ketone was used to impregnate Catalyst No. 1, following the procedure used by Innes for determining catalyst porosity.<sup>(8)</sup> The solvent was removed by heating at 60°C and atmospheric pressure overnight, followed by two hours at 200°C and 1 mm Hg pressure. The final catalyst contained 19% zinc chloride.
8. Zinc Chloride on Alumina - American Cyanamid gamma alumina stabilized with 2% silica was impregnated with 19% zinc chloride by the same procedure as for Catalyst No. 7. The alumina had a surface area of over 225 m<sup>2</sup>/g, and an average pore diameter of 80-100 Å.
9. Mixtures - Runs 2 and 3 were made with mixtures of Catalyst No. 1 and a salt catalyst. These were added separately to the autoclave.

### Equipment

The basic unit for the hydrocracking tests was an American Instrument Co., Catalog No. 40-2150 rocking autoclave. The normal rocking motion of 36 cycles/sec. about the axis of the autoclave was found to give good catalyst mixing only if the catalyst was 35x65 mesh or finer. In order to test catalysts of 1/16-inch diameter such as were being used on continuous units, the autoclave and furnace were mounted on the end of a 12-inch arm, so that a shaking motion resulted rather than rocking. The autoclave was driven at 86 cycles/sec. through an angle of 30° at the end of the 12-inch lever arm as shown in Figure No. 1.

Other features of the test unit are evident from Figure No. 1. Hydrogen can be frequently added to the autoclave during the run to maintain pressure. Hydrogen consumption is measured directly by the change in pressure on the 300 ml accumulator. The accumulator is isolated from the compressor during a run and a precision Heise gauge indicates the pressure to ± 10 psi.

### Procedure for Hydrocracking Tests

The 300 ml autoclave is weighed and 50 grams of feed plus the required weight of catalyst added. The autoclave is then closed, evacuated through valve V-2, and pressure tested with 1000-1500 psig of hydrogen from the accumulator. Heating is then commenced with V-3 closed.

When the temperature approaches the area where reaction will begin (ca. 300°C), V-3 is opened and the reactor pressure watched for evidence of hydrogen consumption. Hydrogen is thereafter supplied as needed in frequent increments from the accumulator until the full hydrogen pressure is reached when reaction temperature is reached. Thereafter, pressure is maintained, if necessary, by more hydrogen additions. The rate of temperature rise is controlled to average 10°C/min. to 375°C. From 375°C to the maximum temperature requires 5 to 15 minutes depending upon the temperature used and the extent of the exothermic reaction obtained. The temperature is then held at the desired level for a set time (usually one hour), and then lowered rapidly to 250°C via an air blast. After reaching 250°C, the motion is stopped, valve V-3 is closed, and the temperature maintained during depressuring of the lines. The line from the accumulator to the autoclave is disconnected at V-3 and replaced with the line (dashed) to the recovery train. The train is evacuated through V-4, and the contents bled off through a dry-ice-acetone cold trap, an Ascarite trap to remove acid gases, and into a gas holder.

### Analysis of Hydrocracked Products from Runs Using Zinc Chloride

The gases passing through the cold trap from the 250°C bleed-off are metered and analyzed on a molecular sieve gas chromatograph column (Linde 5A, Medium Grade). The hydrogen gas remaining after the run is subtracted from that fed from the accumulator to give the overall hydrogen consumption for the run. The volatile materials in the cold trap are bled into an evacuated bottle by placing the cold trap in ice water until the sample bottle reaches 1 atm. The cold trap is then connected to an evacuated stainless steel bomb immersed in dry-ice-acetone and the original trap allowed to rise to room temperature. The volatile products collected in the glass sample bottle and the stainless bomb are subsequently analyzed for C<sub>1</sub> to C<sub>7</sub> hydrocarbons on a gas chromatograph (hexamethylphosphoramide supported on Chromosorb W). The light oil and water remaining in the original cold trap are separated and analyzed.

The product remaining in the autoclave at 250°C is removed after cooling to room temperature, using a mixture of organic solvent (carbon disulfide for pyrene runs, benzene for extract hydro residue runs) and water. The residue is repeatedly washed with water in a Waring Blender and filtered until free of chloride ion. The filtrates are separated into water and organic phases and each washed until water is free of organics and the organic phase free of chloride.

The filter cake from the final water wash is Soxhlet extracted with methyl ethyl ketone (MEK). The soluble fraction is combined with the organic filtrate phase and distilled.

The MEK-Insoluble material in the Soxhlet thimble includes zinc oxide and zinc sulfide as well as organic residue. The amounts of each are determined by analysis.

The procedures for tin chloride or combined catalyst runs followed the above format with very minor modifications. Where only a supported catalyst was involved, the procedure simplified to pressure filtration (20 psi), MEK extraction of the catalyst and sampling of the filtrates.

### Product Boiling Range

Boiling ranges of the pyrene products were determined by gas chromatography using a silicone rubber column at 170°C with flame ionization detector. This permitted CS<sub>2</sub> to be used as a solvent for solid fractions without interference. A fairly simple pattern of about 20 peaks resulted.

Products from runs in which hydro residue was fed were vacuum distilled to give the distillate distribution because of the more complicated nature of the feed.

Hydrogen consumption is determined directly from hydrogen fed and recovered. Conversion is calculated by subtracting the recovered residue (+400°C) from the weight of feed and dividing the difference by the weight of feed.

A measure of the asphaltic nature of extracts and hydro residue (Table I) is given by solvent fractionation. "Benzene-Insolubles" is the fraction of extract insoluble in benzene at its atmospheric boiling point (Soxhlet apparatus). "Asphaltenes" is the benzene-soluble, cyclohexane-insoluble fraction, determined by mixing one part of benzene-soluble material with nine parts of benzene and 100 parts of cyclohexane, by weight, and filtering at room temperature. The fraction soluble in this mixture is termed "oil".

## RESULTS AND DISCUSSION

### Contact Catalysts with Cracking Promoters

The first approach used in attempting to enhance the cracking activity of the contact-type catalyst was to add cracking promoters. One method used was to incorporate the promoters in the contact-type catalysts either by impregnation with zinc chloride or by fluorination in the vapor phase with anhydrous hydrofluoric acid. Another method employed was to impregnate the hydrogenating metals on an active silica-alumina cracking catalyst base. Still another method was investigated in which the cracking catalyst, i.e., zinc chloride was not impregnated on the support but was simply added as a separate component to the autoclave. Finally, the use of a cracking catalyst by itself, i.e., zinc chloride impregnated on  $\gamma$ - $\text{Al}_2\text{O}_3$  was investigated without the addition of hydrogenating metals. The activity tests with pyrene feedstock are summarized in Table II. All runs were carried out at standardized conditions, i.e., a total hot pressure of 4200 psig and 1 hour residence time at the operating temperature of 427°C.

Runs 2 and 5 contained the same quantity of zinc chloride in each case, the only difference being that in the former case the zinc chloride was added as a separate component while in the latter case it was first impregnated on the nickel molybdate catalyst.

No detailed structural investigation was made of the products of the reaction. The boiling ranges of Table II, however, correspond roughly to the following classes of compounds as given below:

340 x 390°C	Partially Hydrogenated Pyrenes
280 x 340°C	Alkylated and Partially Hydrogenated Phenanthrenes
200 x 280°C	Alkylated and Partially Hydrogenated Naphthalenes
$\text{C}_5$ x 200°C	Alkyl Benzenes, Single Ring Naphthenes and Paraffins

In interpreting results, it should be noted that the hydrocracked product consists only of products boiling below 340°C. The pyrene is very readily hydrogenated such that in almost all cases very little remains completely unconverted.

In almost all cases an increase in hydrocracking activity was obtained by addition of the cracking promoter. This is evidenced by an increase in the yield of  $\text{C}_5$  x 340°C distillate products as well as a substantial increase in the hydrogen consumption. A lone exception was stannous chloride. Here, the very low cracking activity of the metal halide was more than compensated for by a decreased activity of the contact catalyst. The latter may be due to coating of the contact catalyst with the molten salt. Zinc chloride, however, is such a strong cracking catalyst that it acts as a net promoter in spite of the fact that the same type of deactivation by coating of the

contact catalyst is possible here too. As a matter of fact, it appears to be slightly more active when added separately than when it is impregnated on the catalyst before use.

It is interesting to note that  $ZnCl_2$  on  $Al_2O_3$ , even without the hydrogenating metals, has hydrocracking activity although it is less than that of the nickel molybdate catalyst by itself. It also shows a relatively high coke yield which may possibly be attributed to the absence of hydrogenating metals. It is clear, however, as was shown by Schmerling and Ipatieff,<sup>(16)</sup> that zinc chloride even in the absence of hydrogenating metals is capable of activating hydrogen for the hydrogenation and hydrocracking of polynuclear aromatic hydrocarbons.

The activities of the other two "dual function catalysts" investigated, i.e., fluorided nickel molybdate and Co-Mo-Ni on a cracking catalyst base (Houdry S-90) are also higher than that of the nickel molybdate catalyst and are even slightly more active than the zinc chloride promoted catalysts for total conversion. They produce, however, more middle range boiling distillates and less gasoline. The yield of  $C_5 \times 200^\circ C$  distillate was 27.1% of the feed in the case of the zinc chloride catalyst and only 13.5% of the feed for the S-90 catalyst.

#### Ammonia Tolerance of Promoted Catalysts

The development of the dual function catalysts was aimed at their use, as mentioned above, in the hydrocracking of refractory residues from the hydrogenolysis of coal extract. These residues, as the data given in Table I show, contain substantial quantities of nitrogen of the order of 1 wt. % or more. Therefore, if these catalysts were to be of much use in such an operation, they must be relatively resistant to poisoning by  $NH_3$  and other nitrogen bases released during the hydrocracking process.

The investigation was therefore directed towards determining the activity of these catalysts as a function of the partial pressure of  $NH_3$  in the gas phase. In order to guide the experimental work, rough absorption isotherms for  $NH_3$  were determined for two of the above catalysts, i.e.,  $ZnCl_2$  on nickel molybdate and Co-Mo-Ni on S-90. These are shown in Figure 2.

The results are at least roughly correct since the  $350^\circ C$  isotherm for Catalyst No. 7 approaches the theoretical asymptotic value of 32 cc  $NH_3/gm$ . This value corresponds to the addition of 1 mole of  $NH_3$  to 1 mole of  $ZnCl_2$ .

Experiments were now conducted in which controlled amounts of  $NH_3$  were added such that the partial pressure of  $NH_3$  could be estimated after correction for the amount absorbed on the catalyst.

The results for three types of catalysts are summarized in Figure 3 where yields of distillates are plotted as a function of  $NH_3$  pressure. It is noted that even the nickel molybdate catalyst by itself suffers a loss of activity on addition of  $NH_3$ . The S-90 catalyst appears to be able to tolerate somewhat larger quantities of  $NH_3$  than the  $ZnCl_2$ -impregnated catalyst probably because the acidic sites are weaker and are more readily dissociated. This fact is evident from the absorption isotherms given in Figure 2.

Thus, to obtain a substantial improvement in activity over the nickel molybdate catalyst, the  $NH_3$  pressure must be maintained below about 5 psi for the  $ZnCl_2$  promoted catalyst or slightly higher for the S-90 catalyst. To achieve such low partial pressures of  $NH_3$  with high nitrogen feedstocks would require, in general, impractically high rates of hydrogen circulation. Consider a feedstock, for example, which releases 1 wt. % nitrogen as ammonia in a hydrocracking process wherein the hydrogen partial pressure is maintained at 200 atms. A hydrogen circulation rate of greater than 160 SCF/lb feed would be required in this case to maintain the partial pressure of  $NH_3$  below 5 psia in the outlet gas.

Autoclave tests were run with the hydro residue itself wherein the S-90 catalyst was compared with the nickel molybdate catalyst. The results of these tests are shown in Table III. It is seen that the high nitrogen content of the feedstock as expected has poisoned the activity of the S-90 catalyst such that it is less active than the nickel molybdate.

The activity of fused zinc chloride catalyst itself with no support or other additive was tested in massive quantities on this same feedstock with the results shown in Table III. In spite of the fact that a lower temperature was used, the molten zinc chloride catalyst more than doubled the conversion and hydrogen consumption. The selectivity of the process as measured by the quantity  $(C_1-C_3) \times 100/\text{conversion}$  is also improved with the molten zinc chloride catalyst.  $C_1-C_3$  here refers to the weight percent yield of methane, ethane plus propane.

Very noteworthy, likewise, is the high selectivity of the process for production of gasoline. Ninety-one percent of the distillate oils (b.p. below  $400^\circ\text{C}$ ) boil in the gasoline range in the case of the  $\text{ZnCl}_2$  catalyst, and only 52 percent in the case of the nickel molybdate catalyst.

Another distinctive feature of catalysis with massive quantities of zinc chloride is the high ratio of iso paraffins to n-paraffins produced as evidenced by the ratio of isobutane to n-butane of over 6/1. This phenomenon is observed with conventional "dual function" hydrocracking catalysts when the feedstock is free of nitrogen poisons. In this case the same phenomenon is observed by "over whelming" the nitrogen poisons with an excess of catalyst.

In contradistinction runs 8 and 9 using contact catalysts show a low ratio of iso to n-butane indicating that the acid cracking sites have been poisoned by the nitrogen bases in the feedstock.

These results point to the clear superiority of massive zinc chloride melts as a hydrocracking catalyst. The development is proceeding with the central concept of continuously circulating the molten halide catalyst to a regeneration step where the nitrogen poisons would be removed. Data on the effect of basic nitrogen on catalyst activity will be given in a subsequent paper.

#### Activity Tests of Molten Halide Catalysts with Pyrene Feedstock

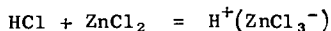
A series of further tests were made with pyrene feedstock to provide more background information for development of the molten halide catalyst system. Experiments were conducted to further clarify the effect of the quantity of catalyst used, the effect of the addition of cracking and hydrogenation promoters as well as a comparison of the activity of fused zinc chloride with other molten halide salts. The experimental results are summarized in Table IV.

It is noted that when the zinc chloride catalyst is used in relatively small amounts (in 7 percent by weight of the pyrene feed, Run 11), that the activity is quite low. The main reaction appears to be hydrogenation of pyrene to partially hydrogenated pyrenes with some hydrocracking to light distillates. The extent of hydrocracking is also much less than when the same amount of zinc chloride is used dispersed on an alumina support (cf. Run 7, Table II). However, when massive quantities of zinc chloride melt are used, i.e., Run 12, the hydrocracking of pyrene proceeds very vigorously. A much greater degree of hydrocracking is obtained than with any of the promoted contact catalysts discussed above. The result is also quite similar to that observed when massive quantities of zinc chloride melt were used for hydrocracking of extract residue (cf. Run 10, Table III). The characteristic high ratio of iso to n-butane (5.6/1) and high proportion of gasoline boiling range liquid, i.e., 91%, in the total  $C_5 \times 340^\circ\text{C}$  distillate is again observed.

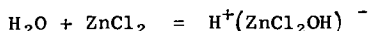
The coke plus tar yield was rather high in Run 12, i.e., 7.5% of the feed in spite of the relatively high pressure employed. Runs 13 and 14 were conducted to determine

if the addition of hydrogenating components to the melt, i.e.,  $\text{SnCl}_2$  and  $\text{MoO}_3$  would reduce the coke plus tar yield. Stannous chloride in the small amounts used was completely inert, i.e., no difference in results is apparent between Runs 12 and 13. Molybdc oxide (Run 14) did increase the hydrogen consumption and decrease the gas yield slightly, but actually caused an increase rather than a decrease in tar plus coke yield.

Runs 15 and 16 were conducted to determine what the effect of the addition of cracking promoters to the melt would be.  $\text{HCl}$  potentially can form the unstable Friedel Crafts acid by the reaction,



while water can undergo a similar reaction,



The original melt was not completely anhydrous and usually contained about 1 wt. %  $\text{H}_2\text{O}$ . Thus, the addition of further quantities of water can increase the amount of acidic cracking catalyst by the above reaction.

It is seen that the addition of  $\text{HCl}$  is unfavorable in that it causes a large increase in the amount of coke. Water addition on the other hand increased the overall hydrogen consumption with only a slight increase in the amount of tar plus coke.

Run 17 was conducted to determine whether massive quantities of stannous chloride melt would behave similarly to zinc chloride. It is seen that it is a very weak catalyst and that practically no hydrocracking takes place. The only process observed is hydrogenation to partially hydrogenated pyrenes. It would appear that the relatively good activity of tin catalysts for hydrogenolysis of coal and coal extract must in some way be related to their activity with respect to scission of specific weak bonds that are not present in pyrene or its partially hydrogenated homologues.

Finally, one experiment (Run 18) was conducted using massive quantities of an  $\text{AlBr}_3$  melt. Due to the very high activity of this catalyst, it was not possible to run at comparable conditions used for the  $\text{ZnCl}_2$  catalyst. The experiment was run at a much lower temperature, i.e.,  $300^\circ\text{C}$ ; and a lower pressure, i.e., 3000 psig. As a matter of fact the absorption of hydrogen was initially so rapid that the pressure fell considerably below 3000 psig at first. This may be the reason for the fairly high yield of tar obtained.

It is obvious, however, that  $\text{AlBr}_3$  is a much more active catalyst than zinc chloride. The conditions chosen were too severe in that, outside of the tar produced, the feed pyrene was almost completely degraded to low molecular weight paraffins in the range of  $\text{C}_1$  to  $\text{C}_6$ . The  $\text{C}_5 \times 150^\circ\text{C}$  distillate, as determined by gas chromatography, showed the composition given below:

	Wt. % of Cut
Isopentane	48.2
n-Pentane	18.2
2,2-Dimethyl Butane	1.8
2,3-Dimethyl Butane )	
2-Methyl Pentane )	8.2
3-Methyl Pentane	3.7
n-Hexane	2.5
Methyl Cyclopentane	0.4
$\text{C}_7 +$	18.0
Total	100.0

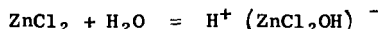
The zinc chloride catalyst is almost completely inactive for hydrocracking of single-ring aromatic hydrocarbons as the data of Table V show where benzene is used as a model compound. This is one reason that high yields of gasoline boiling range hydrocarbons are obtained with zinc chloride melt catalyst. In other words, the hydrocracking process is suspended after aromatic hydrocarbons boiling in gasoline range are produced. Other experiments showed that the whole gasoline fraction including aromatics, naphthenes and paraffins are resistant to further hydrocracking by zinc chloride catalyst.

This is not true of aluminum halide catalysts since it is clear that continued hydrocracking to produce predominantly propane and butanes occurred under the conditions used. The effect of using milder operating conditions with aluminum halide catalysts is now being investigated.

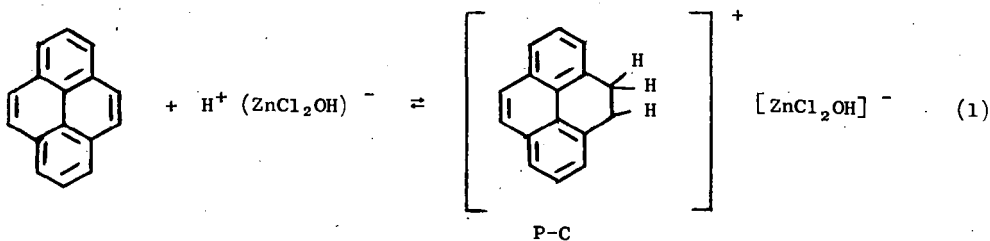
Mechanism of Hydrocracking with Molten Halide Catalysts

The investigation was not aimed at specifically unravelling the mechanism of the hydrocracking process so that one can only speculate on this question.

The nature of the active catalyst is not clear but is likely a Friedel Crafts acid. As stated above, no precautions were used to completely dehydrate the zinc chloride melts used and they usually contained about 1 wt. % of water. Thus, the active catalyst may be the acid produced by interaction of zinc chloride with water

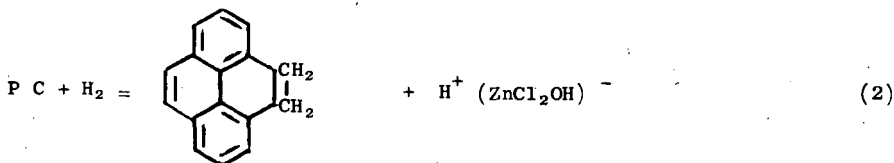


The first step in hydrocracking is likely the addition of the Friedel Crafts acid to the labile unsaturated bond between the 9 and 10 carbon atoms of the pyrene ring.



This is similar to the first step in the mechanism proposed by Schmerling<sup>(15)</sup> and others for alkylation of isoparaffins with olefins using Friedel Crafts catalysts.

The aromatic-catalyst complex, written as P C, can then react with hydrogen to regenerate the catalyst and produce 9,10-dihdropyrene as follows:



This basic mechanism for hydrogenation can continue for further absorption of hydrogen, scission reactions leading to ring opening and dihydroalkylation, etc.

Experiments were carried out to determine the miscibility of  $ZnCl_2$  and pyrene in one another. After mixing an equal weight of the two components at  $350^\circ C$ , no appreciable separation of phases could be detected on standing for one hour. Whether one is dealing with a true solution or relatively stable emulsions is not certain at this time.

The high dependence of reaction rate on catalyst concentration would not be surprising if one is dealing with a homogenous solution of catalyst and hydrocarbon reactant.

It is not clear at present whether the results reported here are unique to molten halide Friedel-Crafts catalysts. It is possible that similar results can be obtained with some liquid protonic acids such as phosphoric acid, hydrofluoric acid, hydroxy fluoboric acid, etc., once proper conditions are selected. Experiments are now in progress to check these possibilities. Preliminary results indicate that phosphoric acid is inactive for hydrocracking of pyrene at  $300^\circ C$  and 3000 psig hot pressure.

#### ACKNOWLEDGMENT

The sponsorship of the U. S. Office of Coal Research for this investigation is gratefully acknowledged.

#### LITERATURE CITED

- (1) Armand, Paul, *Compt. Rend.* 244, pp. 1785-7 (1957).
- (2) Beuther, Harold and Larson, O. A., *Ind. Eng. Chem.* 4, 177 (1965).
- (3) Calloway, N. O., *Chem. Reviews*, 17, 376 (1935).
- (4) Cochran, C. and Sawyer, E. W., *Ind. Chemist* 35, 221-9 (1959).
- (5) Donath, E. E., "Hydrogenation of Coal and Tar".  
*Chemistry of Coal Utilization*, H. H. Lowry, Editor  
Supplementary Volume, pp. 1041-1080,  
John Wiley and Sons, Inc., New York, 1963.
- (6) Faingold, S. I. and Vallas, K. R., *Izvest. Akad. Nauk. Eston. SSR  
Ser Tekhi Fiz. - Mat. Nauk*, 6, 245-51 (1957).
- (7) Gordon, K., *J. Inst. Fuel*, 20, 42-58 (1956).
- (8) Gorin, Everett - U. S. Patents  
3,018,241 Jan. 23, 1962  
3,018,242 Jan. 23, 1962  
3,117,921 Jan. 14, 1964  
3,143,489 Aug. 4, 1964  
3,162,594 Dec. 22, 1964
- (9) Innes, W. B., *Oil Gas J.*, 54, No. 80, p. 162, Nov. 12, 1956.
- (10) Kling, André and Florentin, Daniel, *Compt. Rend.* 182, 526 (1926).  
*Ibid.* 184, 822 (1927).
- (11) Kronig, W., *Die Katalytische Druckhydrierung*, Berlin Springer (1950).
- (12) Losev, I. P. and Trostyanshaya, E. B., *J. Gen. Chem. USSR* 17, 122-9 (1947).

- (13) Pelipetz, M. G., Kuhn, E. M., Freedman, S. and Storch, H. H., *Ind. Eng. Chem.* 40, 1259 (1948).
- (14) Sato, F., Morikawa, K., Morikawa, R., Okamura, T., *J. Soc. Chem. Ind., Japan* 45, 892-903 (1942).
- (15) Schmerling, Louis - Chapter XXV, Vol. II, Part 2 in Friedel Crafts and Related Reactions  
Interscience Publishers, New York 1964.
- (16) Schmerling, Louis and Ipatieff, V. A.  
U. S. Patent 2,388,937 - November 13, 1945.
- (17) Storch, H. H., "Hydrogenation of Coal and Tar".  
Chemistry of Coal Utilization, H. H. Lowry, Editor  
Vol. II, pp. 1750-1796  
John Wiley and Sons, Inc., New York, 1945.
- (18) Weller, S. - Catalysis, Vol. IV, Chapter 7, pp. 513-527, Edited by P. H. Emmett.  
Reinhold Publishing Co., New York 1956.
- (19) Weller, S. and Pelipetz, M. G., *Ind. Eng. Chem.* 43, p. 1243 (1951).
- (20) Weller, S., Pelipetz, M. G., Freedman, S., and Storch, H. H.  
*Ind. Eng. Chem.* 42, pp. 330-334 (1950).
- (21) Winter, H. and Free, G., *Brennstoff Chem.* 12, pp. 451-453 (1931).

TABLE I

Analysis of Feedstocks

<u>Feed</u>	<u>Pyrene</u>	<u>29% Residue (+400°C) from Extract Hydrogenation</u>
H	4.94	6.82
C	94.87	90.79
N	0.02	1.17
O	0.06	1.07
S	0.11	0.15
Benzene-Insolubles	--	3
Asphaltenes	--	30
Oil	--	67

TABLE II

Comparison of Activity of Various Contact Catalysts  
Effect of Promotion with Acid Cracking Catalysts

Hydrocracking of Pyrene at 427°C and 4200 psig Hot Pressure  
Residence Time at Temperature = 60 min.

Run No.	1	2	3	4	5	6	7
Contact Catalyst	Sulfided Nickel Molybdate	ZnCl <sub>2</sub>	SnCl <sub>2</sub>	Fluorided Nickel Molybdate	ZnCl <sub>2</sub> on Nickel Molybdate	Co-Mo-Ni on S-90	ZnCl <sub>2</sub> -Al <sub>2</sub> O <sub>3</sub>
Other Catalyst	None	ZnCl <sub>2</sub>	SnCl <sub>2</sub>	None	--	--	--
Contact Catalyst (Wt. Ratio) Pyrene	0.30	0.30	0.30	0.30	0.37	0.30	0.37
Other Catalyst (Wt. Ratio) Pyrene	0	0.07	0.07	0	--	--	--
Yields, Wt. % of Pyrene Feed							
CH <sub>4</sub>	0.0	0.4	0.2	0.0	0.4	0.2	0.5
C <sub>2</sub> H <sub>6</sub>	0.3	1.3	0.8	0.2	1.2	0.6	1.4
C <sub>3</sub> H <sub>8</sub>	0.7	1.7	1.4	0.5	1.3	1.1	1.6
C <sub>4</sub> H <sub>10</sub>	0.0	0.6	0.1	0.2	0.3	0.5	0.5
C <sub>5</sub> x 150°C Dist.	2.7	15.8	2.9	5.8	22.1	6.4	4.1
150 x 200°C Dist.	0.0	8.4	1.3	0.2	5.0	7.1	2.2
200 x 280°C Dist.	27.1	17.5	11.1	9.3	11.4	15.4	8.5
280 x 340°C Dist.	18.7	20.5	15.8	68.5	16.3	45.9	16.8
340 x 390°C Dist.	52.6	35.6	59.9	21.4	42.7	26.8	47.4
Pyrene	2.6	1.9	9.0	0.0	3.2	0.6	13.6
Coke on Catalyst	0.6	2.8	1.6	0.9	2.1	1.9	7.0
Total Including H Consumed	105.3	106.5	104.1	107.0	106.0	106.6	103.6
H Consumed, Wt. %	5.33	6.56	4.12	6.98	5.98	6.62	3.56

TABLE III

Comparison of Contact Catalysts with ZnCl<sub>2</sub> Melt for Hydrocracking of Extract Hydro Residue

Total Pressure = 4200 psig - Residence Time at Temperature = 60 min.

Run No.	<u>8</u>	<u>9</u>	<u>10</u>
Catalyst	Co-Mo-Ni on S-90	Sulfided Nickel Molybdate	ZnCl <sub>2</sub> Melt
Temperature, °C	441	441	427
Catalyst/Feed, Wt. Ratio	0.3	0.3	1.00
<u>Yields, Wt. % MAF Feed</u>			
CH <sub>4</sub>	1.1	1.1	1.2
C <sub>2</sub> H <sub>6</sub>	1.2	1.2	1.5
C <sub>3</sub> H <sub>8</sub>	1.6	1.6	4.6
iC <sub>4</sub> H <sub>10</sub>	0.2	0.1	5.0
nC <sub>4</sub> H <sub>10</sub>	1.0	1.2	0.8
C <sub>5</sub> x 150°C Dist.	7.0	9.1	52.5
150 x 200°C Dist.	1.7	8.4	10.4
200 x 400°C Dist.	16.9	16.1	6.3
MEK-Sol. + 400°C Residue	67.5	60.2	19.0
MEK-Insol. + 400°C Residue	2.9	2.4	3.4
Conversion, Wt. % Feed	29.6	37.4	77.6
H <sub>2</sub> Consumed, Wt. % Feed	2.64	3.14	6.85
(C <sub>1</sub> -C <sub>3</sub> ) x 100/Conversion	13.4	10.5	9.5

TABLE V

Hydrocracking of Benzene with Zinc Chloride Catalyst

Temperature = 427°C - Residence Time at Temperature = 60 min.  
Total Hot Pressure = 4200 psig

Yields, Wt. % of Benzene Feed

CH <sub>4</sub>	-	.04
C <sub>2</sub> H <sub>6</sub>	-	.09
C <sub>3</sub> H <sub>8</sub>	-	.92
iC <sub>4</sub> H <sub>10</sub>	-	.43
nC <sub>4</sub> H <sub>10</sub>	-	.14
C <sub>5</sub> H <sub>12</sub>	-	.24
Other C <sub>6</sub> 's	-	.42
Benzene	-	<u>99.00</u>
Total		101.28

H<sub>2</sub> Consumed = 0.94 wt. %

TABLE IV

Comparison of Molten Salt Catalysts for Pyrene Hydrocracking

All Runs - 60 min. Residence Time at Temperature

Run No.	11	12	13	14	15	16	17	18	
Temperature, °C	427	↔							300
Total Hot Pressure, psig	4200	↔							3000
Catalyst	ZnCl <sub>2</sub>	↔							SnCl <sub>2</sub> AIBr <sub>3</sub>
Catalyst/Pyrene, Wt. Ratio	0.07	1.0	1.0	1.0	1.0	1.0	1.0	1.0	
Catalyst Additive	None	None	SnCl <sub>2</sub>	MoO <sub>3</sub>	HCl	H <sub>2</sub> O	None	None	
Additive/Pyrene, Wt. Ratio	--	--	.02	.05	.021	0.08	--	--	
Yields, Wt. % Pyrene	↔								
CH <sub>4</sub>	0.0	0.8	0.8	1.0	2.3	1.0	0.0	1.8	
C <sub>2</sub> H <sub>6</sub>	0.1	1.4	1.6	2.3	4.3	2.3	0.2	1.8	
C <sub>3</sub> H <sub>8</sub>	0.5	11.2	11.4	9.7	11.1	10.6	0.2	25.2	
iC <sub>4</sub> H <sub>10</sub>	0.6	9.6	9.8	8.1	8.5	8.2	0.0	24.1	
nC <sub>4</sub> H <sub>10</sub>	0.1	1.7	1.6	1.2	1.8	1.1	0.0	19.1	
C <sub>5</sub> x 150°C Dist.	6.3	52.7	52.4	53.2	45.3	{ 0.0		24.5	
150 x 200°C Dist.	0.3	1.7	1.8	2.1	1.3	{ 66.8		--	
200 x 280°C Dist.	2.0	1.9	2.7	6.2	1.6	{ 0.9		--	
280 x 340°C Dist.	1.0	3.3	3.3	4.7	0.9	{ 3.0		--	
340 x 390°C Dist.	36.8	11.5	12.2	7.2	0.6	{ 11.8		--	
Pyrene	53.1	6.5	4.8	2.4	0.4	{ 49.9		--	
+Pyrene	--	2.5	2.7	3.1	9.1	{ 3.6		0.0	
Coke	--	5.0	4.2	8.6	21.5	{ 4.8		0.0	
Total	101.2	109.2	109.3	109.8	108.7	110.2	101.8	112.4	
H <sub>2</sub> Consumed, Wt. % Pyrene	1.23	9.21	9.31	9.85	8.68	10.23	1.8	12.4	

Figure 1  
**FLOW DIAGRAM**  
**FOR AUTOCLAVE UNIT**

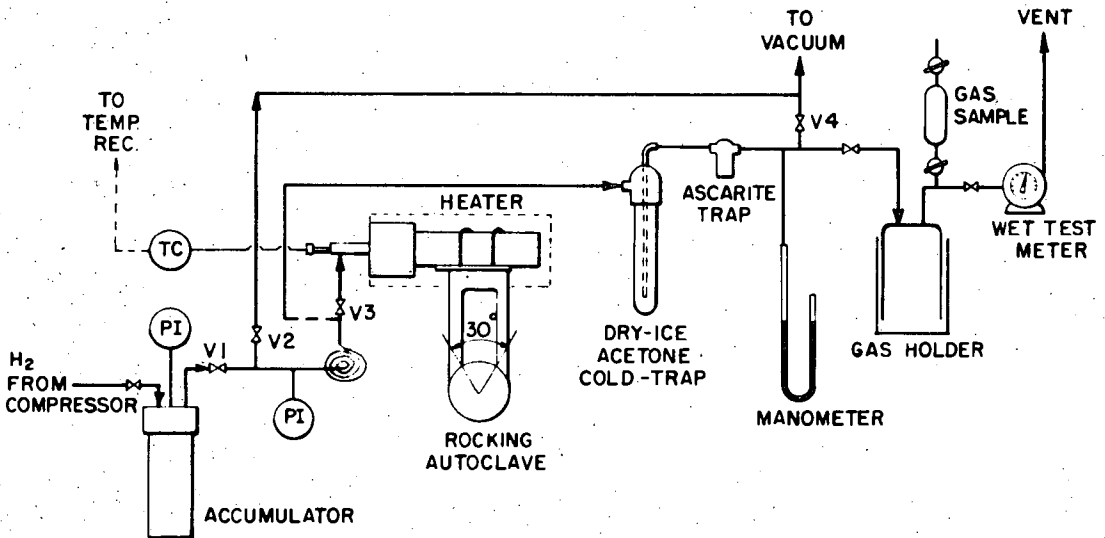


FIGURE NO. 2

Ammonia Adsorption Isotherms

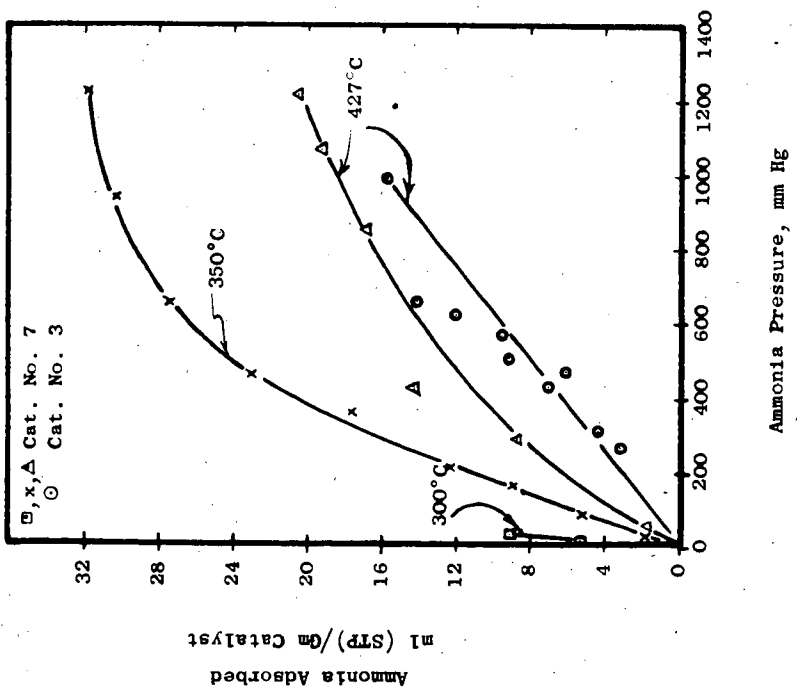
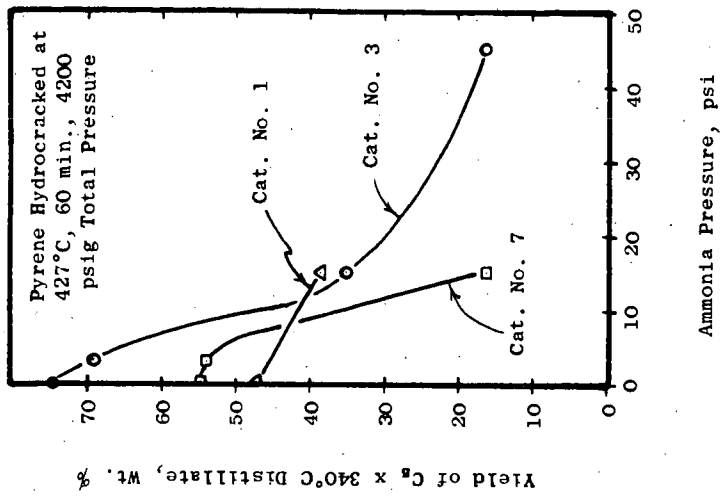


FIGURE NO. 3

The Effect of Ammonia Partial Pressure on Distillate Yields



MOLTEN ZINC HALIDE CATALYSTS FOR THE HYDROCRACKING OF COAL EXTRACT AND COAL

C. W. Zielke, R. T. Struck, J. M. Evans, C. P. Costanza, and E. Gorin

Research Division  
Consolidation Coal Company  
Library, Pennsylvania

INTRODUCTION

The background information leading to the development of fused metal halide catalysts for the hydrocracking of coal extract was discussed in a previous paper.<sup>(10)</sup> It was shown, therein, that metal halides which are strong Lewis acids are active catalysts for the hydrocracking of polynuclear hydrocarbons and residues from the hydrocracking of coal extract with contact catalysts.

The present paper describes the initial steps in the development of molten zinc chloride catalysts for the hydrocracking of coal extract and even coal itself. An extensive survey of the variables in the hydrocracking of coal extract with massive quantities of zinc chloride melt is presented. Comparative data are also presented with other catalyst systems. All data given here were obtained in batch autoclave experiments.

In addition to the zinc halides, several possible Lewis acid catalysts were considered such as  $\text{AlCl}_3$ ,  $\text{AlBr}_3$ ,  $\text{BF}_3$ , etc. These were rejected primarily because they would be completely destroyed by the steam released during the hydrogenation of coal extract. Also, as a consequence of the halogen acids released during hydrolysis of the catalyst, these materials would be much too corrosive to be useful in potential commercial systems.

Zinc bromide was found to be equivalent in activity to zinc chloride. It was rejected from further consideration because of cost.

Zinc chloride has been widely used as a catalyst in experimental work in coal hydrogenation although it has never been employed in commercial plants. No literature data are available on its activity for the hydrocracking of coal extract.

Small amounts of catalyst<sup>(9)</sup> of the order of 3 wt. % or less of the coal were used and frequently the catalyst was impregnated on the coal before use. There appears to be no record of the use of massive quantities of molten zinc chloride catalyst in the coal hydrogenation literature.

$\text{ZnCl}_2$  almost universally has been regarded as being inferior in activity to  $\text{SnCl}_2$  or halogen-promoted tin compounds<sup>(2,5,7,8,9)</sup> as a catalyst for coal hydrogenation. One exception to this is found in some Japanese work,<sup>(6)</sup> on hydrogenating coal to heavy oil at the relatively mild operating conditions of 410°C and 200 atm.

The work was carried out on a fairly large pilot plant scale using 1% of zinc chloride and other catalysts. Zinc chloride was found to be the best catalyst of these tested including tin.

## EXPERIMENTAL

The basic unit used in this work was a 300 ml shaking autoclave. This unit and the procedures involved have been described previously.<sup>(10)</sup> One added feature used in two series of runs at constant hydrogen pressure was the use of a palladium probe. A palladium tube, 1/8-inch I.D., .010" wall and 7 inches long from J. Bishop and Co., was inserted into the autoclave and suitably connected to a gauge to read hydrogen pressure. The ends were silver soldered and the interior of the tube nearly filled with a stainless steel wire for support. At temperatures of 750°F and above, diffusion of hydrogen through the tube was rapid enough to give adequate response to changing pressure. A new tube was used each time to ensure freedom from sulfur poisoning, although burning off between runs was also found to restore activity. The probe was protected from splashing autoclave contents by baffles.

The feedstock for most of this work was "standard" extract prepared by continuous extraction of Pittsburgh Seam coal, Ireland Mine. Tetralin solvent was used with a residence time of 46 minutes at 380°C. Unextracted coal and ash were removed by filtration of the extractor effluent in a pressure filter at 200°C. The final extract represents 53% of the MAF coal. Properties are given in Table I.

The zinc chloride used was Fisher Scientific Co. Certified Reagent, 96-98% pure, dried before use by heating in a vacuum at 110°C. After this treatment, it contained 1-1.5 wt. % water and up to 1.8 wt. % zinc oxide.

The nickel molybdate catalyst is a commercial hydrofining catalyst containing 6.8% molybdenum, 3.8% nickel, and 0.1% cobalt supported on alumina gel. It has a surface area of 200 m<sup>2</sup>/g, a porosity of 77%, and an average pore diameter of 200 Å. It was used as 1/16-inch diameter beads, presulfided with 15% H<sub>2</sub>S-85% H<sub>2</sub> at 500°F.

The extent of reaction of zinc chloride with nitrogen and sulfur was determined by elementary analyses. The work-up procedure for product analysis was as described previously.<sup>(10)</sup> All the inorganic nitrogen was found in the water washings and was analyzed as NH<sub>3</sub> by distillation after adding caustic. The NH<sub>3</sub> is assumed to be present as ZnCl<sub>2</sub>·xNH<sub>3</sub> or ZnCl<sub>2</sub>·yNH<sub>4</sub>Cl. The chlorine present in excess of that required for ZnCl<sub>2</sub> is assumed to be in the form of the double salt; ZnCl<sub>2</sub>·yNH<sub>4</sub>Cl. All of the sulfur in the MEK-insoluble fraction is assumed to be ZnS.

The analysis of the gasoline for individual saturated components was carried out by gas chromatography after suitable calibration with pure hydrocarbons. A temperature programmed stainless steel capillary column 0.02" dia. by 300' long coated with squalene was used in conjunction with a hydrogen flame ionization detector.

The analysis for individual aromatic hydrocarbons was carried by first isolating the aromatic fraction of the gasoline by liquid displacement chromatograph using silica gel as the absorbent. The aromatic fraction was then analyzed by gas chromatography in the same capillary column coated with 2,5-xyleneol phosphate.

## RESULTS AND DISCUSSION

### Comparison with Other Catalysts and Effect of Catalyst/Extract Ratio

Table II gives a comparison of three types of catalysts at low catalyst concentrations between 1 and 2.5 percent of the extract fed. The literature on coal hydrogenation which states that tin chloride in small concentrations is a superior catalyst is confirmed. In spite of the lower concentration of catalyst used and lower pressure, the tin catalyst gave the highest conversion and highest selectivity for production of liquid products. However, in view of the high cost of tin and its low activity for pyrene hydrocracking when used in massive quantities,<sup>(10)</sup> no further test work was done with massive quantities of SnCl<sub>2</sub> in extract hydrocracking.

The activity of the nickel molybdate hydrofining catalyst increases markedly with increasing catalyst concentrations. Extra conversion tends to level off, however, as the catalyst extract ratio is increased beyond 0.3. These data are illustrated in Figure 1.

Two important features are evident from Figure 1. One is that conversion with the molten zinc chloride catalyst at a comparable catalyst extract ratio is always higher than with the contact catalyst type system and that the conversion reached at high catalyst extract ratios is much greater with the molten zinc chloride catalyst system. Another important feature illustrated in Figure 1 is the high conversion to gasoline boiling distillates obtained with the zinc chloride catalyst system. This especially becomes apparent at high catalyst to extract ratios, i.e., above about 0.3. This again is in distinction to the results obtained with the contact catalyst system where the gasoline range boiling distillates always comprised only a minor fraction of the total distillate oils produced. Thus, an important potential advantage of the molten zinc chloride catalyst system is the possibility of obtaining single-stage direct conversion of coal extract to high octane gasoline.

Figure 2 gives another comparison of results obtained under comparable conditions between the two catalyst systems. Especially interesting here is the rapid increase in the isobutane-to-normal butane ratio with increasing  $ZnCl_2$ -to-extract ratio. At high catalyst/extract ratios gasoline is produced which contains a very high proportion of isoparaffins quite comparable to what is normally produced by hydrocracking of hydrofined petroleum feedstock with dual function contact catalysts. The isobutane-to-normal butane ratio is always higher than with the hydrofining catalyst system as illustrated at the bottom of the figure. This shows that no acid cracking function exists in the case of the hydrofining catalyst system. The sharp inflection point on the isobutane-to-normal butane ratio occurs at a catalyst ratio of about 0.3.

The data shown in Figure 2 illustrate that a high selectivity in conversion of extract to gasoline is possible with massive quantities of zinc chloride. The selectivity here is measured by the percent by weight of the extract that is converted to  $C_1$  through  $C_3$  hydrocarbon gases. At very high catalyst:extract ratios the gas yield becomes fairly large, but this would be reduced in an actual continuous system by continuous removal of the products to prevent further cracking of the gasoline components. It is also noted that, at catalyst extract ratios up to about .4, the selectivity is better than obtained with the hydrofining catalyst system. The experiments with the hydrofining catalysts were with fresh catalyst not contaminated with ash and carbon such that the activity is substantially greater than one would have in an actual practical system.

#### Effect of Residence Time, Temperature and Pressure

The influence of these variables with a constant zinc chloride/extract ratio is illustrated in Figures 3, 4, and 5, respectively.

Figure 3 again illustrates the higher conversion rates that can be obtained with molten zinc chloride catalysts as compared with the hydrofining catalyst system. Three hours are required to reach a conversion of 75% with the hydrofining catalyst system, as compared with less than 5 minutes residence time required to reach the same conversion level with the molten zinc chloride catalyst.

Figure 4 gives a very rapid survey of the effects of temperature and pressure on extract conversion with zinc chloride catalyst. It is seen that substantial conversions can be achieved even at low pressures (of the order of 2000 pounds) at quite low temperatures. It also appears that at low temperatures the conversion achieved may not be too sensitive to the actual pressure. Thus, by operating at

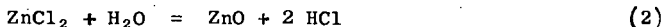
very low temperatures of the order of 650°F, substantial conversions can be achieved even at very low pressures perhaps as low as 1500 pounds. This remains to be confirmed by future work.

Figure 5 shows the effect of operating temperature at constant time and pressure on the single stage gasoline yields, i.e., the fraction of the total liquid product which boils within the gasoline range. It also shows the effect of operating temperature on selectivity of the process. It is seen that the gasoline yield increases with operating temperature, but even at temperatures as low as 625°F more than half of the liquid product boils within gasoline range. Thus, in any case, it would appear to be possible to recycle the heavier liquid to obtain ultimate conversion of all distillate products to gasoline. It is seen also that the selectivity of the process becomes better as temperature of operation is reduced, and that accordingly the ultimate gasoline yields, upon recycling of higher boiling liquids to extinction, would be very high at temperatures below about 760°F.

#### Reactions of Catalyst With Hydrocracked Products

The coal extract is rich in hetero atoms, i.e., N, O, and S, as the analyses of Table I shows. These are released during hydrocracking in the form of NH<sub>3</sub>, H<sub>2</sub>O and H<sub>2</sub>S, respectively.

The following reactions with the catalyst are then possible:



The equilibrium constant for reaction (1) has been determined experimentally by Kapustinsky,<sup>(1)</sup> and that for (2) may be calculated from available thermodynamic data on zinc compounds<sup>(3)</sup> with results given below:

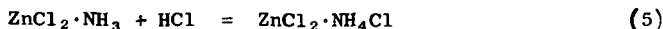
$$\log K_2 = \log \frac{P_{\text{HCl}}^2}{P_{\text{H}_2\text{O}}} = \frac{-6930}{T} + 8.03 \quad (4)$$

The dissociation pressure of NH<sub>3</sub> over zinc chloride melts has been measured by Krasnov.<sup>(4)</sup>

The equilibrium data of Kapustinsky<sup>(1)</sup> for reaction (1) indicates that nearly quantitative absorption of H<sub>2</sub>S to produce ZnS should take place. This was confirmed experimentally, in that no H<sub>2</sub>S could be detected in the product gas, and all of the sulfur released was absorbed by the melt.

The data for reaction (2) indicates that zinc chloride should be quite resistant to hydrolysis but that a small amount of HCl should be present in the gas. Experimentally nothing more than trace quantities of HCl could ever be found. The discrepancy may be due to a high degree of absorption of water by the melt which reduces the partial pressure of steam to a low value.

Krasnov's data<sup>(4)</sup> indicate that the NH<sub>3</sub> pressure over melts containing less than 25 mole percent of ammonia would be quite small at temperatures in the normal range used for hydrocracking. Quantitative absorption of ammonia by the melts is thus to be expected, which was, in fact, confirmed experimentally. It is usual in the hydrocracking of standard extract to produce at least one mole of NH<sub>3</sub> for each mole of hydrogen chloride formed by reaction (1). The hydrogen chloride so produced is absorbed by the melt by the following reaction:



Equilibrium data for reaction (5) will be presented in a subsequent paper.

The melt fed to the autoclave experiments usually contained 2.5 to 3.0 mole percent of ZnO as determined by the ability of the anhydrous melt to chemically react with hydrogen chloride to produce water. The ZnO, of course, reacts with hydrogen chloride released by reaction (1) during hydrocracking by reversal of reaction (2). It is possible to add sufficient ZnO to neutralize all of the HCl produced. In this case no  $\text{NH}_4\text{Cl}$  would be formed in the melt. The ZnO acceptor for HCl can be produced during regeneration of the melt, for example, by oxidation of the ZnS formed by reaction (1).

#### Effect of $\text{NH}_3$ and $\text{NH}_4\text{Cl}$ on Melt Activity

It is, therefore, clear that depending upon operating conditions used and whether or not zinc oxide acceptor is employed, both ammonia and ammonium chloride in widely ranged proportions can be present in the melt during hydrogenation. It is therefore of interest to see what effect these materials have on the hydrocracking activity of zinc chloride melt toward extract. The data in Figure 6 illustrate this point.

In these runs, the temperature and pressure were held constant at 750°F and 3000 pounds, respectively, and the amount of ammonia or ammonium chloride added was varied. It is seen that with both ammonia and ammonium chloride there was a decrease in extract conversion, but that the decrease is much more rapid in the case of ammonia than in the case of ammonium chloride.

Another interesting item illustrated in Figure 7 is the effect of ammonia and ammonium chloride addition on selectivity. It is seen that both additives have a favorable effect on this count in that they caused a very dramatic decrease in the gas yield. The effect of other additives was also studied, in particular the effect of the addition of zinc oxide. Zinc oxide prevents the formation of ammonium chloride by absorbing the HCl produced. Zinc oxide was found to have marked inhibiting effect when used in large quantities. The inhibiting effect is quite moderate when only small quantities are used.

The data of Figure 6 were obtained with a zinc chloride/extract weight ratio of 2. Similar data were obtained at other feed ratios of 1 and 3, respectively. Conversions were slightly lower when the feed ratio was lowered, particularly when the amount of  $\text{NH}_3$  added was small. The major effect of the zinc chloride/extract ratio at low  $\text{NH}_3$  concentrations was that the gas yield decreased rapidly as the feed ratio decreased.

When higher concentrations of  $\text{NH}_3$  were used, there was no perceptible effect of feed ratio in the range of 1 to 3.

It is therefore concluded that one controlling factor in determining the amount of melt circulation required in an extract hydrocracking process is the accumulation of nitrogen poisons. It would appear from the prior experience with pyrene,<sup>(10)</sup> however, that even with a feed low in nitrogen poisons that there is a kinetic advantage in the use of massive quantities of catalyst. The present data indicate, however, that no further advantage is gained by increasing the weight ratio of catalyst to feed beyond 1.

It is abundantly clear, therefore, that a commercial process for hydrocracking with zinc chloride melts would require continuous regeneration to remove the nitrogen poisons. Methods of regeneration will be discussed in a subsequent paper.

Some data on the effect of  $\text{NH}_3$  at higher temperatures, i.e., at 800°F were also obtained. They are summarized in Table III. Under these conditions a small amount

of  $\text{NH}_3$ , i.e., 0.09 mole percent has a favorable effect, in that the conversion is increased, the selectivity is greatly increased because of the lower gas yield and the yield of MEK-Insolubles is decreased. As a matter of fact, the increase in conversion due to  $\text{NH}_3$  addition can be ascribed entirely to the decrease in the MEK-Insoluble yield. It appears likely that the favorable effect of small amounts of  $\text{NH}_3$  is due to moderation of the cracking activity of the melt which is too high for best results at the conditions used. Even larger quantities of ammonia possibly could be tolerated with favorable results at temperatures above  $800^\circ\text{F}$ .

It is noted that at a 1/1 mole ratio of  $\text{NH}_3/\text{ZnCl}_2$  the hydrocracking activity is reduced to about the equivalent to that obtained when only 2 percent of  $\text{ZnCl}_2$  (with no  $\text{NH}_3$  added) is used (cf. Table II).

Further addition of  $\text{NH}_3$  decreases the catalytic activity of the melt even further. The data for the melt containing 2 moles  $\text{NH}_3/\text{mole ZnCl}_2$  indicates that at this level the catalytic activity is almost completely poisoned.

The data of Table III also show the effect of increasing amounts of ammonia in decreasing the  $i\text{C}_4/n\text{C}_4$  ratio. It is thus apparent that the main effect of ammonia is to reduce the acidic cracking properties of the melt by neutralizing the Friedel Crafts acids.

Friedel Crafts acids in the case of extract hydrocracking can be generated by formation of several different zinc chloride complexes such as with phenolic groups in the extract, with water and with  $\text{HCl}$  formed by reaction (1).

It is also noted in Table III, from the catalyst analyses given, that as discussed above a very high percentage of the original nitrogen and sulfur in the feed extract is retained by the catalyst when the extract conversion is high.

#### Five-Stage Run

The above discussion indicates that if the  $\text{NH}_3$  accumulates mostly as  $\text{NH}_4\text{Cl}$  relatively little deactivation of the catalyst occurs. This would be attractive from the practical point of view since it is desirable to reduce the melt circulation rate between regeneration and hydrocracking.

A five-stage run was carried out to demonstrate this. After each stage, the autoclave was cooled to  $250^\circ\text{C}$  and depressurized with removal of volatile liquid products and gas. After further cooling, fresh zinc chloride and extract were added (in a weight ratio of 0.23/1) to the catalyst and high-boiling liquid remaining in the autoclave from the previous stage. The autoclave was repressurized with hydrogen and heated back to the operating conditions of  $750^\circ\text{F}$  and 3000 psig.

The results after a single-stage are compared with the cumulative results of the five-stage run in Table IV. It is noted that the cumulative results of the five stages are very nearly equivalent to that of the first stage. However, a favorable net reduction in catalyst/extract ratio from 1 to 0.38 is achieved by this technique.

The composition of the catalyst after stages 1 and 5 is also shown in Table IV. It is seen that 82 percent of the nitrogen and 95 percent of the sulfur in the feed accumulate in the melt. The  $\text{NH}_3$  is present mostly as  $\text{NH}_4\text{Cl}$  which explains the relatively small loss in catalyst activity.

A chlorine balance around the five-stage run indicates that 85 percent of the  $\text{HCl}$  released by reaction (1) was retained in the melt. The nature of  $\text{HCl}$  loss is not clear, however, as none could be found in the off-gas.

### Kinetics of the Hydrocracking Process

The maximum extract conversion achieved in 60 minutes residence time in the experiments reported above was 91 percent. It, of course, is desirable to achieve substantially complete conversion. In order to accomplish this it is first of all necessary to substantially reduce the yield of MEK-Insolubles. Secondly, it is necessary to hydrocrack the +400°C MEK-Solubles to distillate oils.

Another characteristic of the previous experiments is that although the total hot pressure was maintained constant, the partial pressure of hydrogen decreased with time due to accumulation of gas and volatile reaction products. The hydrogen pressure is the most important variable in controlling the MEK-Insoluble yield. A series of runs were therefore carried out wherein the hydrogen pressure was maintained constant using a palladium probe to indicate hydrogen partial pressure.

The results of two series of runs at various times carried out at 750°F wherein the hydrogen partial pressures were maintained constant at 2500 psi and 3500 psi, respectively, are shown in Figure 7.

The MEK-Insoluble yield rapidly falls to a nearly constant value after 15 to 30 minutes time after which very little further reduction occurs. The final yield is, of course, lower at the higher hydrogen pressure, i.e., 1.5 percent vs. 3.5 percent.

The rate of total conversion decreases rapidly with time and becomes very slow after one hour. Even after three hours the total conversion only reaches 92.1 percent at 3500 psi and is slightly lower at 2500 psi H<sub>2</sub> pressure.

The cause of the difficulty is shown in Figure 8 where the reaction rate for conversion of the +400°C MEK-Solubles is plotted as a first order reaction, i.e.,

$$k(t - 15) = \ln C_0/C_t$$

where  $C_0$  and  $C_t$  are the weight percent MEK-Solubles present after 15 minutes and time "t", respectively.

It is seen that the initial rate follows the first order rate law but that the rate falls off rapidly as high conversions are reached. The first order rate increases about 20 percent in going from 2500 to 3500 psi, i.e., less than proportional to increase in pressure.

The higher pressure does not likewise prevent the decrease in rate at high conversions. As a matter of fact at both pressure levels the same yield of MEK-Soluble residue, i.e., 6.2 wt. % remains after three hours.

The decrease in reaction rate is due to formation of a refractory residue and not to decrease in catalytic activity of the melt. That this is so is obvious from the fact that over 95 percent of N and S catalyst poisons have accumulated in the melt after one hour residence time, i.e., long before the rate starts to decrease. It was also confirmed by recovery and separate hydrocracking of the MEK-Soluble residue.

It is clear that to obtain higher conversions a staged hydrogenation system with progressive increase in temperature would be required.

### Effect of Feedstock - Direct Hydrogenation of Coal

The use of molten zinc chloride hydrocracking catalyst is not limited, of course, to coal extract but may be applied to a wide range of feedstocks varying from coal itself to middle boiling range petroleum distillates.

A comparison of results with several other coal derived feedstocks is given in Table V. Ireland Mine coal, a Pittsburgh Seam coal from Northern West Virginia, is the coal used for production of the standard extract used in most of this work. It was necessary to use a high ratio of catalyst to coal in this case in order to have sufficient volume of liquid present to produce a handleable coal slurry. As stated above, the use of a catalyst ratio above 1 with extract only increases the conversion slightly but has a relatively marked effect on gas yield. Thus, allowing for the difference in quantity of catalyst used, it is seen that coal and extract behave with remarkable similarity.

Results are also shown for another extract, i.e., "Spencer" extract. This extract was procured from the Spencer Chemical Co., and was prepared by extraction of a West Kentucky No. 11 coal under a pressure of 1000 psig of hydrogen at about 425°C. The depth of extraction was reported by Spencer Chemical to have been over 90%. Inspections of the extract are given in Table I.

Comparison should be made with the 750°F standard extract results of Table IV (Stage 1). Again a remarkable similarity is noted although the yield of middle range distillate is higher and the overall conversion slightly lower.

Results with a higher quality feedstock, i.e., benzene-soluble component of standard extract, are also shown in Table V. In this case a notable improvement in results is noted. The conversion is substantially increased while the yield of MEK-Insoluble residue is substantially decreased.

#### Gasoline Composition

The gasoline produced by the zinc chloride process contains a high proportion of branched paraffins and a substantial amount of aromatics. The aromatic content of the gasoline varies with conditions used from about 20 to 50 vol. percent. High aromatic contents are obtained in operations at the higher temperatures around 800°F and with catalyst/extract ratios below one.

A sample of gasoline from a large number of autoclave runs at different conditions was composited for a micro octane number test with results shown in Table VI along with inspections of the gasoline. The gasoline sample tested had substantially all the  $C_4$ 's and  $C_6$ 's removed but in spite of this had a clear research octane of 89. It is clear that a motor gasoline with the appropriate  $C_4$ 's and  $C_5$ 's added for volatility would have a clear octane number of well over 90.

Another sample of gasoline was obtained by running a number repetitive autoclave runs at Stage 1 conditions shown in Table IV. A more complete analysis of this gasoline is given in Table VI along with a breakdown into individual components.

The ratio of branched-to-normal paraffins is clearly quite large in the  $C_5$  and  $C_6$  fractions.

#### Potential Commercial Considerations

It is premature to discuss in detail the potential commercial application of the zinc chloride hydrocracking process. Data are required both on continuous hydrocracking and continuous melt regeneration systems. Work is presently in progress on both of these subjects and will be reported in future papers. Some aspects of the regeneration process is discussed in a subsequent paper.

Corrosion control is one of the important aspects of a potential commercial process. Weight loss data over the duration of the autoclave program indicate that the average penetration rate with 316 stainless is less than 80 mpy. Separate

corrosion tests, however, have indicated that pitting may be a problem with 316 stainless when substantial quantities of  $\text{NH}_4\text{Cl}$  are allowed to build up in the melt. In this case more expensive alloys such as Hastelloy B or Inconel 625 may be required.

The formation of  $\text{NH}_4\text{Cl}$  can be eliminated by addition of zinc oxide acceptor. Corrosion test work in this case indicates that 316 stainless may be a satisfactory alloy, i.e., penetration rates below 5 mpy were observed with test specimens.

Therefore, from the corrosion standpoint the zinc-oxide acceptor system is preferred. The disadvantage is the lower catalyst activity for a given nitrogen level. The inhibiting effect of  $\text{ZnO}$  can be minimized by maintaining at all times a very low concentration of zinc oxide in the hydrocracking zone and by providing for a staged increase in temperature to over  $800^\circ\text{F}$  to partially compensate for decrease in catalyst activity by accumulation of  $\text{NH}_3$  in the melt. Figure 9 illustrates schematically a continuous operation using the above principles. It should be noted that the zinc chloride melt is miscible with extract, as it was with pyrene.<sup>(10)</sup>

#### ACKNOWLEDGMENT

The sponsorship of the U. S. Office of Coal Research for this investigation is gratefully acknowledged.

#### BIBLIOGRAPHY

- (1) Britzke, E. V. Kapustinsky, A. F., and Wesselowsky, B. K.  
Zeit. Anorg. Chem. 213, 65 (1933).
- (2) Kandiner, H. J., Hiteshue, R. W., and Clark, E. L.  
Chem. Eng. Progress 47, 392-396 (1951).
- (3) Kitchener, J. A. and Ignatowicz, S., Trans. Farad. Soc. 47, 1278 (1951).
- (4) Krasnov, A. Z., J. Applied Chem. (USSR) 12, 1595-1597 (1939).
- (5) Kuo-Chuan Chen and Fuh-Liang Chang,  
Jan Liso Hsueh Pao 3, 23-34 (1958).
- (6) Kurokawa, M., Hirota, W., Takeya, G., and Takenaka, Y.  
J. Soc. Chem. Ind., Japan 44, 776-779 (1941).
- (7) Pelipetz, M., Kuhn, E. M., Freedman, S., and Storch, H. H.  
Ind. Eng. Chem. 40, 1259-1264 (1948).
- (8) Sato, F., Morikawa, K., Morikawa, R., Okamura, T.  
J. Soc. Chem. Ind., Japan 45, 892-903 (1942).
- (9) Weller, S., Pelipetz, M. G., Freedman, S., and Storch, H. H.  
Ind. Eng. Chem. 42, 330-334 (1950).
- (10) Zielke, C. W.; Struck, R. T., Evans, J. M., Costanza, C. P., and Gorin, E.  
"Molten Salt Catalysts for Hydrocracking of Polynuclear Hydrocarbons."  
Presented Before the Division of Fuel Chemistry, ACS,  
Atlantic City, N. J., September 12-17, 1965.

TABLE I      Analysis of Feedstocks

Feedstock	Ireland	"Standard"	"Spencer"	Benzene Solubles
	Mine Coal	Extract	Extract	
	<u>MF Basis</u>			
Volatile Matter	40.32			
Fixed Carbon	46.66			
FeS	0.08			
FeS <sub>2</sub>	4.19			
Other Ash	10.15			
	<u>MAF Basis</u>			
H	5.73	6.14	5.03	7.04
C	81.90	83.73	87.62	85.30
N	1.58	1.46	1.49	.94
O	8.61	6.87	4.75	5.10
Organic S	2.18	1.80	1.11	1.62
<u>Solvent Fractionation</u>				
Benzene Insolubles		46.9	37.2	.5
Asphaltenes		37.2	31.2	59.6
Oil		15.9	31.5	39.0

TABLE II      Comparison of Catalyst Activity at Low Concentration Levels - 1 Hr. Residence Time

Temperature, °F	← 800 →		
	4200	4200	3000
Total Hot Pressure			
Catalyst	Nickel Molybdate on Al <sub>2</sub> O <sub>3</sub>	ZnCl <sub>2</sub>	SnCl <sub>2</sub>
Catalyst/Extract, Wt. Ratio	.025	.02	.01
<u>Yields, Wt. % Feed</u>			
C <sub>1</sub> -C <sub>3</sub>	5.0	5.1	4.1
C <sub>4</sub>	) 14.9	1.0	1.8
C <sub>5</sub> x 200°C		14.7	13.0
200 x 400°C	14.5	19.8	24.6
MEK-Soluble +400°C Residue	60.3	52.9	53.5
MEK-Insoluble +400°C Residue	0.6	3.0	0.1
Other (NH <sub>3</sub> , H <sub>2</sub> S, H <sub>2</sub> O, etc.)	7.3	7.6	6.7
Total	102.6	104.1	103.8
H <sub>2</sub> Consumption, Wt. % Feed	2.55	4.13	3.71
Conversion, Wt. % Feed	39.0	44.1	46.5
(C <sub>1</sub> -C <sub>3</sub> ) x 100/Conversion	12.8	11.5	8.8

TABLE III

Activity of Zinc Chloride Catalyst as Affected

by NH<sub>3</sub> Addition

Temperature = 800°F, Total Pressure = 4200 psig

ZnCl<sub>2</sub>/Extract Wt. Ratio = 1.0, Time = 60 mins.

NH <sub>3</sub> /ZnCl <sub>2</sub> , Mole Ratio	0	0.091	1.0	2.0
<u>Yields, Wt. % MAF Feed</u>				
CH <sub>4</sub>	1.8	1.5	1.6	1.8
C <sub>2</sub> H <sub>6</sub>	2.6	1.7	1.2	1.4
C <sub>3</sub> H <sub>8</sub>	8.6	3.0	1.2	1.2
i C <sub>4</sub> H <sub>10</sub>	9.6	2.5	0.4	0.1
n C <sub>4</sub> H <sub>10</sub>	1.6	0.5	0.5	0.5
(NH <sub>3</sub> +H <sub>2</sub> S+H <sub>2</sub> O+CO+CO <sub>2</sub> )	7.4	7.4	5.5	2.3
C <sub>5</sub> x 200°C Dist.	60.4	68.2	15.8	10.3
200 x 400°C Dist.	3.1	11.4	19.1	9.5
+400°C MEK-Soluble Residue	6.3	6.2	54.5	54.1
+400°C MEK-Insoluble Residue	3.9	2.6	2.4	20.3
N to Catalyst	1.3	1.3	} 1.6	} 1.4
S " "	1.8	1.4		
H " "	0.3	0.3		
Total	108.7	108.0	103.8	102.9
Conversion, Wt. % MAF Feed	89.8	91.2	43.2	25.6
H <sub>2</sub> Consumed, Wt. % MAF Feed	8.7	8.0	3.8	2.9
(C <sub>1</sub> -C <sub>3</sub> ) x 100/Conversion	14.5	6.8	9.3	17.1

TABLE IV

Results of 5-Stage Run

Temperature = 750°F, Total Hot Pressure = 3000 psig

Residence Time/Stage = 60 mins.

Stage No.		<u>1</u>	<u>2 thru 5</u>	<u>Cumulative</u>
Wt. Extract Feed Per Stage/gms		50	50	250
Wt. ZnCl <sub>2</sub> Feed Per Stage/gms		50	11.4	95.6
Cumulative ZnCl <sub>2</sub> /Extract, Wt. Ratio		1	--	0.383
<u>Melt Composition, Mole %</u>	<u>Feed</u>	<u>After Stage 1</u>		<u>After Stage 5</u>
	ZnCl <sub>2</sub>	81.7		48.5
	ZnO	--		--
	ZnCl <sub>2</sub> ·NH <sub>3</sub>	2.3		4.4
	ZnCl <sub>2</sub> ·NH <sub>4</sub> Cl	8.9		27.4
	ZnS	7.1		19.7
	<u>100.0</u>	<u>100.0</u>		<u>100.0</u>
<u>Yields, Wt. % Total Extract Feed</u>				
	C <sub>1</sub> -C <sub>3</sub>	6.3		6.3
	i C <sub>4</sub> H <sub>10</sub>	3.3		3.2
	n C <sub>4</sub> H <sub>10</sub>	0.4		0.6
	CO	0.1		0.2
	H <sub>2</sub> O	7.3		5.8
	C <sub>5</sub> x 200°C Dist.	59.0		56.0
	200 x 400°C Dist.	9.6		14.3
	+400°C MEK-Soluble Residue	11.9		12.9
	+400°C MEK-Insoluble Residue	6.4		4.5
	H to Catalyst	0.3		0.3
	N " "	1.1		1.2
	S " "	1.6		1.7
Total		107.3		107.0
Conversion, Wt. % MAF Feed		81.8		82.6
H <sub>2</sub> Consumed, Wt. % MAF Feed		7.3		7.0
(C <sub>1</sub> -C <sub>3</sub> ) x 100/Conversion		7.7		7.6

TABLE V

Comparison of Feedstocks in Hydrocracking  
With Molten Zinc Chloride Catalyst

Residence Time = 60 min.

Feedstock	Ireland Mine Coal	Standard Extract	Spencer Extract	Benzene Solubles from Standard Extract
Temperature, °F	725	725	750	750
ZnCl <sub>2</sub> MAF Feed (Wt. Ratio)	3.5	1.0	1.0	1.0
Total Pressure, psig	2000	2000	3000	3000
<u>Yields, Wt. % MAF Feed</u>				
CH <sub>4</sub>	0.9	0.6	0.6	.6
C <sub>2</sub> H <sub>6</sub>	2.3	1.2	0.8	1.2
C <sub>3</sub> H <sub>8</sub>	7.5	1.7	2.1	5.8
i C <sub>4</sub> H <sub>10</sub>	7.8	1.2	2.1	7.3
n C <sub>4</sub> H <sub>10</sub>	1.3	0.1	0.3	1.0
(NH <sub>3</sub> +H <sub>2</sub> S+CO+CO <sub>2</sub> +H <sub>2</sub> O)	6.7	6.9	6.8	7.0
C <sub>5</sub> x 200°C Dist.	48.2	49.5	50.4	66.2
200 x 400°C Dist.	2.9	9.4	17.9	6.2
+400°C MEK-Soluble Residue	15.0	17.0	17.9	7.7
+400°C MEK-Insoluble Residue	10.9	14.8	5.7	1.2
N+S+H to Catalyst	5.2	3.5	2.3	3.1
Total	108.7	105.9	106.9	107.3
Conversion, Wt. % MAF Feed	74.2	68.1	76.4	91.1
H <sub>2</sub> Consumption, Wt. % MAF Feed	8.7	5.9	6.9	7.3
(C <sub>1</sub> -C <sub>3</sub> ) x 100/Conversion	14.3	5.1	4.6	8.3

TABLE VI

Analyses of Product Gasoline

Description	<u>C<sub>5</sub>-200°C Gasoline</u>	<u>C<sub>6</sub>-190°C Gasoline</u>
<u>FIA, Vol. %<sup>(1)</sup></u>		
Aromatics	25.5	30.9
Saturates	74.5	69.1
Olefins	0.0	0.0
Naphthenes	Not Determined	31.7 <sup>(2)</sup>
Research, Clear Octane No.	" "	89
<u>Elemental Analytical, Wt. %</u>		
H	13.42	12.93
C	86.22	87.00
N	0.0	.04
O	.34	.03
S	.02	0.0
<u>Partial Component Breakdown, Vol. %</u>		
<u>Saturates</u>		
i-Pentane	13.4	
n-Pentane	1.2	
Cyclopentane	.8	
2,3-Dimethylbutane	1.1	
2-Methylpentane	4.4	
3-Methylpentane	3.0	
n-Hexane	.5	
Cyclohexane	.6	
Methylcyclopentane	9.3	
<u>Aromatics</u>		
Benzene	2.0	
Toluene	5.9	
Ethyl Benzene	2.4	
Xylenes	3.9	
Cumene	1.1	
n-Propyl Benzene	.5	

(1) Fluorescent Indicator Analysis, A.S.T.M. Method D-1319-61T.

(2) The total saturates are 31.7% naphthenic and 37.4% paraffinic as determined by A.S.T.M. Method D-2159.

Figure 1

**EFFECT OF FEED CATALYST-EXTRACT RATIO ON TOTAL CONVERSION AND CONVERSION TO GASOLINE**

800°F - 4200 psi Total Pressure.  
- 60 min. R.T.

▲ Molten ZnCl<sub>2</sub> Catalyst.  
○ Nickel Molybdate Hydrofining Catalyst.

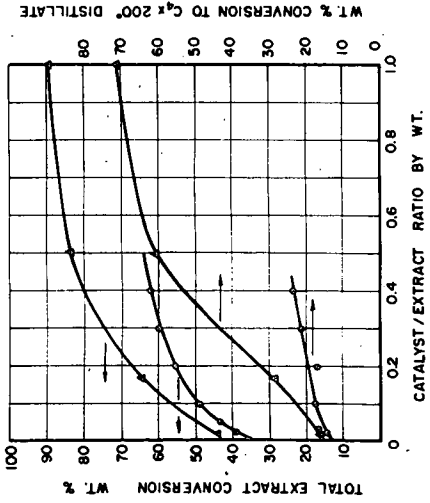


Figure 2

**EFFECT OF CATALYST-EXTRACT RATIO ON C<sub>4</sub>-C<sub>4</sub> RATIO AND SELECTIVITY**

800°F - 4200 psi Total Pressure.  
- 60 min. R.T.

▲ Molten ZnCl<sub>2</sub> Catalyst.  
○ Nickel Molybdate Hydrofining Catalyst.

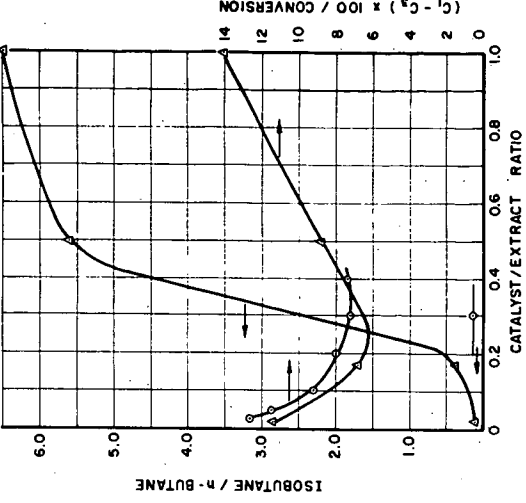


Figure 4  
EXTRACT CONVERSION  
VS  
TEMPERATURE & PRESSURE

Zn Cl<sub>2</sub> / Extract = 1.0  
 Time = 1 Hour

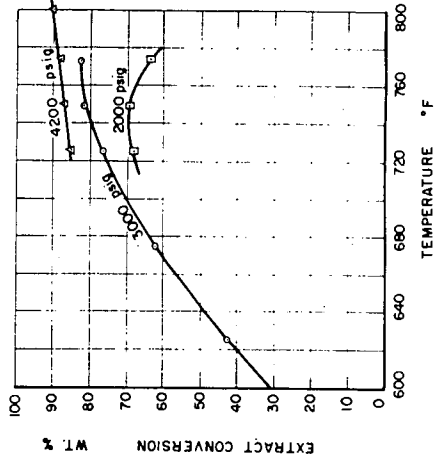


Figure 3  
EFFECT OF RESIDENCE TIME  
ON TOTAL CONVERSION

Δ Zn Cl<sub>2</sub> / Extract = 1  
 ○ Nickel Molybdate / Extract = 0.3

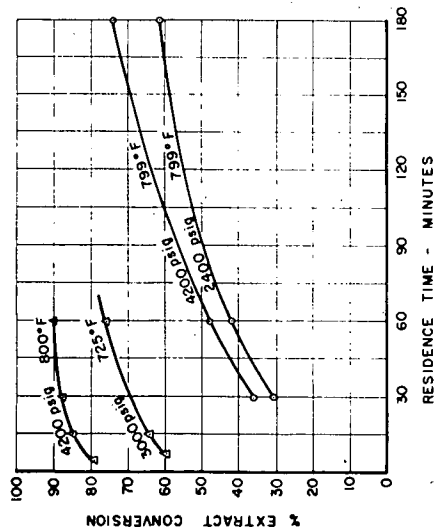


Figure 6  
**EFFECT OF NH<sub>3</sub> & NH<sub>4</sub>Cl ON  
 CONVERSION & SELECTIVITY**

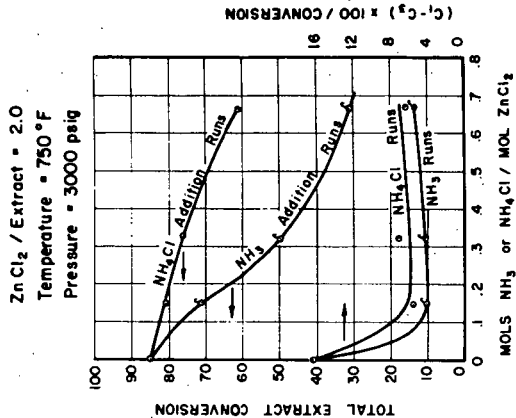


Figure 5  
**GASOLINE YIELD & SELECTIVITY  
 VS  
 TEMPERATURE**

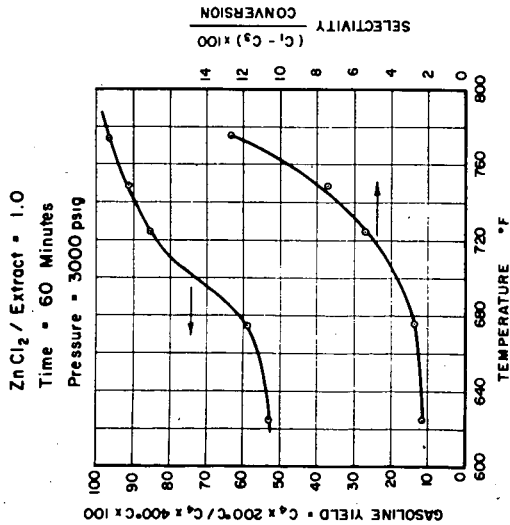


Figure 7  
YIELDS vs TIME IN CONSTANT  
HYDROGEN PRESSURE RUNS  
AT 750° F

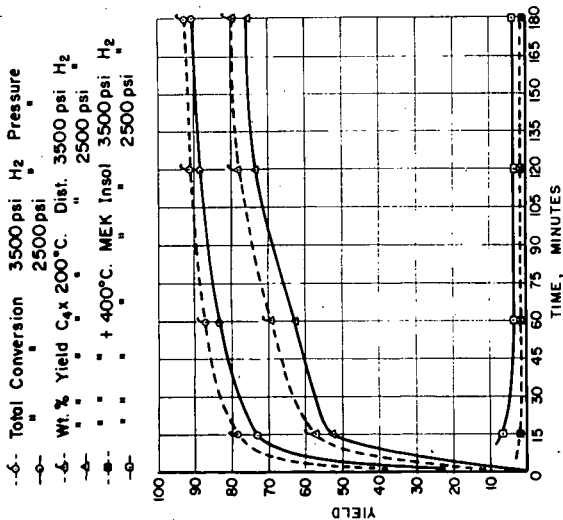
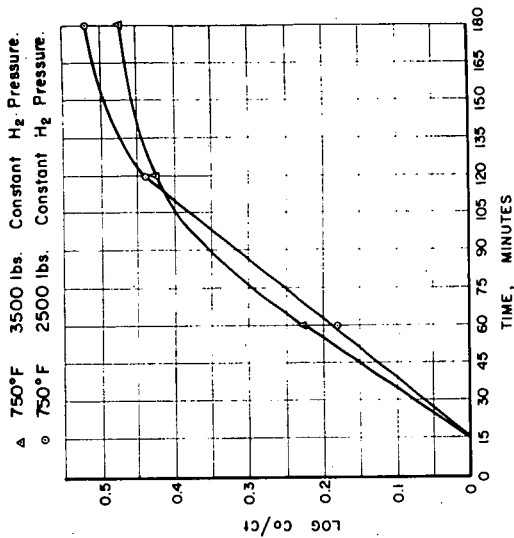
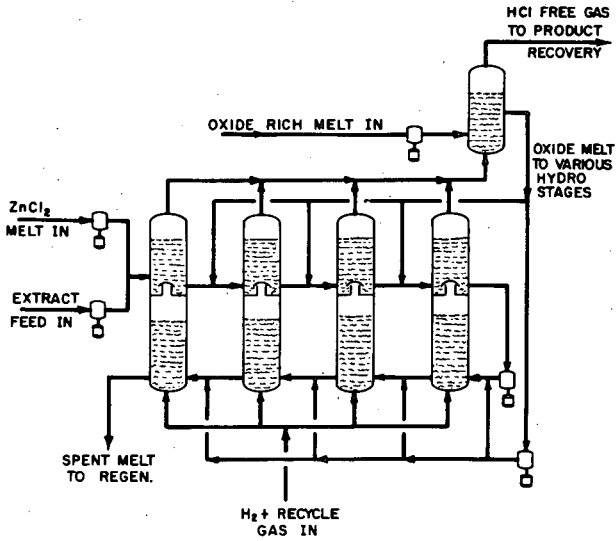


Figure 8  
RATE OF HYDROCRACKING OF  
+400°C MEK SOLUBLE RESIDUE



*Figure 9*

**SCHEMATIC HYDRO SYSTEM WITH MASSIVE  
ZINC CHLORIDE MELT CATALYST  
ZINC OXIDE ACCEPTOR SYSTEM**



REGENERATION OF ZINC HALIDE CATALYSTS USED IN HYDROCRACKING OF COAL EXTRACT

C. W. Zielke, R. T. Struck, and E. Gorin

Research Division  
CONSOLIDATION COAL COMPANY  
Library, Pennsylvania

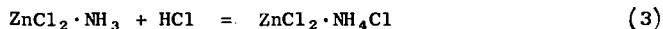
INTRODUCTION

The application of molten zinc chloride catalysis to the hydrocracking of poly-nuclear hydrocarbons, coal extract and coal was discussed in two previous papers.<sup>(a,b)</sup> The zinc chloride, however, is not a catalyst in the chemical sense since it is partially destroyed by reaction with the N and S impurities in the hydrocracker feed. When coal itself is used further complications arise due to reactions with some of the inorganic components in the coal ash.

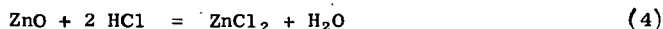
A commercial process utilizing molten zinc chloride catalysis must provide a viable scheme for regeneration of the catalyst.

Two schemes for using the catalyst were discussed in a previous paper, i.e., with and without the concomitant addition of zinc oxide acceptor.

The following reactions occur when no acceptor is added:



The addition of zinc oxide acceptor eliminates reaction (3) and introduces a new reaction



The present paper will discuss only the regeneration of the catalyst for the non-acceptor case. The acceptor case will be discussed in a separate paper.

The melt leaving the hydrocracker thus, in general, will contain in addition to  $\text{ZnCl}_2$  the following compounds:  $\text{ZnS}$ ,  $\text{ZnCl}_2 \cdot \text{NH}_3$  and  $\text{ZnCl}_2 \cdot \text{NH}_4\text{Cl}$ . The addition compounds between zinc chloride and  $\text{NH}_3$  and  $\text{NH}_4\text{Cl}$  are written as the 1/1 adducts not because they necessarily exist as such in the melt but for convenience of discussion. The ratio of the  $\text{NH}_4\text{Cl}$  to the  $\text{NH}_3$  adducts is dependent on the ratio of N to S in the feed. Where the moles of sulfur in the hydrocracker feed is equal to or greater than one-half the moles of nitrogen, substantially all of the  $\text{NH}_3$  will be present as the  $\text{NH}_4\text{Cl}$  double salt.

Regeneration of the melt comprises removal of the bulk of the sulfur and nitrogen and return of the melt as relatively pure zinc chloride.

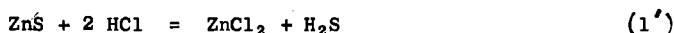
From the economic point of view it would be desirable to recover the sulfur in the form of elemental sulfur and the nitrogen as ammonia such that credits for these materials would partially defray the regeneration cost.

In addition to the inorganic impurities in the spent melt, the melt contains organic impurities which cannot be distilled out of the melt. The organic residue itself can be

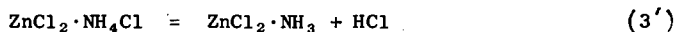
divided into two parts, one soluble in MEK and the other insoluble. The first part is largely convertible to distillate oil on recycle while the latter is mostly unconvertible and can be regarded as semi-coke. The regeneration process thus must in addition remove the organic residue from the melt before it can be recycled, coked or otherwise processed.

The reactions which are involved for specific components of the spent melt are listed below. Most of these reactions involve simple reversal of the reactions by which they were formed, i.e., reactions (1), (2) and (3) above. Where this is the case the number of the reaction is primed.

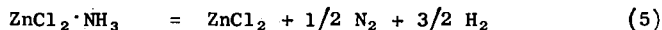
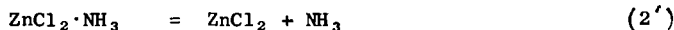
Regeneration of Zinc Sulfide



Regeneration of Ammonium Chloride-Double Salt



Regeneration of  $\text{ZnCl}_2 \cdot \text{NH}_3$



It is the purpose of this paper to present thermodynamic and other data bearing on the feasibility of the particular regeneration scheme shown. The data on the individual process steps involved are presented. The integration of the individual process steps into the overall scheme is also given.

EXPERIMENTAL

Equipment and procedures for hydrocracking of coal extract with zinc chloride catalyst have been given previously.<sup>(8)</sup>

Figure 1 shows the apparatus used to determine the equilibria in the decomposition of the zinc chloride-ammonium chloride double salt. A flow system was used with nitrogen passing slowly through a molten bed of  $\text{ZnCl}_2 + \text{NH}_4\text{Cl}$  and the exit gas being analyzed for HCl. A number of points taken over a period resulted in curves of HCl partial pressure versus the extent of  $\text{NH}_4\text{Cl}$  decomposition.

The zinc chloride and ammonium chloride used were Fisher Scientific Co. Certified Reagents. The zinc chloride was 98 percent pure, the impurities being water and zinc oxide. This material was purified at the start of each run by heating to 425°C in a flow of purified nitrogen to remove water, and then passing anhydrous HCl through it for two hours to convert ZnO to  $\text{ZnCl}_2$ . This was followed by a nitrogen purge of 12 to 36 hours to remove excess HCl from the melt. The nitrogen used was purified by passage through hot copper, Ascarite, and magnesium perchlorate to remove traces of oxygen, carbon dioxide and water.

After purifying the zinc chloride, the reactor temperature was lowered to 343°C to minimize the possible loss of HCl when adding  $\text{NH}_4\text{Cl}$  through a long stem funnel inserted in the stirrer annulus (3 seconds required). The reactor was then brought to the desired temperature with a low flow of nitrogen (1 ml/min). The desired temperature was controlled to  $\pm 2^\circ\text{C}$  and the nitrogen rate raised to the operating flow of 4.7  $\pm 0.2$  cc/min (STP). The nitrogen gas reaches equilibrium HCl content in passing through the molten bed as shown by identical results at flows between 4.7 and 12 cc/min and stirring rates from the 3100 rpm used down to as low as 1500 rpm. The gas from the reactor passes through a caustic trap and is collected in a bottle by water displacement. Two recovery trains used alternately allow continuous collection.

The 0.1 or 1.0 N caustic used in the traps is titrated after use with 0.1 or 1.0 N HCl using methyl red indicator. Caustic traps are used even during lineout periods so the amount of  $\text{NH}_4\text{Cl}$  remaining in the melt can be accurately calculated.

Collection of the effluent nitrogen in bottles allowed accurate measurement of flow rates using weight of water remaining after adjustment of the gas to atmospheric pressure.

When most of the  $\text{NH}_4\text{Cl}$  had decomposed, pressure of  $\text{NH}_3$  over the bed became appreciable, combining with HCl on cooling to form solid  $\text{NH}_4\text{Cl}$  in the glass wool trap. Analyses of these solids confirmed that they were mostly  $\text{NH}_4\text{Cl}$ . At  $427^\circ\text{C}$ , a small amount of  $\text{ZnCl}_2$  was also found in the glass wool trap. The partial pressures of HCl calculated by caustic titration were corrected by adding the additional HCl tied up as solid  $\text{NH}_4\text{Cl}$  in the solids trap.

Equilibrium data for zinc sulfide regeneration (Reaction (1'), Table III) were determined in a static glass system. After adding  $\text{ZnS}$ , the vessel was evacuated and brought to temperature under vacuum. The vacuum was then shut off and aqueous HCl added in increments. After each increment, the slurry was stirred and allowed to reach steady state before the pressure was measured. For purposes of the rough figures reported in Table III, the  $\text{H}_2\text{S}$  pressure was taken as the total pressure minus the vapor pressure of water at the temperature used. The normality of the acid was determined by titration after completion of the run.

The phase separation studies reported in Table II were conducted in the same type of rocking autoclave used for hydrocracking tests.<sup>(8a)</sup> The synthetic spent melt, whose composition is given in Table IIA, was charged to the autoclave along with the desired amount of water or in the final test, with water plus dimethylnaphthalene (Table IIB). After flushing the air with nitrogen, the unit was heated to temperature and rocked for an additional 30 minutes. The autoclave was then tilted vertically and allowed to stand for one hour before bleeding off the contents through the bottom. The products were collected in about 8 increments which were then usually combined as "organic" and "aqueous" phases. The aqueous phase was washed with benzene to remove organics before distilling off the water. The organic phase was likewise distilled to  $+400^\circ\text{C}$  end point to remove any light material before analysis. Methods of analysis for the zinc salts,  $\text{NH}_3$ , and  $\text{NH}_4\text{Cl}$  were given previously.<sup>(8a)</sup>

## RESULTS AND DISCUSSION

### 1. Separation of Organic Residue from Spent Melt

No substantial separation of phases was ever observed for mixtures of zinc chloride melt with high boiling organic materials such as extract, pyrene or hydrocracking residues. A number of different conditions were tried using separation times of up to one hour, with negative results.

The results of one such experiment are summarized in Table I. In this experiment extract was hydrocracked with zinc chloride melt at  $750^\circ\text{F}$  and 3000 psig. When the run was completed the autoclave was placed in a horizontal and then a vertical position for 15 minutes each while maintaining temperature and pressure. A number of samples were successively withdrawn over an additional 15 minute period and analyzed as shown.

It is seen that the amount of  $\text{ZnCl}_2$  and organic residue remained reasonably constant over the first six samples indicating no phase separation. The hydrocarbon distillate showed considerable fluctuation from sample to sample but no definite trend is discernable. The bulk of the distillate was withdrawn with the bulk of the gas in the last sample. It is likely that most of the distillate was actually in the vapor phase as the temperature used was above the critical temperature of most gasoline components.

It therefore does not appear possible to effect a phase separation between the high-boiling organics and the catalyst melt and this must be taken account of in any regeneration scheme. The high-boiling residue still contains substantial quantities of N, O and S which hetero atoms may complex with the zinc chloride catalyst to form a true solution. On the other hand, polynuclear hydrocarbons such as pyrene which do not contain hetero atoms also do not separate.<sup>(8a)</sup> It thus is not ruled out that one is dealing with a relatively stable emulsion.

It is noted likewise that no concentration of ZnS by settling is apparent from Table I. Separate experiments were conducted in which ZnCl<sub>2</sub> melts were mixed with powdered ZnS and allowed to stand. Again, no phase separation was observed. Since the solubility of ZnS in molten ZnCl<sub>2</sub> is known to be small,<sup>(3)</sup> this is clearly a case of a stable dispersion rather than solution.

Recovery of the organic residue therefore requires addition of another component which will cause phase separation to take place. If solution of unconverted extract is due to complex formation with zinc chloride, it would be logical to assume that phase separation could be effected by addition of agents which themselves complex with zinc chloride such as H<sub>2</sub>O, CH<sub>3</sub>OH, NH<sub>3</sub> and NH<sub>4</sub>Cl. All of these materials have been found in preliminary experiments to be capable of effecting the desired phase separation. At the time of this writing, water addition has been most thoroughly investigated and only some of these data at 200 and 250°C are presented. Composition of the separated phases after water addition are given in Table IIA.

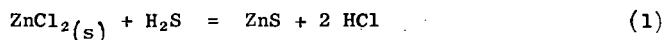
The feed melt composition used in this study was a simulated spent melt and had the composition given in the bottom of Table IIA. Extract was used in place of hydro residue due to shortage of the latter material. Since separation of extract from spent melt is, if anything, more difficult, the results are adequately conservative.

Adequate separation of the extract from the zinc chloride phase takes place at water/melt ratios of 0.3 or greater. The sharpness of separation of the zinc chloride from the organic phase leaves something to be desired, however, especially at low water/melt ratios. The difficulty is due to physical occlusion of aqueous zinc chloride in organic phase. The organic phase is a highly viscous mass that does not flow readily, thus making a sharp separation difficult. The high viscosity is due in part to the inherent high viscosity of the extract and secondly due to dispersion of the zinc sulfide in the organic phase. The zinc sulfide was surprisingly in all cases nearly quantitatively transferred to the organic phase.

The addition of aromatic solvents was investigated in order to improve the sharpness of separation. One such experiment is shown in Table IIB. The added solvent made it possible to withdraw the organic phase as a fluid liquid due to the effect of the solvent in cutting the viscosity. The organic phase was relatively free of inorganic components. In contrast to the previous case most of the ZnS was found in the aqueous phase. This points to physical trapping by the viscous extract as the principle reason for transferral of the ZnS to the organic phase in the previous instance.

## 2. Regeneration of Zinc Sulfide via Reversal of Reaction (1)

The equilibrium in reaction (1) has been measured by Britzke and Kapustinsky<sup>(2)</sup> down to the melting point of ZnCl<sub>2</sub>. Their data were then extrapolated below the melting point using the heat of reaction



$$\Delta H = +16,700 \text{ cal/mole}$$

as determined from the thermochemical data given in Bichowsky and Rossini.<sup>(1)</sup> The result is

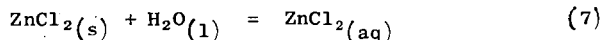
$$\log K_p = \frac{-3360}{T} + 7.62 \quad (6)$$

The equilibrium becomes less favorable with decreasing temperature such that reversal of the reaction becomes feasible at temperatures of the order of 200°C or less, i.e.,  $K_p = 1.0$  at 207°C. For example, at 100°C

$$K_p = P_{HCl}^2/P_{H_2S} = 6.46 \times 10^{-3}$$

Thus, if reversal of the reaction is effected with 0.1 atmosphere of HCl, the ratio  $P_{H_2S}/P_{HCl} = 15.5$  at 100°C.

In actual practice, reversal of reaction (1) can only be effected after addition of sufficient water to maintain a liquid phase. The equilibrium for reversal will now even be more favorable since there is a negative free energy change for the reaction



The effect of using aqueous solutions in facilitating the reversal of reaction (1) is illustrated by some equilibrium data measured by us in dilute aqueous solutions as shown in Table III. The equilibrium is now much more favorable and reversal of reaction (1) with aqueous solution of zinc chloride is to be regarded as a feasible process. Experiments were conducted wherein actual spent melts from hydrocracking of extract were treated with aqueous hydrochloric acid. Rapid evolution of H<sub>2</sub>S was noted.

### 3. Decomposition of Zinc Chloride-Ammonium Chloride Double Salt

The reaction in question is the reversal of reaction (3) which not only supplies the HCl required for regeneration of zinc chloride from zinc sulfide, but eliminates HCl from the melt prior to recovery of the NH<sub>3</sub>. Equilibrium measurements were accordingly made over the range 340-450°C and for initial concentrations of NH<sub>4</sub>Cl in the range of 10 to 20 mole percent. The partial pressure of HCl in equilibrium with the melt as a function of percent NH<sub>4</sub>Cl decomposed is shown in the semi-log plot of Figure 2.

The smoothed data from Figure 2 are replotted to define a "pseudo" equilibrium constant K.

$$P_{HCl} = K \frac{(1 - \alpha)}{\alpha} \quad (8)$$

where  $\alpha$  is the fraction of NH<sub>4</sub>Cl decomposed. Adequate straight lines are obtained (Fig. 3) although slight tailing off is noted in some cases at high conversion levels. This may be due to experimental error as a result of slight losses of NH<sub>3</sub> from the melt. The NH<sub>3</sub> was collected and analyzed as NH<sub>4</sub>Cl and corrections made for its loss. However, if the measurements of volatilized NH<sub>3</sub> were slightly low, it would produce the tailing off observed. The values of K are considerably greater for the 10 mole percent NH<sub>4</sub>Cl series than for the 20 mole percent NH<sub>4</sub>Cl series. No adequate explanation for this phenomenon can be advanced at this time.

A semi-log plot of the HCl pressure versus the reciprocal of the absolute temperature at constant percent NH<sub>4</sub>Cl decomposition is given in Figure 4. The slopes of the lines correspond to the heat of decomposition,

$$\Delta H = 21,000 \pm 600 \text{ cal/mole}$$

It is now possible to express values of K as a function of the temperature in degrees Kelvin by the expressions

$$\log K = \frac{-4590}{T} + B \quad (9)$$

where  $B = 6.32$  and  $6.14$  when the initial  $\text{NH}_4\text{Cl}$  concentrations are 10 and 20 mole percent, respectively, and the  $\text{HCl}$  partial pressure in the expression for  $K$  is given in atmospheres.

In practice,  $\text{HCl}$  would be removed from the melt by stripping with hot gas in a countercurrent tower. The  $\text{HCl}$  concentration in the gas as a function of that in the melt at any point in such a tower is given by the simple material balance relationship

$$P_{\text{HCl}} = \frac{(\Delta - \Delta_f)}{(\Delta - \Delta_f + r)} \cdot \pi \quad (10)$$

The equilibrium pressure of  $\text{HCl}$  over the melt is likewise given by

$$P_{\text{HCl}}^{\text{eq.}} = K \left( \frac{\Delta}{1 - \Delta} \right) \quad (11)$$

where  $\Delta$  = Mole fraction of total  $\text{NH}_3$  in melt combined with  $\text{HCl}$ .

$\Delta_f$  = Value of  $\Delta$  in melt leaving tower.

$\pi$  = Total pressure in atmospheres.

$r$  = Moles of stripping gas/mole of  $\text{NH}_3 + \text{NH}_4\text{Cl}$  in melt.

It is clear that in order to have a net driving force for  $\text{HCl}$  evolution  $P_{\text{HCl}}^{\text{eq.}} > P_{\text{HCl}}$  everywhere in the tower. Consider the case, for simplicity, where the melt is nearly quantitatively stripped of  $\text{HCl}$ , i.e.,  $\Delta_f \cong 0$ . The above condition is satisfied if

$$\left( \frac{dP_{\text{HCl}}}{d\Delta} \right)_{\Delta=0} \leq \left( \frac{dP_{\text{HCl}}^{\text{eq.}}}{d\Delta} \right)_{\Delta=0} \quad (12)$$

Differentiating equations (10) and (11), the inequality may be written,

$$\pi/r \leq K \quad (13)$$

For example, if the temperature at the melt outlet is  $460^\circ\text{C}$ , and the mole fraction of  $\text{NH}_3 + \text{NH}_4\text{Cl}$  in the melt is 0.20, then  $\pi/r \cong .73$ .

A net driving force for  $\text{HCl}$  evolution can still be maintained in such a tower, even if, as will normally be the case, the temperature decreases from bottom to top. The more general inequality can be obtained if the differentiation of equations (10) and (11) above is performed with the equilibrium constant  $K$  as function of  $\Delta$  and therefore also of temperature (i.e.,  $\Delta$  is considered to be a function of temperature). The result is, again for case where  $\Delta_f \cong 0$ ,

$$\frac{K_0}{(1 + \Delta/r)^2} \leq \left( \frac{\Delta}{1 - \Delta} \right) \frac{dK}{d\Delta} + K \left( \frac{1}{1 - \Delta} \right)^2 \quad (14)$$

where  $K_0$  is the value of  $K$  at melt outlet, i.e., where  $\Delta = 0$ . Equation (14) in combination with equation (9) thus can be employed to define the maximum allowable rate of decrease in temperature with respect to  $\Delta$  in the tower and thus is useful for design purposes.

#### 4. Decomposition of Zinc Chloride-Ammonia Adduct

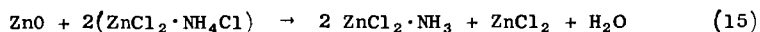
The final regeneration of the spent melt requires that a major fraction of the ammonia be removed. This can be done in principle by thermal decomposition of the adduct which amounts to a reversal of reaction (2). This would be attractive since recovery of  $\text{NH}_3$  would bring substantial by-product credits.

The design of such an  $\text{NH}_3$  adduct decomposition tower requires equilibrium data which give the partial pressure of ammonia over the melt as a function of its ammonia content and temperature. Equilibrium measurements in this system have been made by Kurilov,<sup>(6)</sup> Koeneman<sup>(4)</sup> and Krasnov.<sup>(5)</sup> The above authors in the order named measured the ammonia pressures at successively increasing temperatures and decreasing ammonia content.

The data of these authors are summarized in graphical form in Figure 5. A log-log plot is used to permit some extrapolation outside the range of the data. No experimental points are available below 3.4 wt. percent of  $\text{NH}_3$ .

The ammonia content of the melt sent to the ammonia decomposer in practice will vary between 1.5 and 5.0 wt. % depending upon the melt circulation rate used. It is clear, however, from the data of Figure 5 that it will be very difficult to achieve very low  $\text{NH}_3$  concentrations, i.e., below 1% in the regenerated melt unless temperatures well above those investigated are used.

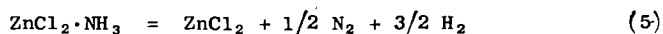
It is not necessary, however, to reduce the  $\text{NH}_3$  content of the regenerated melt to zero. It has been found, for example, that the reaction



goes quantitatively to the right at temperatures in the neighborhood of 400°C. The melt leaving the  $\text{NH}_4\text{Cl}$  decomposer will therefore be free of zinc oxide. This is in contrast to the feed melt to the hydrocracking runs described in a previous paper<sup>(8b)</sup> which contained 2.8 mole % of  $\text{ZnO}$ . Equivalent hydrocracking results will therefore be obtained with a regenerated melt containing .056 moles  $\text{NH}_3$ /mole  $\text{ZnCl}_2$  (0.7 wt. %  $\text{NH}_3$ ) to those reported experimentally which contained .056 moles  $\text{NH}_4\text{Cl}$ /mole  $\text{ZnCl}_2$ . The above result follows since reaction (15) proceeds in the melt used in the experimental work to produce an identical melt composition in both cases. The activity of the melt in this case [cf. Figure 6 of previous paper<sup>(8b)</sup>] is only negligibly less than that of a melt containing no  $\text{NH}_4\text{Cl}$ .

The ammonia decomposition equilibrium at lower  $\text{NH}_3$  concentrations and higher temperatures is presently being investigated in the Consolidation Coal Co. laboratories but no data are available as yet.

One interesting observation has been made, however, that the reaction



is readily catalyzed by oxidized metal surfaces. Thus, it appears to be possible, if desired, to eliminate the last traces of ammonia from the melt by catalytic decomposition at temperatures of the order of 550-600°C.

#### 5. Removal of Ash

Coal extract feed will contain anywhere from 0.1 to 0.4 wt. % ash depending on its method of preparation. Ash must be periodically removed from the melt during its regeneration to prevent its build up. Several methods are available such as filtration after dilution with water and removal of zinc sulfide. It also may be removed by distillation of zinc chloride vapor from a side stream to leave an ash residue.

## 6. Overall Regeneration Scheme

The integration of the various process steps discussed above into a single regeneration scheme is illustrated in Figure 6. Appropriate operating ranges for each process step are likewise given.

A material balance around the operation is given in Table IV. The spent melt entering regeneration is assumed to be the same composition as that from the 5 stage coal extract hydrocracking run reported in a previous paper<sup>(8b)</sup> {cf. Table IV}. The regenerated melt composition is adjusted such that the composition of the spent melt after hydro is consistent with elimination of 98.0% of the sulfur and 87.5% of the nitrogen from the feed extract, i.e., in accord with experimentally observed results in the 5 stage run.

The performance of the  $\text{NH}_3$  decomposition tower was calculated from the data of Figure 5 assuming isothermal operation at  $530^\circ\text{C}$ , 4 theoretical stages and a total pressure of 1.5 atms.

In practice, one would have a temperature increase in the  $\text{NH}_3$  decomposition tower since heat would be supplied by condensing zinc chloride vapor from the boiler. Thus, fewer stages would be required.

Recovery of  $\text{NH}_3$  from the gases leaving the ammonia decomposer can be effected according to the data of Kurilov (cf. Figure 5) by scrubbing with a  $\text{ZnCl}_2$  melt relatively concentrated in  $\text{NH}_3$  at lower temperatures as shown in Figure 6.

The melt is readily decomposed to yield pure  $\text{NH}_3$  gas at temperatures of the order of  $400^\circ\text{C}$ . Of course, other more conventional methods of ammonia recovery could also be used.

The above scheme is likewise adaptable to spent melts used in hydrocracking of coal itself. In this case the melt will contain a larger percentage of ash and accordingly more ash will have to be rejected in the vaporization step. In practice, a higher proportion of the melt will have to be vaporized, and this would be one of the disadvantages of using coal as compared with extract.

### ACKNOWLEDGMENT

The sponsorship of the U. S. Office of Coal Research for this investigation is gratefully acknowledged.

### BIBLIOGRAPHY

- (1) Bichowsky, F. R. and Rossini, F. P., *Thermochemistry of the Chemical Substances*, Reinhold Publishing Co., New York, 1936.
- (2) Britzke, E. V., Kapustinsky, A. F. and Veselovskii, B. K., *Zeit, Anorg. Chem.*, **213**, 65 (1933).
- (3) Gasharov, G. and Levine, A. K., *J. Chem. and Eng. Data* **5**, No. 4, 517 (1960).
- (4) Koeneman, E., *Gesamtbericht II, Weltkraft Conference, Berlin V*, 325 (1930).
- (5) Krasnov, A. Z., *J. Applied Chem. USSR*, **12**, No. 11, 1595-1597 (1939).
- (6) Kurilov, N. N., *Proc. Russ. Akad. Sci., Phys. - Materials Section* **1**, 6 (1895).
- (7) Stull, P. R., *Ind. Eng. Chem.*, **39**, 545 (1947).
- (8) Zielke, C. W., Struck, R. T., Evans, J. M., Costanza, C. P., and Gorin, E.
  - (a) "Molten Salt Catalysts for Hydrocracking of Polynuclear Hydrocarbons."
  - (b) "Molten Zinc Halide Catalysts for the Hydrocracking of Coal Extract and Coal."

Presented Before the Division of Fuel Chemistry, ACS  
Atlantic City, N. J., September 12-17, 1965.

TABLE I

Phase Separation of Organic Residue from Zinc Chloride Melt

Hydro Condition:

ZnCl<sub>2</sub>/Extract, Wt. Ratio = 1  
 Total Hot Pressure = 3000 psig  
 Temperature = 750°F

Sample No.	1	2	3	4	5	6	7	8
Cum. Wt. % of Total Liquid Withdrawn	7.8	17.6	25.4	35.3	45.7	58.0	64.7	100
Cum. Wt. % of Total Gas Withdrawn	1.9	3.2	4.2	5.6	7.0	8.1	10.2	100
Type of Sample	Melt							Lt. Oil + Gas

Analysis, Wt. % of Sample

Hydrocarbon Distillate	-400°C	5.5	10.5	7.8	16.2	9.4	9.8	21.9	100
Organic Residue	+400°C	18.0	20.3	21.6	15.4	18.2	17.3	29.5	--
ZnCl <sub>2</sub>		62.7	54.4	58.2	56.9	61.8	61.9	40.4	--
ZnCl <sub>2</sub> ·NH <sub>3</sub> + ZnCl <sub>2</sub> ·NH <sub>4</sub> Cl		9.3	10.8	8.5	6.5	6.5	6.8	4.0	--
ZnS		4.5	4.0	3.9	11.5	4.1	4.2	4.2	--

TABLE II

A. Phase Separation Studies with Water Addition

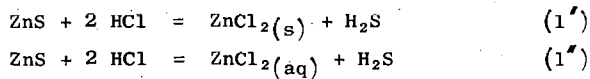
Wt. Ratio H <sub>2</sub> O/Feed Temperature, °C	60 Minute Phase Separation Time Used											
	0.3		0.5		1.0		0.5		1.0		1.0	
	Aqueous Phase	Organic Phase	Aqueous Phase	Organic Phase	Aqueous Phase	Organic Phase	Aqueous Phase	Organic Phase	Aqueous Phase	Organic Phase	Aqueous Phase	Organic Phase
Feed Melt	81.9											
ZnCl <sub>2</sub>	57.6	20.3	71.1	9.1	75.0	3.6	75.8	5.2	79.0	2.3		
ZnS	0.0	4.4	0.0	4.0	0.0	5.5	0.0	3.8	0.0	4.3		
NH <sub>3</sub>	1.0	0.3	1.0	0.2	1.0	0.0	1.3	0.1	1.1	0.0		
Extract	0.4	16.0	0.5	9.2	0.6	13.2	0.9	9.2	0.7	10.3		
Total	59.0	41.0	72.6	22.5	76.6	22.3	78.0	18.3	80.8	16.9		

B. Phase Separation with Water and Dimethylnaphthalene (DMN) Solvent Addition

Wt. Ratio H <sub>2</sub> O/Feed Temperature, °C	0.56		0.22		250	
	Aqueous Phase	Organic Phase	Aqueous Phase	Organic Phase	Feed Melt Composition, Wt. %	
	ZnCl <sub>2</sub>	44.4	--	44.4	--	ZnCl <sub>2</sub>
NH <sub>4</sub> Cl	2.8	--	2.8	--	NH <sub>4</sub> Cl	2.8
ZnS	2.3	0.5	2.3	0.5	ZnS	2.8
Extract	1.4	48.6	1.4	48.6	Extract	50.0
Total	50.9	50.1	50.9	50.1		

TABLE III

Equilibrium Data Compared for Reactions



Temperature, °C	50	66
<u>Normality of Equil. Mixture</u>		
HCl	2.6	0.68
ZnCl <sub>2</sub>	0.4	0.32
P <sub>H<sub>2</sub>S</sub> (atm)	1.52	0.10
P <sub>HCl</sub> (atm) <sup>(1)</sup>	7.9 × 10 <sup>-5</sup>	1.3 × 10 <sup>-5</sup>
P <sub>H<sub>2</sub>S</sub> /P <sub>HCl</sub> <sup>2</sup> obs. for reaction (1'')	2.4 × 10 <sup>8</sup>	5.9 × 10 <sup>8</sup>
P <sub>H<sub>2</sub>S</sub> /P <sub>HCl</sub> <sup>2</sup> Calc. for reaction (1')	4.9 × 10 <sup>3</sup>	1.5 × 10 <sup>3</sup>

(1) From literature data at the measured acid concentration of International Critical Tables Vol. III, pg 301.

TABLE IV

Material Balance in Regeneration of Zinc Chloride Melt from  
5 Stage Extract Hydro Run at 750°F - 3000 psig

Process Step	From Extract Hydro	From ZnS Decomposer	MgCl <sub>2</sub> from Decanter	From NH <sub>4</sub> Cl Decomposer	From Condenser	From Primary NH <sub>3</sub> Decomposer
Temperature, °C	393	~ 100	200	427	400	530
No. of Stages	5	1	1	NC	1	4
<u>Moles/100 lbs Extract Fed to Hydro</u>						
<u>Liquid Phase</u>						
ZnCl <sub>2</sub> (1)	0.197	0.252	0.252	0.252	0.0024	0.343
ZnCl <sub>2</sub> ·NH <sub>3</sub> (1)	0.018	0.018	0.018	0.129	0.0078	0.038
ZnCl <sub>2</sub> ·NH <sub>4</sub> Cl(1)	0.111	0.111	0.111	--	--	--
ZnS(s)	0.055	--	--	--	--	--
+400°C Organic Residue (lbs)	17.4	17.4	--	--	--	--
<u>Gas Phase</u>						
Stripping Gas	--	--	--	NC	0.550	0.550
NH <sub>3</sub>	--	--	--	--	0.091	0.0988
ZnCl <sub>2</sub> (v)	--	--	--	--	--	0.0102
H <sub>2</sub> S	--	0.055	--	--	--	--
HCl	--	--	--	0.111	--	--

(1) Percent of sulfur released from extract feed as ZnS = 98.0

(2) Percent of nitrogen released from extract feed as NH<sub>3</sub> + NH<sub>4</sub>Cl = 87.5

*Figure 1*  
**APPARATUS FOR EQUILIBRIUM STUDIES**

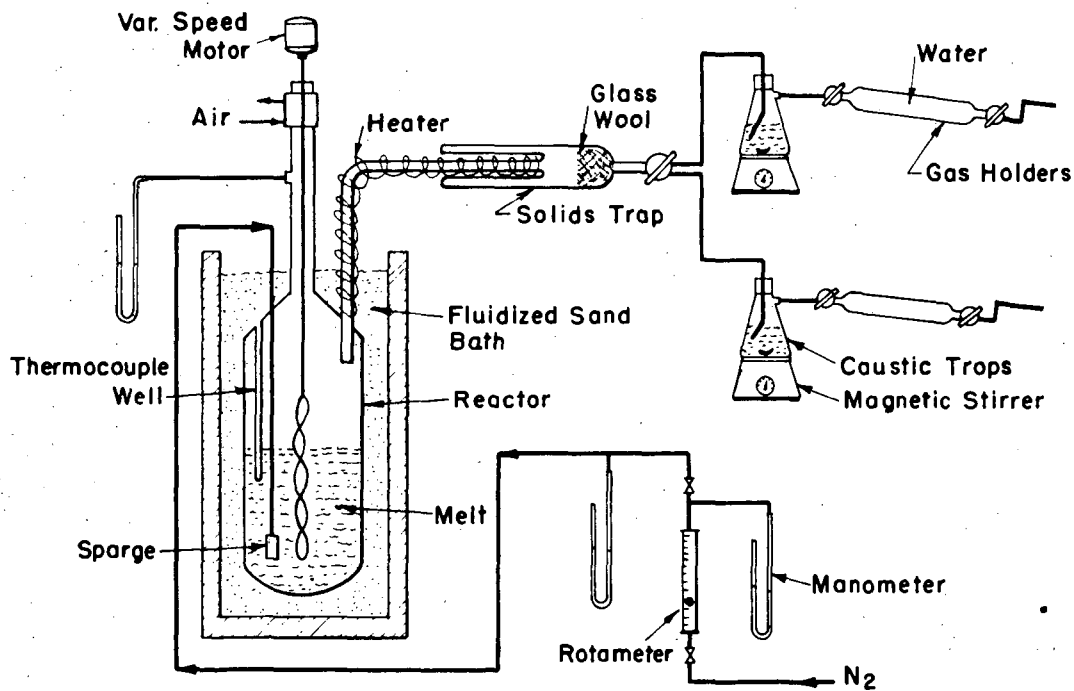


Figure 2

**EQUILIBRIUM PARTIAL PRESSURE OF HCl**  
**VS**  
**% NH<sub>4</sub>Cl DECOMPOSED**

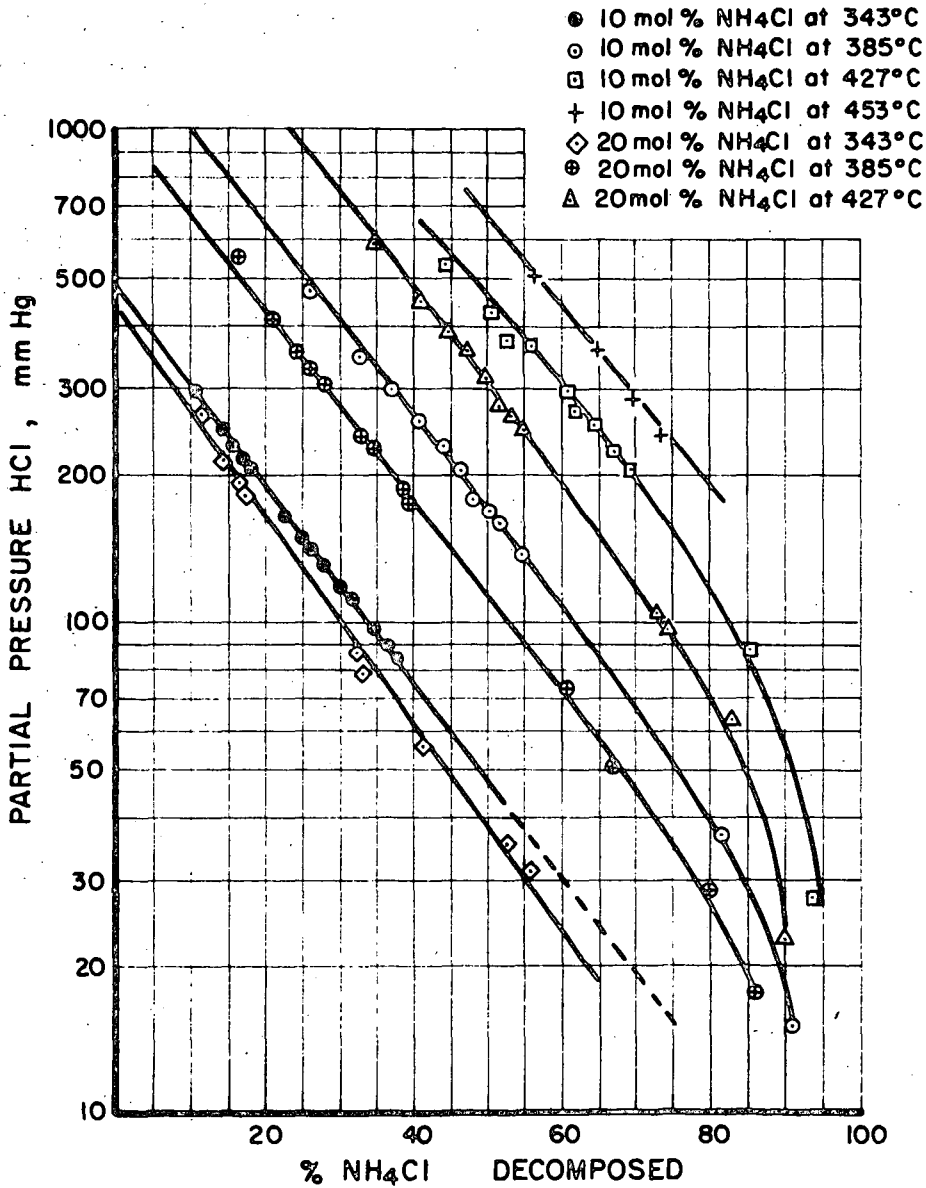


Figure 3  
**EQUILIBRIUM CONSTANT FOR REACTION**  
 $ZnCl_2 \cdot NH_4Cl = ZnCl_2 \cdot NH_3 + HCl$

Initial Concn. NH <sub>4</sub> Cl Mol%	Temp. °C
○ 10	427
◊ 10	385
◻ 20	427
◻ 20	385

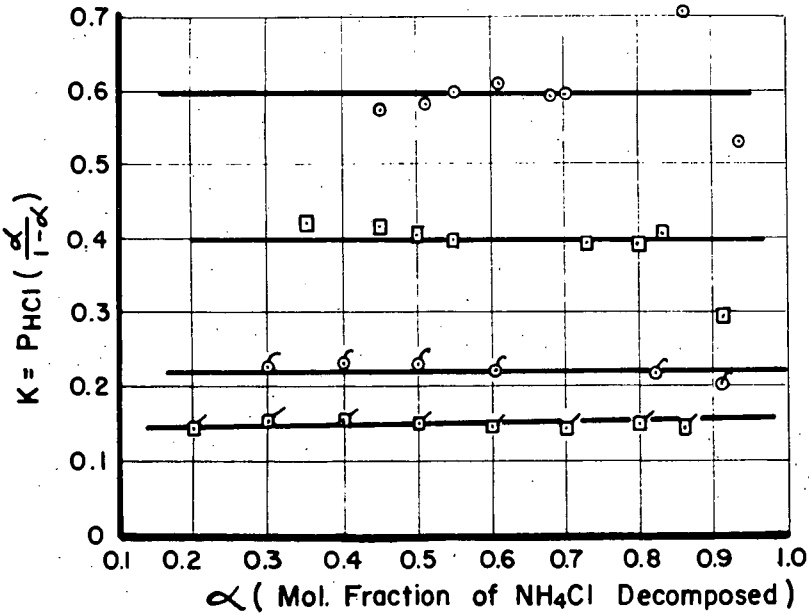


Figure 4

EFFECT OF TEMPERATURE ON  
HCl EQUILIBRIUM PARTIAL PRESSURE

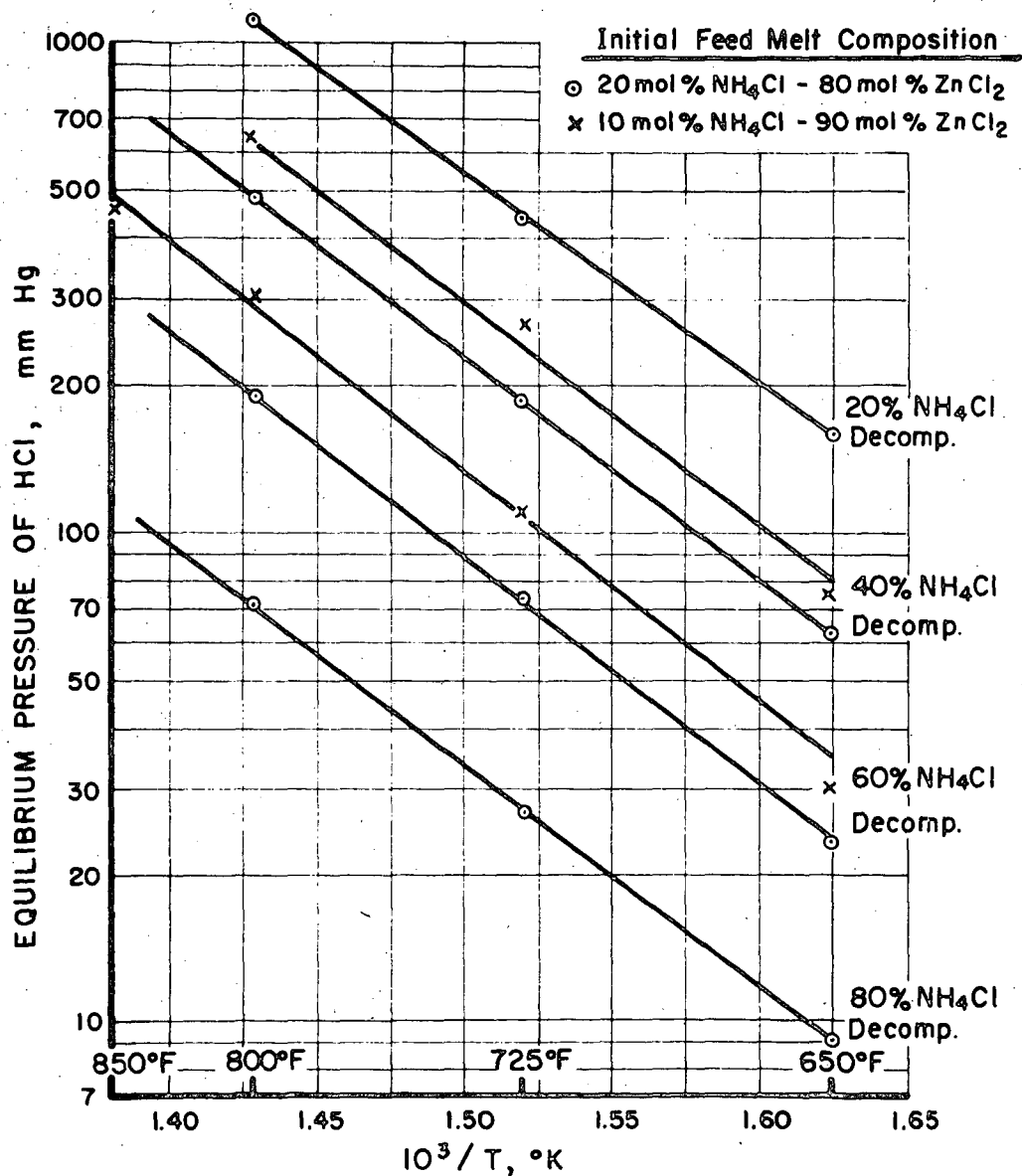


Figure 5

SUMMARIZED DATA ON DISSOCIATION  
PRESSURE OF NH<sub>3</sub> OVER ZnCl<sub>2</sub> MELTS

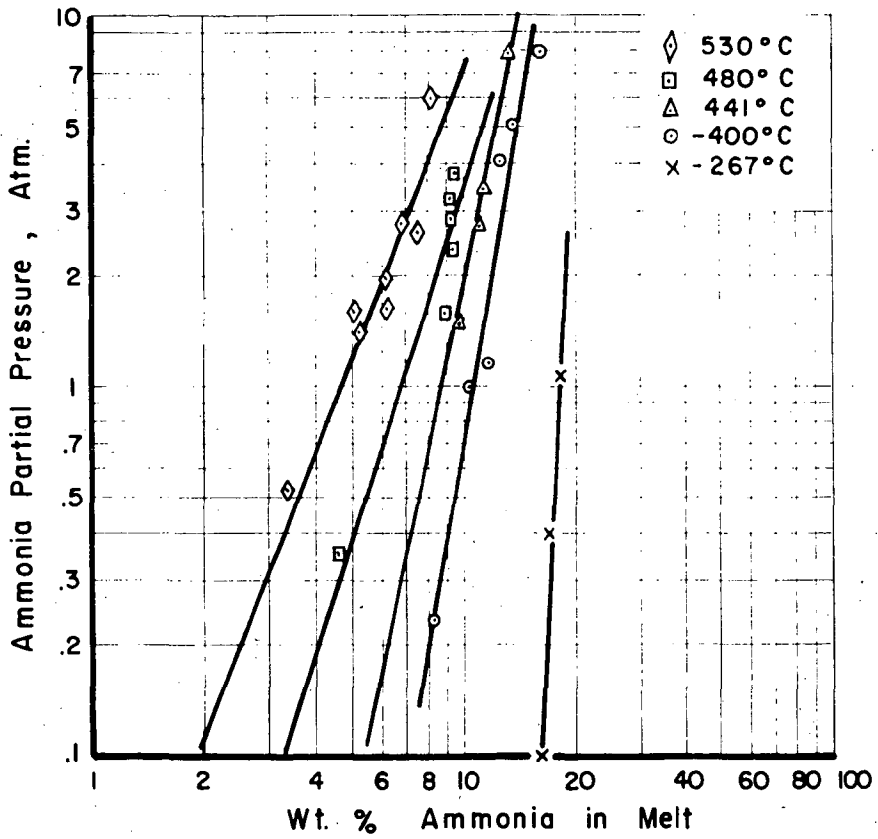
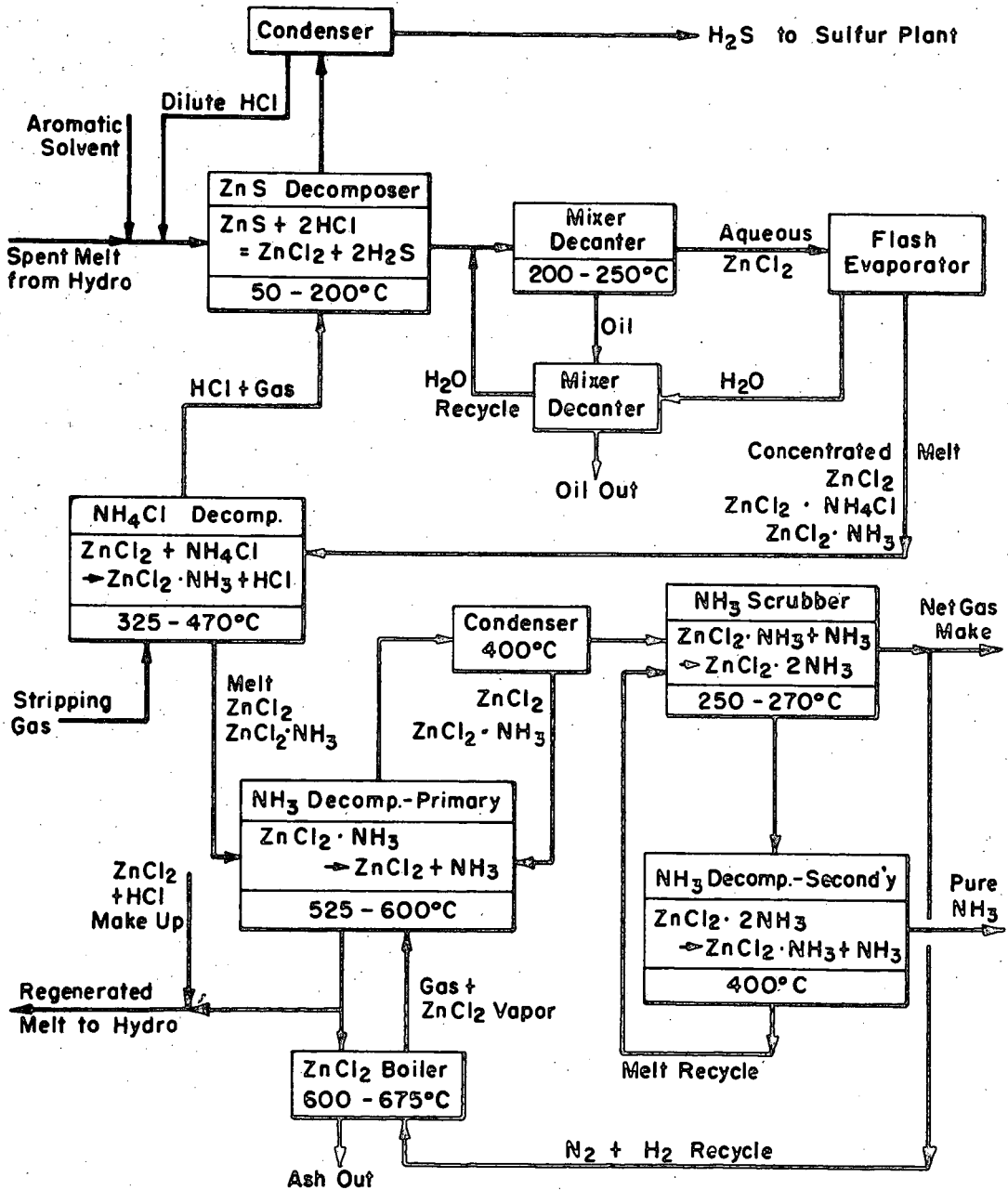


Figure 6

**SCHEMATIC DIAGRAM OF REGENERATION SCHEME**



Elevated Pressure Adsorption of Methane on Activated Carbon;  
Effects of Contaminant Gases and Repeated Cycling

J. W. Mulvihill, W. P. Haynes, R. J. Haren, and J. H. Field  
U. S. Bureau of Mines, 4800 Forbes Avenue  
Pittsburgh, Pennsylvania 15213

INTRODUCTION

Bureau of Mines interest in methane adsorption was developed from research on hydrogasification of coal to produce synthetic pipeline gas. The product from hydrogasification consists principally of methane and hydrogen<sup>2, 6</sup>, the methane content varying from 5 to 80 percent depending on process variables. The minor constituents are nitrogen, carbon oxides, sulfur compounds, unsaturates, higher molecular weight hydrocarbons including aromatics, and water vapor. Synthetic pipeline gas with a heating value of approximately 1,000 Btu's can be produced from hydrogasification product by recovering the methane. The Bureau of Mines has reported that estimated capital and operating costs for separating methane from mixtures of methane and hydrogen are lowest if the methane is adsorbed by activated carbon<sup>8</sup>. The estimate, however, was based on extrapolated data<sup>5</sup> for the adsorption of pure methane at relatively low pressures. The objective of this investigation was to establish adsorption isotherms for methane on activated carbon at 40° C and pressures of 14.2 to 800 psia and study the tendency of activated carbon to lose its adsorptive capacity for methane when the methane is contaminated with other gases and/or there is repeated cycling.

Effects of adding benzene, hydrogen, ethylene, or hydrogen sulfide were investigated. These gases were chosen as contaminants because they are in the gaseous mixture produced by hydrogasification. Two of the contaminant gases, benzene and hydrogen, used in the experiments were given concentrations similar to those found in a hydrogasification product. The other two contaminants, ethylene and hydrogen sulfide, were given much higher concentrations than would be found in a hydrogasification product in order to simulate rapid poisoning of the adsorbent.

The adsorptive capacity of activated carbon can be affected by side reactions. Activated carbon may act catalytically to convert hydrogen sulfide to free sulfur in the presence of trace amounts of oxygen, and the free sulfur may occupy space that could be taken up by the methane.<sup>1</sup>

### APPARATUS AND PROCEDURE

Some of the main components of the fixed-bed adsorption unit are shown in figure 1. The adsorber was made of type 304 stainless steel as were the valves, fittings, tubing, and gas collection reservoirs, because of their contact with hydrogen sulfide. The adsorber was 24 inches long with 1/2-inch outside diameter and 3/8-inch inside diameter. It had a maximum working pressure of 1,500 psi and a maximum working temperature of 450° C. During desorption, heat was supplied electrically using the adsorber wall as an electrical resistor. Power for heating was supplied by a 7.5 KVA, 10:1 step-down transformer. During the cooling cycle, the adsorber was rapidly cooled along its entire length by air blown from a series of small nozzles.

During the rapid cycling studies, the adsorption, desorption, and cooling cycles were automatically controlled by a time cycle controller. A complete cycle consisted of a 9-minute adsorption period at 40° C, 6 minutes desorption at 450° C, and 3 minutes cooling.

Figure 2 is a schematic flow diagram of the rapid cycling, fixed-bed adsorption system. The desired feed gas of known composition is supplied to the unit from high-pressure storage cylinders. The gas flow rate is measured by pressure drop through a calibrated capillary manometer. The gas saturator was used to add benzene to the feed gas when the contaminating effect of benzene was studied.

A weighed sample of fresh activated carbon was placed in the adsorber prior to each series of experiments. The activated carbon was degassed under vacuum for 2 to 3 hours at 450° C. At the end of this period the pressure in the adsorption chamber, measured by a McLeod gage, was about 15 microns Hg. The "dead space" in the reactor system was the volume of the adsorption chamber bounded by three solenoid valves, SV-1, SV-2, and SV-3. It represented the adsorbent pore volume, the interparticle void space, plus the volume of the apparatus capillary lines inside the respective boundaries. Dead space was determined by introducing measured amounts of helium at atmospheric pressure into the evacuated adsorption chamber, noting the equilibrium pressure, and applying the ideal gas law. Adsorption of helium was assumed to be negligible under these conditions.

In determining the amount of methane adsorbed for the pure methane experiments (static studies), methane was fed into the adsorption chamber until equilibrium conditions were attained. Equilibrium was attained rapidly, in some cases within 15 minutes. The gas was then desorbed from the adsorption chamber into a 500-cc calibrated collection reservoir. The desorption temperature was 450° C for all the experiments. A slow helium purge was also used in conjunction with the high temperature to remove the last traces of methane. The amount of methane adsorbed on the activated carbon was the difference between the total methane collected and that contained in the dead space.

In the mixture experiments (dynamic studies), it was assumed that methane equilibrium was attained in approximately the same length of time required during the pure methane experiments (static studies). After methane equilibrium was attained, the gas remaining in the dead space and on activated carbon's surface was desorbed into the 500-cc calibrated collection reservoir. The amount of methane adsorbed was determined in a manner similar to that used for the static studies.

The ideal gas law was used for computing the amount of adsorbed gas when the total adsorption pressure did not exceed 50 psi. Generalized compressibility factors<sup>9/</sup> were used in conjunction with Amagat's law when total pressure exceeded 50 psi.

All gases were analyzed by chromatography and mass spectrometry. The methane used in the experiments contained 0.2 percent ethane and 0.1 percent nitrogen. The adsorbent was a 12x30 mesh Pittsburgh Coke and Chemical Co. Type BPL activated carbon manufactured from various grades of bituminous coal combined with suitable binders.

#### RESULTS AND DISCUSSION

When adsorption takes place in a unimolecular layer, or part of a layer, the data can often be fitted satisfactorily by means of the simple Langmuir equation<sup>7/</sup>

$$x/m = \frac{a b P}{1 + a P}$$

In this formula

- x = weight of gas adsorbed.
- m = weight of solid adsorbent.
- P = Partial pressure of the gas in question at equilibrium.
- a, b = experimental constants.

The Langmuir equation is based on the assumption that the molecules of the adsorbed gas are present on the surface of the adsorbent as a monolayer. The greater the fraction of the surface covered by the monolayer, the less tendency there is to accumulate more molecules and the greater the partial pressure must be to continue such accumulation.

The Langmuir formula may be rewritten as the equation of a straight line,

$$P/(x/m) = (1/b) P + 1/(a b).$$

The experimental constants a and b can be calculated if the plot of  $P/(x/m)$  versus P is a straight line. Figure 3 shows Langmuir plots of our experimental data and data of four other investigators, Per K. Frolich<sup>4/</sup>,

L. Szepesy<sup>11/</sup>, G. C. Ray<sup>10/</sup>, and R. J. Grant<sup>5/</sup>. Curve 5 represents Grant's extrapolated data. These extrapolated data were used in our original cost estimates.

Plots of both Szepesy's and our data, curves 2 and 3, produced straight lines. The upper portion of Frolich's data, curve 1, is also a straight line. The experimental constants for curves 2 and 3 become:

1) Curve 2:  $a = 9.64 \times 10^{-3} \text{ psia}^{-1}$ ,  $b = 7.41 \text{ g/100 g}$ .

2) Curve 3:  $a = 12.85 \times 10^{-3} \text{ psia}^{-1}$ ,  $b = 5.56 \text{ g/100 g}$ .

Freundlich's equation,  $x/m = a P^{1/n}$ , is used frequently to correlate adsorption data. The letters x, m, and P have the same meaning as in the Langmuir equation, and the letters a and 1/n represent empirical constants.

The validity of the formula for the experimental data can be tested by plotting the logarithm of x/m against the logarithm of P, since rewriting the formula in its logarithm form,  $\log(x/m) = \log a + (1/n) \log P$ , gives the equation of a straight line.

Figure 4 shows Freundlich plots of our experimental data and data of the four other investigators previously mentioned. None of the curves obeys the Freundlich equation.

Table 1 shows the effect of 76.5 percent hydrogen in the methane feed gas upon activated carbon's adsorptive capacity for methane. In these series of experiments, two methane partial pressure levels were investigated, 50 and 300 psia. Activated carbon's equilibrium capacity for methane was reduced 10.0 and 22.8 percent, respectively, owing to the presence of hydrogen. Experiments with a methane-hydrogen mixture showed that the selectivity of the carbon for methane over hydrogen was 11:1 at 50 psia partial pressure, and 28:1 at 300 psia.

Figure 5 shows the effect of methane contamination and repeated cycling upon activated carbon's adsorptive capacity of methane. Benzene, hydrogen, ethylene, and hydrogen sulfide were the contaminants tested. After the first adsorption step, all the contaminants reduced the capacity of activated carbon for methane. The initial reductions in capacity for methane owing to the presence of the contaminants are given in percent in table 2. The presence of 8.3 percent hydrogen sulfide produced the greatest initial loss of capacity, reducing the carbon's capacity for methane by 53 percent. Benzene, hydrogen, and ethylene reduced the methane capacity of the carbon by 13, 25, and 37 percent, respectively.

Additional adsorption-desorption cycles using the contaminated methane feed gases incurred no further decrease in carbon capacity for methane except in the tests using 10.3 percent ethylene in the methane feed gas. After 150 cycles, activated carbon's capacity for methane was reduced an additional 13 percent from 37 to 50 percent.

TABLE 1.- Effect of hydrogen upon activated carbon's adsorptive capacity for methane

Feed gas	Adsorption temperature, °C	equilibrium pressure, psia	Activated carbon's capacity for methane,	Activated carbon's capacity for hydrogen,	Selectivity, Carbon capacity(CH <sub>4</sub> ) Carbon capacity(H <sub>2</sub> )
			<u>g CH<sub>4</sub></u> <u>100 g carbon</u>	<u>g H<sub>2</sub></u> <u>100 g carbon</u>	
a) CH <sub>4</sub> <sup>1/</sup>	40	50	2.49	--	--
23.7 pct CH <sub>4</sub> b) + 76.3 pct H <sub>2</sub>	40	50	2.24	0.02	11:1
a) CH <sub>4</sub> <sup>1/</sup>	40	300	5.49	--	--
23.7 pct CH <sub>4</sub> b) + 76.3 pct H <sub>2</sub>	40	300	4.23	0.15	28:1

<sup>1/</sup> Containing 0.2 pct C<sub>2</sub>H<sub>6</sub> and 0.1 pct N<sub>2</sub>.

TABLE 2.- Reduction in activated carbon's capacity for methane by contaminating gases and repeated cycling <sup>1/</sup>

Contaminating gas, vol-pct	Percent		Saturation of activated carbon with impurity
	Initial reduction in capacity for methane (without recycling)	Reduction in capacity for methane after 150 cycles	
0.35 C <sub>6</sub> H <sub>6</sub>	13.0	14.0	10.0
76.3 H <sub>2</sub>	25.0	25.0	100.0
10.3 C <sub>2</sub> H <sub>4</sub>	37.0	50.0	75.0
8.3 H <sub>2</sub> S	53.0	53.0	100.0

<sup>1/</sup> Conditions: Adsorption temperature 40° C; Methane equilibrium pressure 300 psia.

In these contaminating and cycling tests, hydrogen and hydrogen sulfide were the only two contaminants that completely saturated the activated carbon. Benzene and ethylene only reached 10 and 75 percent carbon saturation, respectively. In all of the tests conducted, methane attained equilibrium conditions or 100 percent saturation before desorption was initiated. Degree of saturation was determined through adsorber tail gas analyses.

Experiments were conducted about five times for each pure methane equilibrium point. Standard deviation from the mean value was  $\pm 1-2$  percent for these experiments. Standard deviation for the methane-hydrogen mixture experiments conducted at the two partial pressure levels was  $\pm 15$  percent. Greater scattering of data occurred when the small quantities of hydrogen adsorbed were being determined.

#### CONCLUSIONS

1. Increased total pressure favors the preferential adsorption of methane from methane-hydrogen mixtures. However, methane is less strongly adsorbed from the mixture than when it is present at the same partial pressure in the pure state. Lower values for methane adsorption at high partial pressures were found experimentally than those extrapolated from existing data at lower pressures.

2. Each impurity of hydrogasification product gas tested decreased activated carbon's capacity for methane. Although the carbon was not completely saturated with benzene and ethylene, these impurities still contributed significantly to the initial lowering of the adsorbent's capacity for methane.

3. Repeated cycling, up to 150 cycles, in the presence of the contaminants did not further decrease activated carbon's capacity for methane except when ethylene was added.

4. These results indicate that the cost estimates reported earlier<sup>8/</sup> were too low because the extrapolated values for methane adsorption were too high. The efficiency of activated carbon in adsorbing methane is lowered by other gases mixed with the methane and, when ethylene is present, by repeated cycling. However, for most of the cases of separation investigated ( $\text{CH}_4$  concentrations of 5, 20 and 50 pct), the economics of adsorption by activated carbon are now considered to be approximately the same as separation by liquefaction of methane.

1. Barry, H. M. Fixed-bed Adsorption. Chem. Eng., v. 67, No. 3, Feb. 8, 1960, p. 115.
2. Channabasappa, K. C., and H. R. Linden. Fluid-Bed Pretreatment of Bituminous Coals and Lignite. Direct Hydrogenation of Chars to Pipeline Gas. Ind. Eng. Chem., v. 50, No. 4, April 1958, pp. 637-644.
3. Freundlich, Herbert. Colloid and Capillary Chemistry (Translated from the third German edition by H. Stafford Hatfield), E. P. Dutton and Co., New York, N. Y., 1931, p. 111.
4. Frolich, Per K. Adsorption of Methane and Hydrogen on Charcoal at High Pressure. Ind. and Eng. Chem., v. 22, No. 10, Oct. 1930, pp. 1058-1060.
5. Grant, R. J., M. Manes, and S. B. Smith. Adsorption of Normal Paraffins and Sulfur Compounds on Activated Carbon. A. I. Ch. E. J., v. 8, No. 3, July 1962, pp. 403-406.
6. Hiteshue, R. W., R. B. Anderson, and S. Friedman. Hydrogenation of Coal and Chars. Ind. and Eng. Chem., v. 52, No. 7, July 1960, pp. 577-579.
7. Langmuir, I. The Adsorption of Gases on Plane Surfaces of Glass, Mica, and Platinum. J. Am. Chem. Soc., v. 40, No. 9, Sept. 1918, p. 1361.
8. Mulvihill, J. W., W. P. Haynes, S. Katell, and G. B. Taylor. Cost Estimates of Processes for Separating Mixtures of Methane and Hydrogen. BuMines Rept. of Inv. 6530, 1964, 43 pp.
9. Nelson, L. C., and E. F. Obert. How to Use the New Generalized Compressibility Charts. Chem. Eng., v. 61, No. 7, July 1954, pp. 203-208.
10. Ray, G. C., and E. O. Box, Jr. Adsorption of Gases on Activated Charcoal. Ind. and Eng. Chem., v. 42, No. 7, July 1950, pp. 1315-1318.
11. Szepeesy, L., and V. Illes. Adsorption of Gases and Gas Mixtures. Acta Chim. Hung. Tomus., v. 35, 1963, pp. 37-50; 53-59.

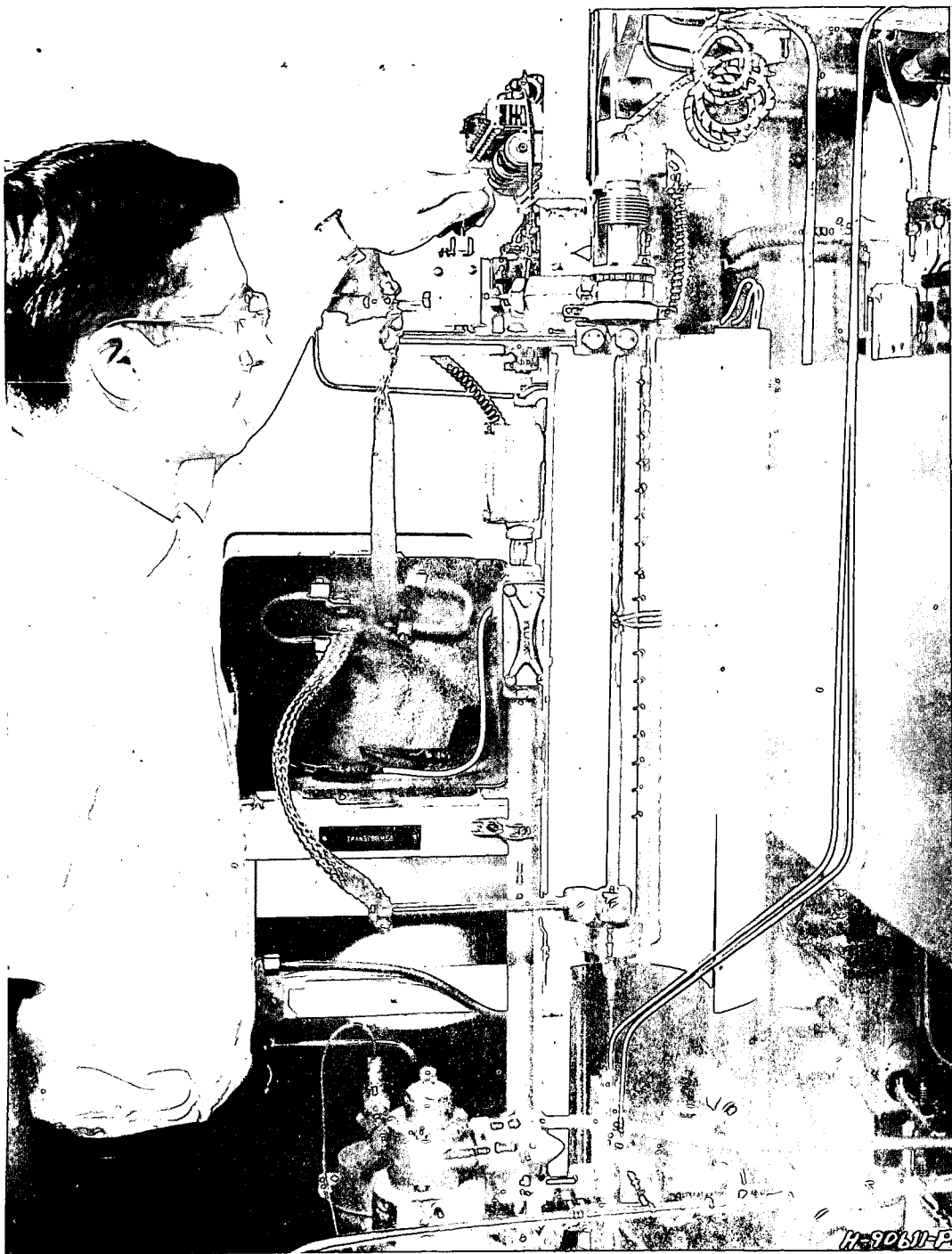


Figure 1.-RAPID CYCLING, FIXED BED ABSORBER

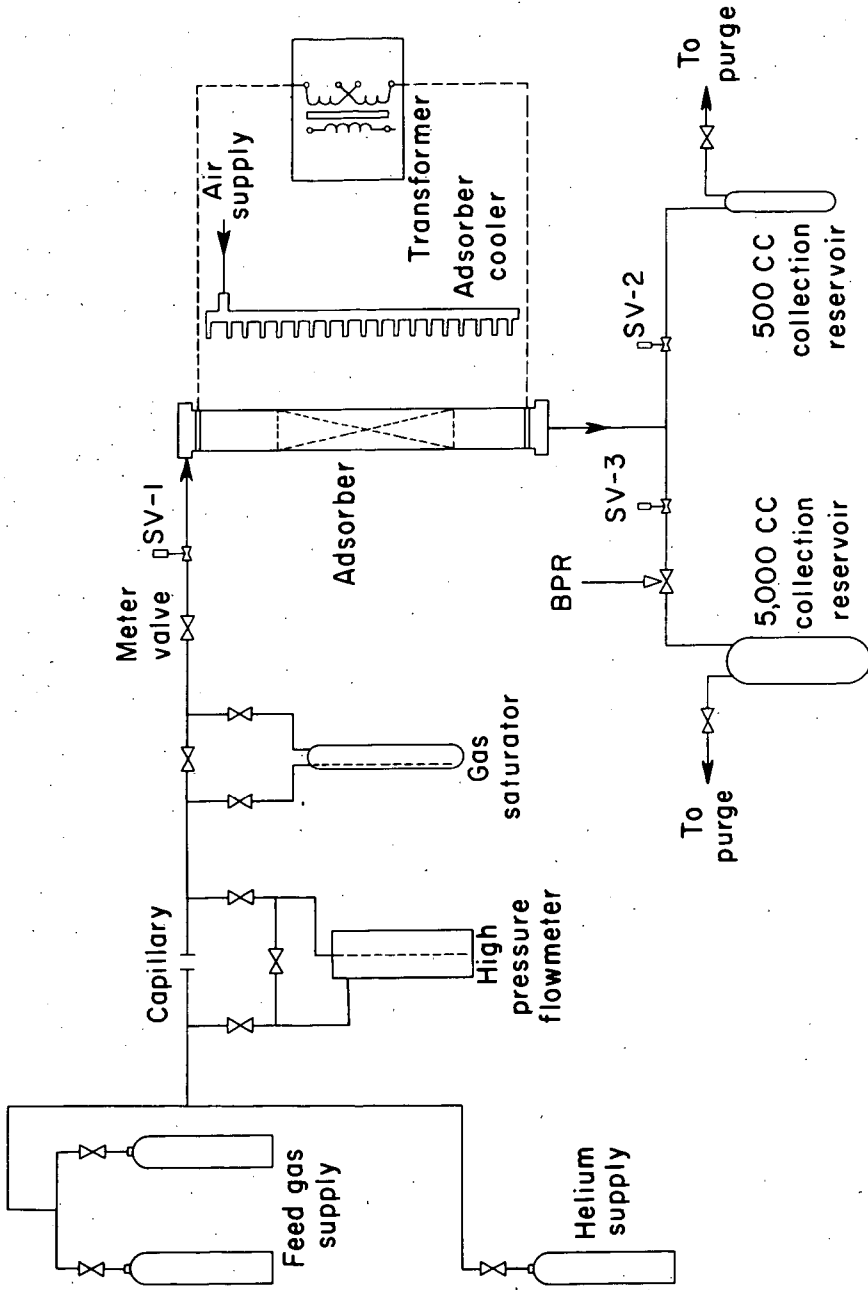


Figure 2.-Overall flowsheet of bench-scale adsorption unit.

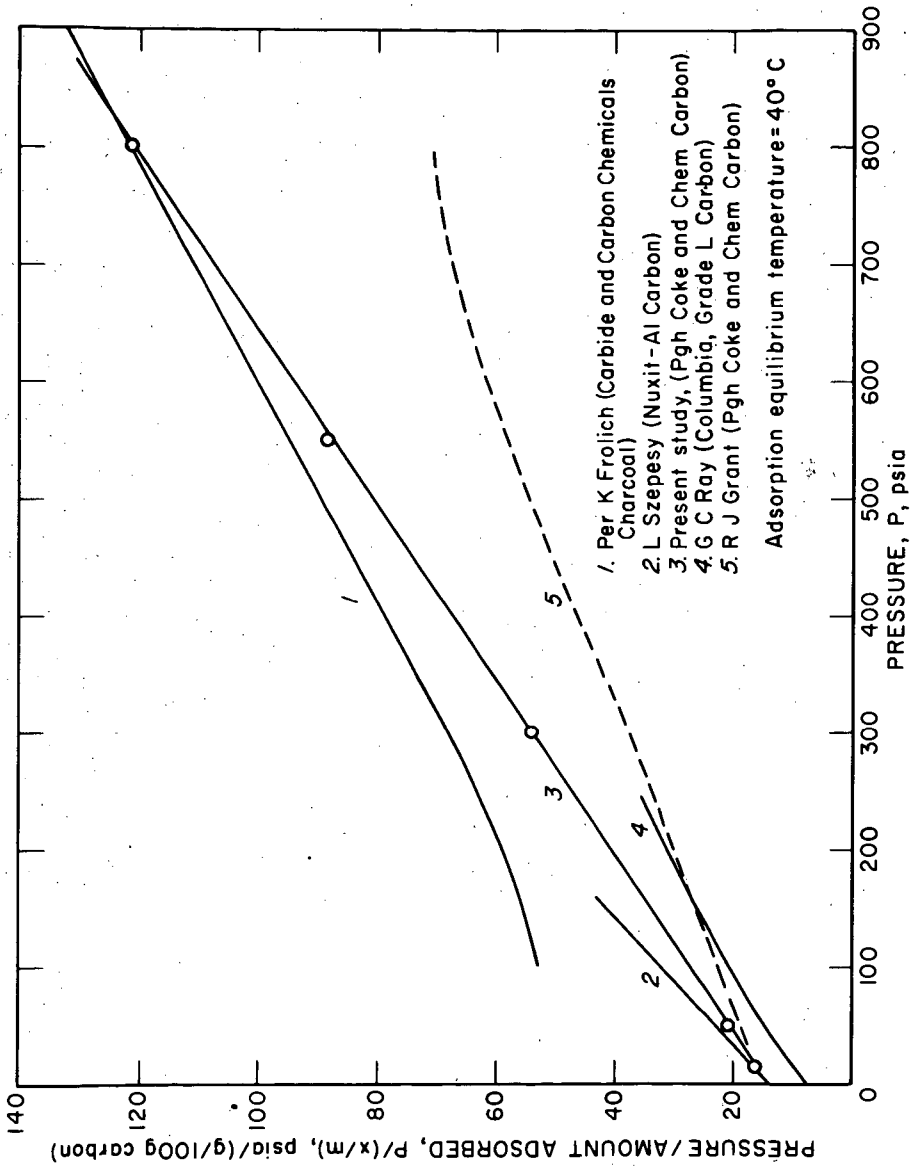


Figure 3.- Adsorption isotherms for methane on various types of activated carbon, Langmuir plots.

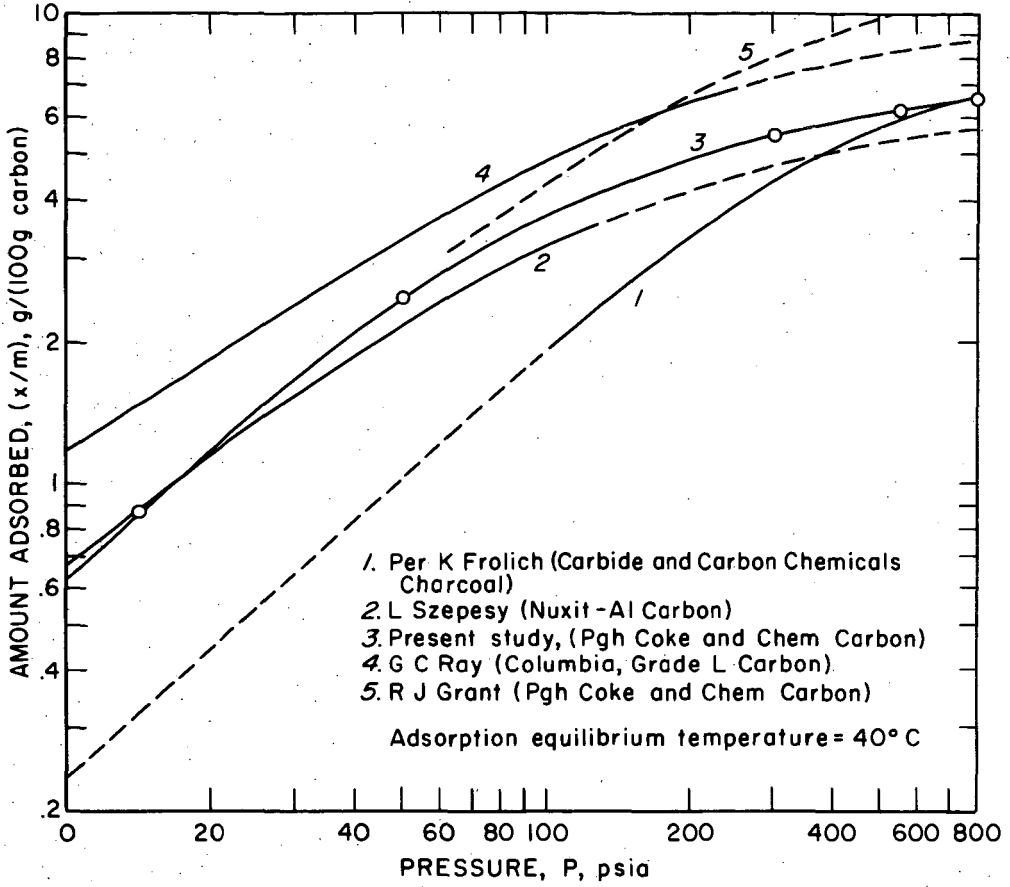


Figure 4.-Adsorption isotherms for methane on various types of activated carbon, Freundlich plots.

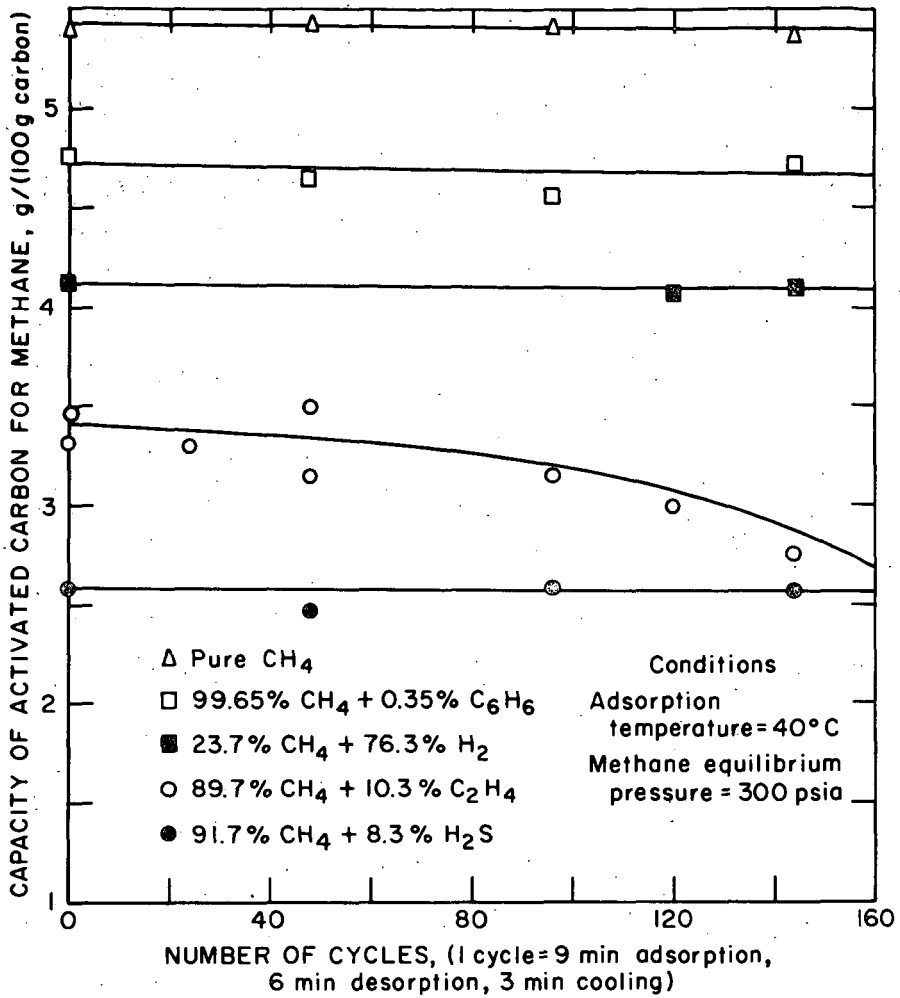


Figure 5.—Effect of contaminating gases and repeated cycling upon activated carbon's capacity for methane.